UiT
THE ARCTIC
UNIVERSITY
OF NORWAY

Faculty of Science and Technology, Department of Geosciences

Source of CO_2 in large Talc-Carbonate veins in serpentinites of the Zermatt-Saas Fee unit

—

Tonje K. Strømø

Master thesis in GEO-3900, July 2018

Supervised by Lukas P. Baumgartner and Jiri Konopasek

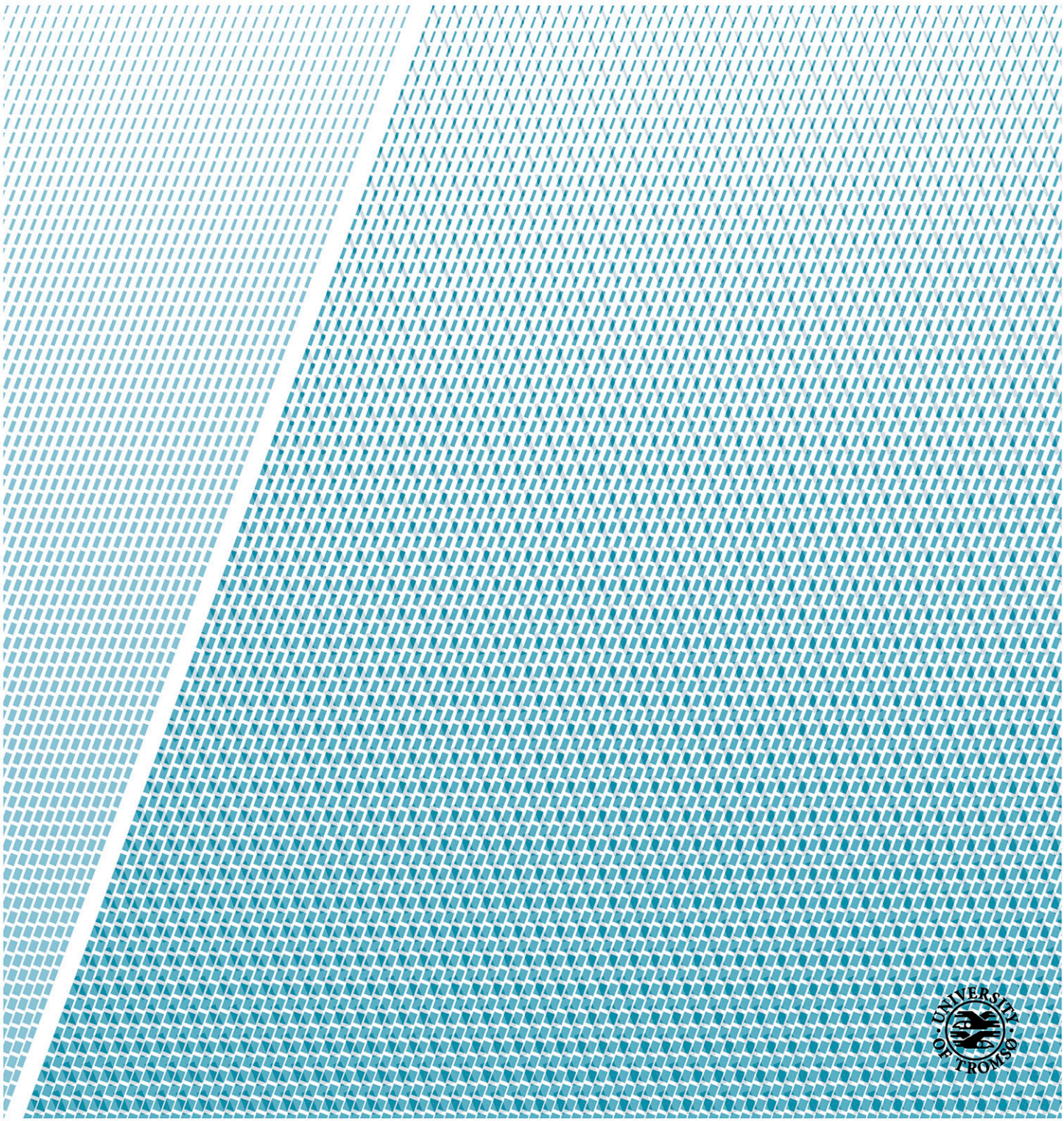

Acknowledgements

I am using this opportunity to express my gratitude to everyone who has been involved in the successfull accomplishment of this master thesis.

Foremost, I would like to address my sincere gratitude to my project director Prof. Lukas Baumgartner for this wonderful field work and master project opportunity and for your continuous support, patience and enthusiasm.

A huge thanks also goes to all the people in the lab. Thank you Torsten Venneman and Benita Putlitz for teaching me how to do the stable isotope analysis and for your good advices. Thank you Martin Robyr for all the valuable help at the microprobe.

Thank you to all my office mates, Joana, Selena, Thibault, Thierry, Dimitri, Christoph and Jules for the good vibes and support all throughout the year! You are all great!

Abstract

The Zermatt-Saas Fee zone represents an ophiolitic sequence within the Western Alps derived from the paleo ocean Liguro-Piemontaise. The melting of the Unterer Theodulgletcher glacier newly uncovered some Tc-Mgs and Atg-Dol veins within serpentinite host rock. Both the serpentinite and veins are fresh as they have been protected from weathering by the glacier, which makes this area ideal for investigation.

The SW-NE orientation of the veins indicates that the veins were formed in context with the backfolding event of the Alpine orogeny. Temperature estimations indicate that the veins formed at 350-450°C at middle- to lower greenschist facies conditions during or shortly after the backfolding event. The veins are metasomatic and formed due to infiltration of a CO2 and Ca rich fluid which reacted with the serpentinite to form carbonate veins. Stable isotope d13C analysis implies that the fluids might be derived from the overlying metasediments – the Bündnerschiefer.

Table of Content

Table of Figures

List of Tables

Fant ingen figurlisteoppføringer.

Acronyms and Abbreviations			
Atg	Antigorite	Mgs	Magnesite
Cal	Calcite	Trem	Tremolite
Chl	Chlorite	Tc	Talc
Di	Diopside	Ol	Olivine
Dol	Dolomite		
Techniques			
EPMA	Electron Probe Micro-Analyzer		
SEM	Scanning Electron Microscope		
XRF	X-Ray Fluorescence		
Other terms			
ZSF	Zermatt-Saas Fee	ca.	circa (about)
PPL	Plane polarized light	e.g.	exempli gratia (in example)
XPL	Cross Polarized light		
ppm	parts per million		

1. Introduction

For the last decade a lot of studies on CO2-sequestration in serpentinites and peridotite have been made to combat the global warming. The idea is based on the reaction of serpentine with CO2 to form talc and magnesite. This way CO2 is "trapped" in the form of a carbonate mineral, which will remain stable for a long time. A lot of studies have been completed in this field to better understand the mechanism of how CO2-rich fluids react with serpentinite in nature, a process which is hoped to be similar to anthropogenic CO2 immobilized. This way, nature can be used to help creating a feasable method for CO2-sequestration.

1.1 Motivation and Goals

The overall goal of this project is to collect data which could provide clues about the source of the carbonating fluids that infiltrated the serpentine in the Zermatt-Saas Fee ophiolitic sequence. Specifically, the goals were to:

- Determining the origin/source and relative timing of CO2-rich fluids. The results will be compared with Seydoux (2013) for the black walls and the potential source rocks.

  The approach used is to:

  - Describe and map the veins and their immediate environment in the field.
  - Determining the temperature (and metamorphic facies) under which the veins were formed using stable isotopes.
  - Do mass balance calculations using the ISOCON approach to establish mass transport for both major and trace elements.
  - Analyse the stable isotopic composition of carbonates and silicates to determine potential sources of the fluid (plot of carbon-isotope against oxygen-isotopes).

1.2 Geological Overview

The study area in the Zermatt-Saas Fee Zone (ZSF) is located in the Swiss part of the Western Alps. The zone has a general NE-SW orientation. It underlain by the Mt. Rosa and the Grand Saint Bernard nappe in the North (Reference?). The latter are of European/Briançonnais origin (Reference). In the South, it is overlain by the Tsaté and the Dent Blanche unit, which is of Apulian origin. In the East it borders to the highly metamorphosed Lepontine dome. There is also an area within the ZSF-zone which shows the overlaying nappes; Mont Fort nappe, Tsaté nappe.

The area of study is situated in Canton du Valais, approximately 6 km south of the Zermatt village (blue star on the map, Figure 1). The field area is situated within the Zermatt-Saas Fee Nappe, which represents a part of the obducted paleo ocean called Tethys, of the Piemont-Ligura paleogeographic domain (Figure 2).

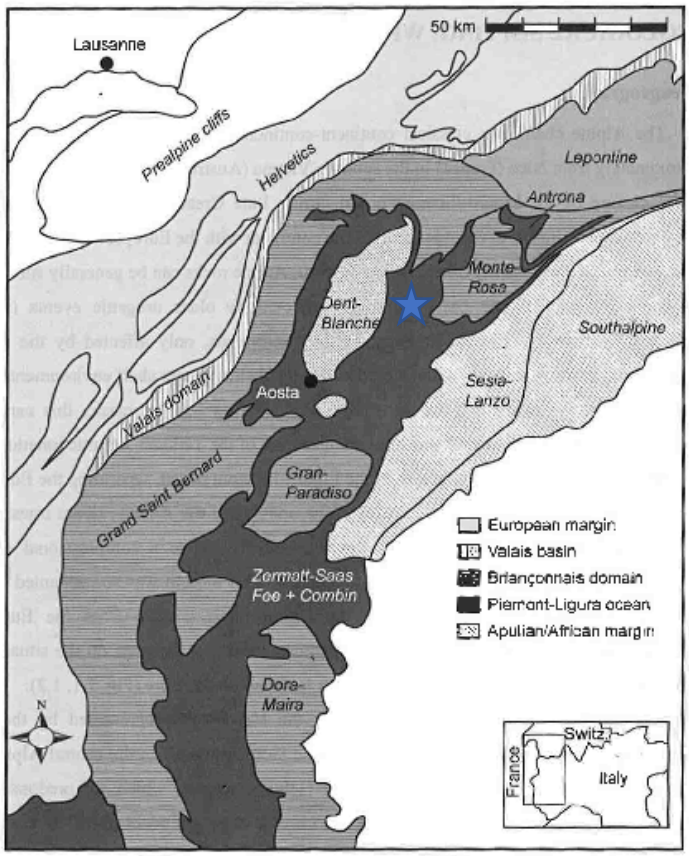

Figure 1: Geological map over the Western Alps, showing the principal geological units and their distribution (After Marthaler, 2001).

The ophiolite sequence is comprised of several lithologies. In this project the focus is on the serpentinites and the carbonate bearing veins. The serpentinites are overlain by Bündnerschiefer (schist lustre) of the ZSFzone. Slices of eclogitic Bündnerschiefers can also be found below the serpentinites studied here (for more detail see Seydoux, 2013). The serpentinites of the Zermatt-Saas Fee Ophiolite cover an area of 30 km^2, and stretches from Breithorn south of Zermatt to Riffelalp in the North. The field work was carried out alongside the glacier "Unterer Theodulgletcher", on the western side of the glacier front (Figure 4).

1.2.1 Paleogeography

The Alpine mountain range is a result of a classic continent-continent collision. It formed during the closing of the Liguro-Piemonte Ocean in late Cretaceous – early Tertiary, followed by the collision between the continents Africa and Europe (Hunziker, 1974).

During the rifting between the European and the African continent in middle to late Jurassic, the Liguro-Piemonte Ocean was formed (Steck, 2008). For a long time the spreading axis of the Atlantic Ocean and Tethys were oriented in the same East-West direction, but from the end of Jurassic to the beginning of Cretaceous (~130-100 Ma) the evolution of the Atlantic Ocean changed direction towards North. This led to the establishment of a triple junction - Tethyan-Atlantic Junction. The northward spreading along the Atlantic mid-ocean ridge caused compression between the European and African continent as the European plate was rotated clockwise, while the African plate rotated counter-clockwise (Dietz & Holden, 1970). As a result of this motion (compression) a fragment of the European continental margin, Briançonnais, drifted away and formed the Valasian Basin (Trümpy, 1980). The paleogeographic situation described above is depicted in Figure 2.

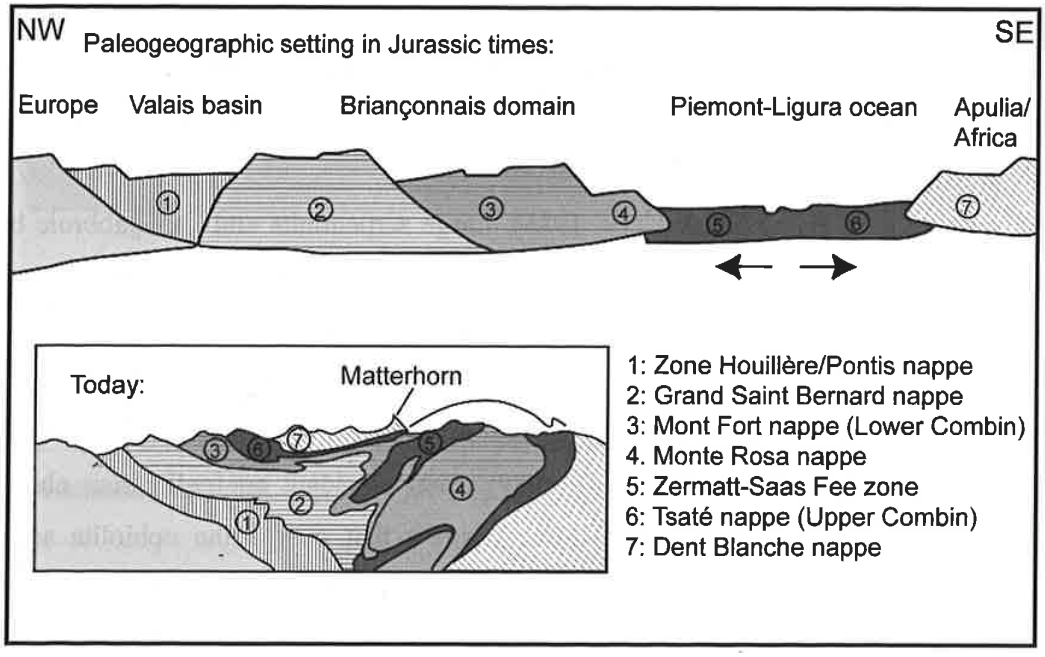

Figure 2: Illustration of the paleogeographic setting in a profile from NW to SW during rifting and formation of the Liguro-Piemonte Ocean in Jurassic. The smaller profile illustrate the current tectonic situation (from Labhart, 1992).

The initiation of subduction of the Liguro-Piemonte ocean started in early/middle Cretaceous, and led the European and African continent to collide. As the subduction proceeded, an accretionary prism formed at the margin of the African plate. Part of the Piemont was subducted, and an accretionary prism was formed. With oceanic crust and marine sediments from the Liguro – Piemonte Ocean. The microcontinent, Briançonnais, was also partly subducted below the accretionary prism (Trümpy, 1980).

Eventually, in the middle/late Cretaceous the African and European plates collided. The collision lasted until the Tertiary (~40 Ma). At his point, the African plate (now in the Dent Blanche nappe) was underlain by the Piemonte accretionary prism, the ZSF-zone, the Mt Rosa of the Briançonnais domain. The Valasian accretionary prism formed(Trümpy, 1980).

However, the micro continent, Briançonnais, was not so easily subducted due to its high buoyancy. As the subduction continued and the pressure and temperature increased, Briançonnais became ductile. Pliable, buoyant fragments of Briançonnais were forced back up along ductile shear zones, along with fragments of the Piemont ocean. The nappes of buoyant continental crust within the relatively heavy oceanic accretionary prism increased the overall buoyancy of the subducted material. This led to a combination of compressional and an up-ward lifting forces which caused backfolding. The backfolding event led to the current geometry of the various nappes (Escher et al., 1997, Steck et al., 2008).

1.2.2 Timing of the high pressure metamorphism

Based on paleomagnetic anomalies, Dewey et al. (1989) interpreted the subduction of the oceanic crust to start during the upper Cretaceous at approx. 110-90 Ma. The earliest HP event were dated at 65-69 Ma (Rubatto et al., 1999; Duchêne et al., 1997) within the Sesia-Lanzo Zone, which contain an eclogitic-micaschist complex. Peak metamorphism was estimated to 13-17 kbar and 500-600°C (Compagnoni, 1977; Venturini, 1995). The PT estimates in the Zermatt-Saas Fee zone are based on blueschist/eclogites, and metapelites, and yield a pressure of about 15-20 kbar and 500-600°C (Barnicoat and Fry, 1986). In addition, UHP conditions of ~27-29 kbar and 600-630°C have been recorded in Lago di Cignana (Reinecke 1991; Reinecke 1998). The dating of the UHP event suggest 44-40 Ma, which partly overlaps with the HP ages estimated for the Monte Rosa nappe. See Skora et al. (2015) for a recent detailed review.

1.2.3 Zermatt-Saas

The Zermatt-Saas Fee unit is a classic example of an ophiolitic sequence, which contains the different layers of oceanic crust. Ultramafic rocks such as serpentine and peridotite (Li et al. 2004), metagabbros (Meyer, 1983), and eclogites containing meta-pillow lavas overlain by radiolarites and carbonate bearing sediments (Bearth (1959), Oberhänsli (1982) and Barnicoat (1988)) are all typical rock types identified and described within Zermatt-Saas Fee unit. The age of the protolith of the oceanic crust is was determined to be 164 Ma, based on U/Pb dating of zircons in the Allalin Gabbro (emplacement). Minimum ages were obtained by U/Pb dating of zircons in the detrital sedimentary cover (Rubatto et al., 1998).

Of special interest for this study are the high pressure Bündnerschiefer units of the ZSF, as well as the serpentinites described in more detail below.

1.2.3.1 Bündnerschiefer

Up in the mountain side 800 m SW of the studied outcrop (below Gandegghütte), a layer of Bündnerschiefer has been observed within the serpentinite. The layer has been folded, with a NW-orientation of the axis (Seydoux, 2013).

The Bündnerschiefer are metasediments derived from the sediments deposited at the bottom of Liguro-Piemonte Ocean and is a part of The Zermatt-Saas Fee unit (Sartori 1987, Marthaler and Stampfli 1989, Dal Piaz 1999, Stampfli and Borel 2002, Bosquet 2008).

These clastic, carbonate bearing sediments are typical flysch sediments found in the narrow Piemont ocean. They are often also called schist lustre (the French nomenclature). The calcschist has a light foliated texture and consist of calcite, quartz, epidote, mica, chlorite and oxides (For detailed description, see Seydoux, 2013). They are a possible source of the CO_2 fluid needed for the formation of the carbonate/talc/ serpentinite veins.

1.2.3.2 Serpentinites at Unterer Theodulgletcher

The serpentinite are partially hydrated mantle peridotites, derived from the Liguro-Piemonte ocean. Compared to other serpentinites in the ZSF-zone, the outcrop next to the Unterer Theodulgletcher was less affected by the subduction and the orogenic folding events. Less deformation and alteration has led to partial preservation of mantle mineralogy and geometry, including pyroxenite and chromite layers, gabbro and basaltdikes. The predominant mineralogy is magnetite (Mt)olivine (Ol)l- antigorite (Atg). Large, neo-formed metamorphic olivine was formed during the Alpine metamorphism, followed by partial re-serpentinisation during the exhumation. Talc (Tc)-magnesite (Mgs) veins crosscut all other veins in the area and are nearly undeformed. These observations indicate that Tc-Mgs veins are the youngest ones in the area. Late greenschist facies fluid flow converted some of these carbonate bearing veins to serpentinite/dolomite veins. The Tc-Mgs veins formed at greenschist facies conditions linked to the backfolding event. They post-date the deformation (Kempf, 2014).

2. Theoretical Background

2.1 Metamorphic fluid

Metamorphic fluids form by dehydration and/or decarbonation of rocks during prograde metamorphism. The fluids are expelled from the rock and will infiltrate other rocks on their way to the surface. These fluids play an essential role in metamorphic processes, as they take part in many reactions and are the agents of dissolution and transportation of elements. To what extent the fluid is able to dissolve and transport elements depends on the composition of the fluid - e.g. the disequilibrium between the host and the fluid - and the infiltrated rock, the acidity of the fluid, and the temperature of the system (Spear, 1995).

2.2 Metasomatism

Metasomatism is a form of metamorphosis, in which the chemical composition of a rock is altered by removal from or addition to the rock of chemical components due to interaction with fluids. Metasomatism occurs when the chemical composition of the rock is not in equilibrium with the chemical composition of the introduced/external fluid. In order to re-equilibrate, an exchange of elements takes place, and the chemical composition of the rock changes. In contrast, 'standard' metamorphism the mineral assemblages re-equilibrate due to changes in pressure and temperature, but the overall chemical composition of the rock remains the same. (Putnis and Austrheim, 2010). Metasomatism is separated from melting by the fact that the rock remains in a solid state during metasomatism (Zharikov et al., 2007). Exclusion of the volatile components in the rock (Putnis and Austrheim, 2010).

2.3 Stable-isotope signatures of fluid-rock interaction

The Stable isotope signature of a metamorphic rock depends on six factors, as defined by Valley (1986): (1) The composition of the pre-metamorphic protolith; (2) the effects of devolatilization; (3) the temperature of exchange; (4) exchange kinetics; (5) chemical composition of the interacting with the rock, and (6) the amount of fluid interacting with the rock. The fluids chemical and isotopic composition varies depending on the fluids origin; oceanic, meteoric, magmatic or metamorphic (Hoefs, 2015). See Figure 3 for the typical compositions of solids in different environments for oxygen and carbonates. Temperature at which fluid and rock interact is an important factor, since isotope fractionation strongly depends on temperature. Interaction at high (igneous) temperatures results in small fractionations, while low temperature of sedimentary environments gives large isotope fractionation. The Isotope fractionation is mass-dependent. Heavier isotopes have a higher affinity for the chemical compounds in which the element is bound most strongly (Bigeleisen, 1965). Heavier isotopes are therefore most likely to be fractionated into a solid phase over a liquid phase, and a liquid phase over a vapor phase.

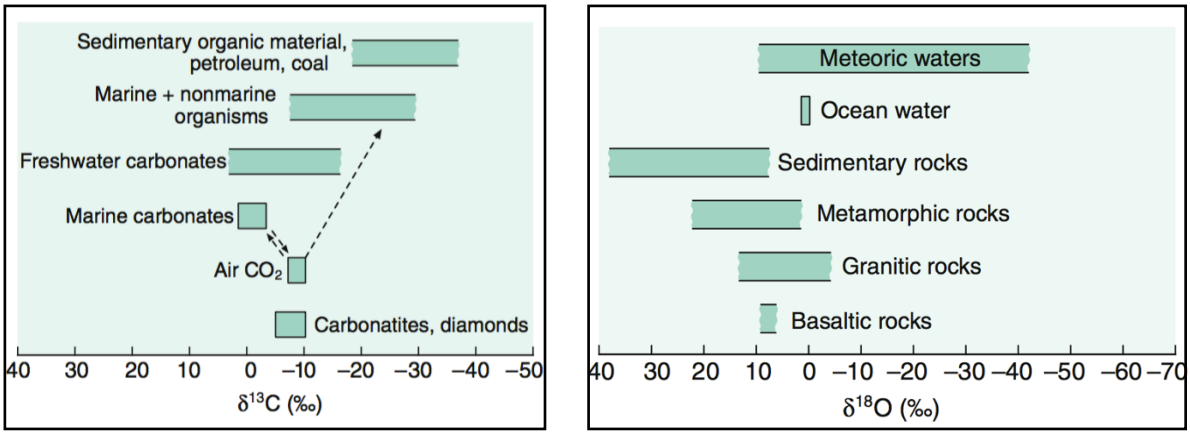

Figure 3: Isotope-fractionation values of important geological reservoirs for d13C and d18O (Hoefs, 2015).

2.4 Serpentinisation

Serpentinisation is the process of hydration of (mantle) peridotite in the oceanic crust. Mantle peridotite is characterized by its high olivine content. Water circulating in the cracks of the oceanic crust reacts with the olivine and forms serpentine, brucite, magnetite and dihydrogen gas. The general formula for the hydration of a dunite is shown in Eq. 1 below.

$$\text{MgFe-Olivine} + H_2O \rightarrow \text{MgFe-serpentine} + \text{MgFe-brucite} + \text{Mt} + H_2\,(aq) \qquad \text{(Eq. 1)}$$

Serpentine has different polymorphs: ; chrysotile and lizardite form at low temperatures (T= 50-300°C), while antigorite forms at higher temperatures (T=400-600°C) (O'Hanley and Wicks, 1995; O'Hanley, 1996, p.160).

2.5 Carbonatisation

Carbonation of serpentine takes place when CO_2-bearing fluids infiltrates the rock. For this process, the concentration of CO2 in the fluid and the temperature of the system is important. When CO_2 is mixed into water, a carbonic acid (H_2CO_3) is formed , along with $CO2_{aq}$, (eq.2). Further, carbonic acid dissociates to form the bicarbonate ion (HCO_3^-) (eq. 3).

$$CO_2 + H_2O \rightarrow H_2CO_3 \qquad \text{(Eq. 2)}$$

$$H_2CO_3 \rightarrow HCO_3^- + H^+ \qquad \text{(Eq. 3)}$$

The increased acidity will cause the ultra-mafic rock to partly dissolve. In this case it is serpentinite (antigorite) + olivine + (cpx?)that dissolves. The cations extracted from the minerals are Mg^{2+}, Ca^{2+}, Fe^{2+}. Mg^{2+} and Ca^{2+} will react with the bicarbonate ion and precipitate in form of carbonates such as magnesite, calcite, and dolomite (Eq. 4a,b,c), while the Fe^{2+} will be partially taken up by the carbonates, but will also react to form f magnetite, depending on the oxygen fugacity.

$$HCO_3^- + Mg^{2+} \rightarrow MgCO_3 + H^+ \qquad \text{(Eq. 4)}$$
$$HCO_3^- + Ca^{2+} \rightarrow CaCO_3 + H^+$$

$$2HCO_3^- + Ca^{2+} + Mg^{2+} \rightarrow CaMg(CO_3)_2 + H^+$$

Talc is often found as a matrix surrounding the carbonates in these type of carbonation reactions. This is because Talc is a product of the excessive cations from the carbonation process (Eq. 5)(Garcia, B. et al., 2010).

$$\underset{\text{Atg}}{2Mg_3Si_2O_5(OH)_4} + 3CO_2 \rightarrow \underset{\text{Mgs}}{3MgCO_3} + \underset{\text{Tc}}{Mg_3Si_4O_{10}(OH)_2} + 3H_2O \quad \text{(Eq. 5)}$$

3. Field Observations

The area where the field work was done had been covered by the glaciers until recently. This provides nice outcrops with freshly polished serpentine which has not yet been weathered. Within the serpentine outcrops one can observe several vein types, including Atg-Dol and Tc-Mgs veins oriented in SW-NE direction, as drawn onto the map (Figure 4). As these veins mainly consists of carbonates, talc and tremolite, they were easily eroded by the glacier and water runoff, resulting in sharp, steep cracks in an otherwise smooth/glacier-polished area.

The strategy of the field work was to obtain samples of the Atg-Dol and Tc-Mgs veins, as well as the host rock. All samples were drilled in a manner to obtain a cross section through the veins. Some samples were drilled in the centre of the zones, and some from the transitions between zones. This enabled to study how the petrology and geochemistry changes from the outer rim of the vein all the way to the centre. The orientation of the veins were mapped and additional deformational features associated with the veins were measured.

There are small changes observable in the mineralogy as a function of location: veins in the south (higher up) are slightly different from veins in the north (lower down), which will be discussed in more detail in the following chapters.

3.2 Host rock

The serpentine in the area contains well-developed magnetite grains. The magnetite grains are slightly elongated, with the long axis oriented in direction NNW-SSE, which is oblique to the veins (Figure 4). The magnetite concentration varies in the field and creates layers of higher and lower concentration. Small veins of olivine can also be found in the serpentine. In addition, veins of clinohumite, and chlorite veins (likely representing altered basalt dykes) are present throughout the area. There seem to be at least two generations of olivine-veins, cutting each other (Figure X).

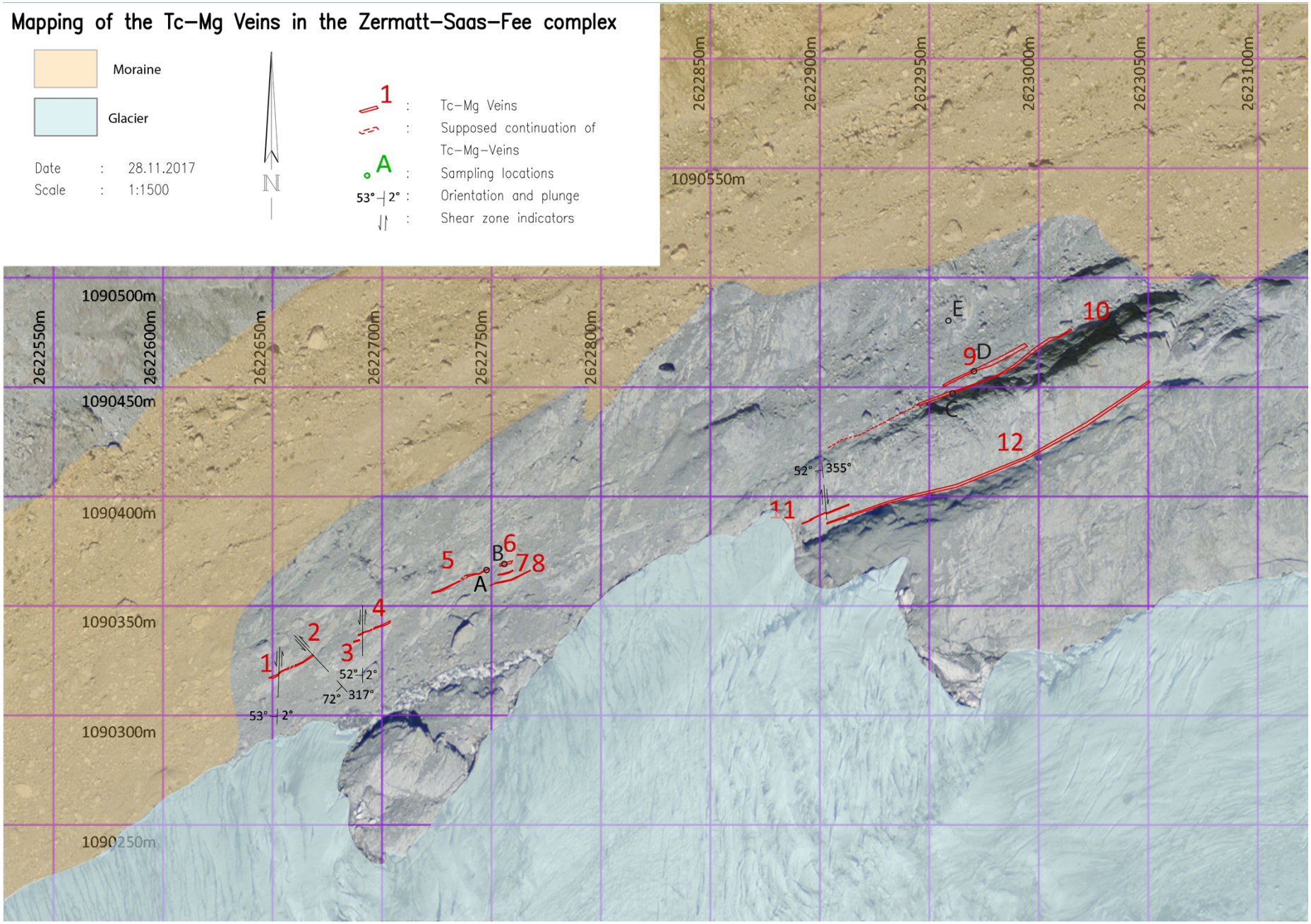

Figure 4: Map with an overview of the field area and the veins.

3.3 Description of studied veins

Three different vein types were studied in the field. They have different mineral zonation. The different types of veins will be categorized and named based on the sample site referenced on the map in (Figure. 4: A, B, C…see map). Mineral composition will be discussed in more detail in the Petrology chapter.

3.3.1 Vein A

Sample site A (Figure 5) is located only a few meters south of Vein 5. The vein shows clear signs of surface weathering. The carbonates are rusty-red due to oxidation. The vein is symmetric and has 4 zones. These are, from host rock towards the center of the vein: the host rock (Host-A) is comprised of serpentine with some Mt-grains; Zone A1 is the most weathered zone. It consists of both carbonates and serpentine. As serpentine is more resistant to weathering and erosion than carbonates, the serpentine stands out. The distribution of serpentine and carbonates seem to be a bit "clustered"; Zone A2 is also formed by serpentine and carbonates. It has a quite even distribution of the two minerals. In Zone A3 the mineralogy changes to tremolite. The tremolite is blue-grey, fibrous and oriented perpendicular to the vein. Zone A4 is also comprised of tremolite, but a white/grey variety.

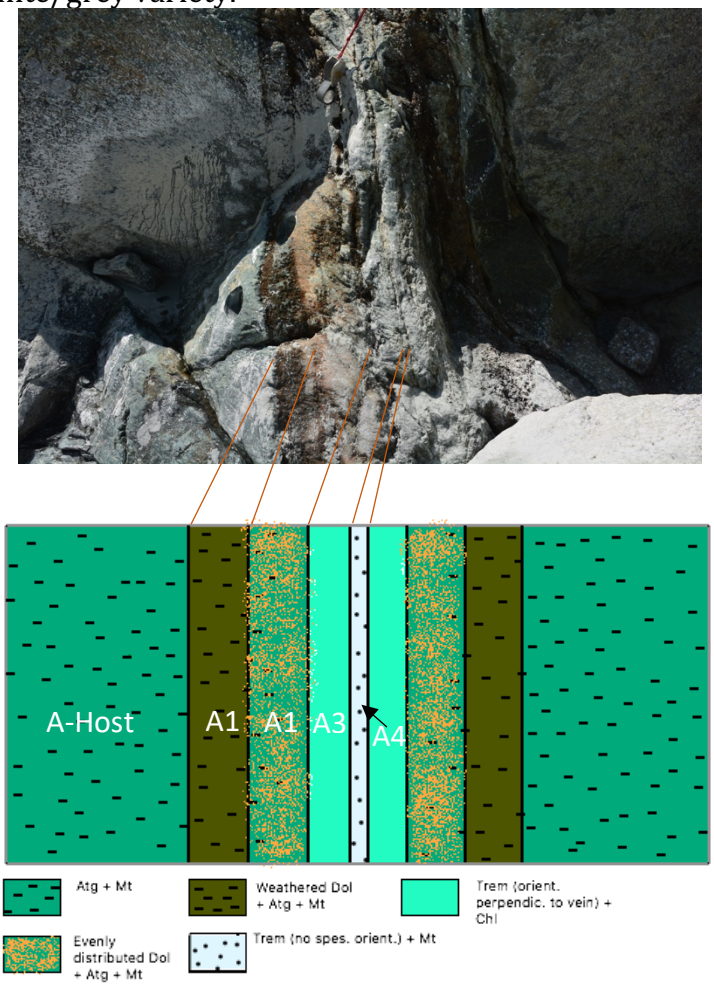

Figure 5:Illustration of the zones observed in sample site A.

3.3.2 Vein B

Sample site B (Figure 6) samples Vein 6 (see map, Figure 4). Vein 6 is representative for Vein 1 - Vein 8. Looking at the outcrop surface of the vein, one can distinguish 6 different zones (B1-B6). The most distal zone, B1, is characterized by serpentine with small, elongated wholes on the surface oriented parallel to the vein and magnetite grains perpendicular to the vein. The cavities are due to weathering of carbonate grains exposed at the surface. Zone B2 has a clear green color and is comprised of mainly serpentine with magnetite grains bending slightly as they approach the vein. The border between zone B2 and B3 is very sharp and linear. Zone B3 has the color of green serpentine with brown oxidized carbonates in it. Zone B4 has a white/grey and rusty-red color to it, and seem to be the zone with the highest concentration of carbonates. The magnetite grains are still present in the vein -deflected. The border between Zone B4 and Zone B5 is marked by a complete change in mineralogy: Zone B5 consist of grey/blue tremolite. The tremolite grains are elongated, fibrous and oriented perpendicular to the vein. Zone B6 consist of white, blocky tremolite with no specific orientation, diopside and newly grown magnetite. The initial magnetite is missing, suggesting that Zone B5 and B6 are mineral zones deposited in an fracture, hence a "crack-infill".

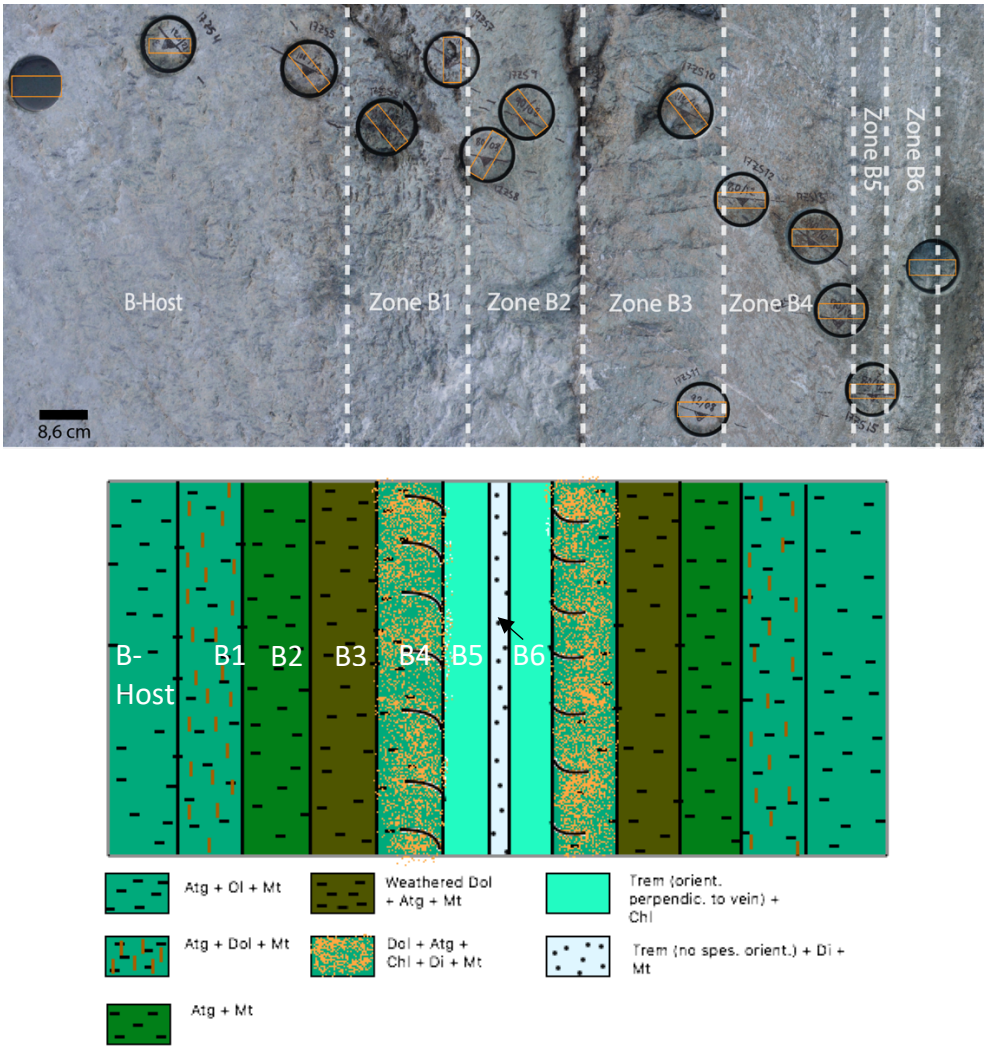

Figure 6:Illustration of the zones observed in sample site B.

3.3.3 Vein C

Sample site C is located in Vein 10, and is a good representative for Vein 9 and 12(Figure 7) as well (see map, Figure 4). From what is observable in the field, there is no zones like the ones in A and B. The reason for this is that the veins have undergone a high degree of erosion which formed large valley in the terrain. Only the most distal part of the vein is preserved within the walls of the cracks, and the centre of the veins are covered by moraine material (Figure 5). The transition from host rock to vein is sharp and undeformed (Figure 7 and 8). Partially outcropping central zones suggest that tremolite is in the centre of the veins.

Typical for these veins are chlorite veins that cut through the Talc-Magnetite vein part of the veins. However, these chlorite veins do not cause any deformation of the vein (Figure X).

Figure 7: Vein 12. Heavily eroded in the center. Moraine material at the bottom of the vein. Person for scale.

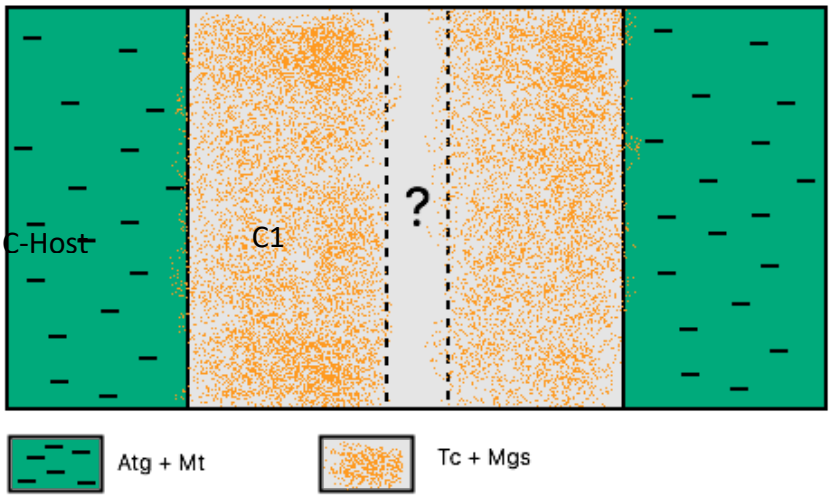

Figure 8: Illustration of zones observed in sample site C.

3.4 Deformational features in the veins

3.4.1 Y-shaped vein

Vein 1 (see map, Figure 4) is the uppermost vein in the terrain which was possible to map. Further up the slope (south-west) the serpentines are covered by moraine material and the glacier. It is also the only vein observed which does not seem to have a continuity as the tip of the vein terminates within the massive host rock. The vein has an orientation of 55-60° NE with a plunge of 80°. This suggests that Tc/Serp-veining might be localized to the present outcrop domain.

Vein 1 has a Y-shape, with needle shaped tips/ends (Figure 9a). The zonation pattern follows the geometry of the vein. However, the zones do not show the "typical" pattern illustrated in Figure 6. The outer zones (Zone B1 and B2) seem to be less defined. Instead, one can find larger 'patches' of carbonates dispersed in the area around the vein. The yellow line in Figure 9a marks the first vein "offset" observed in field, oriented toward North with a dip of 50°.

The lower part of the vein has several cracks cutting perpendicular to it (Figure 7b). They have approx. the same orientation as the offset in Figure 7a, but does not show any displacement. Some of the cracks cut all the way through the host rock and the vein while some only cut through the vein itself. Vein 1 crosscut a chlorite vein, which indicates that the carbonate veins are younger than the chlorite veins (9b).

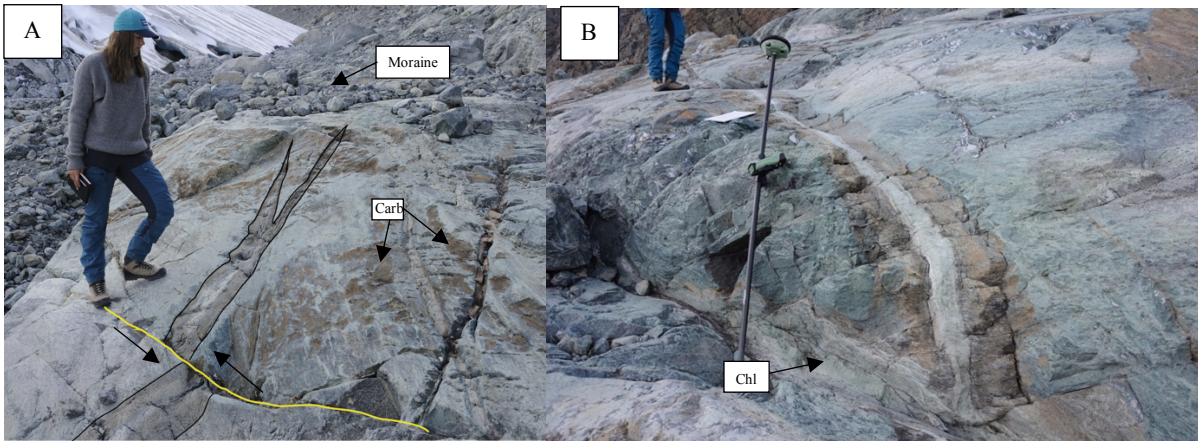

Figure 9: Y-shaped vein (Vein 1). On the left: The top of the vein with a vein offset marked with yellow line and shear sense indicators. On the right: The lower part of the vein with perpendicular cracks, including a cross-cutting serpentine shear zone.

3.4.2 SW-NE oriented shear zone indicators

Vein 1 to 8 (see map, Figure 4) show a dextral shear sense in SW-NE direction. The shear sense is indicated by a sigmoidal trend in different features described below.

Vein 1 (Figure 10) has been locally tectonized, and is highlighted by the orange with arrows indicating the dextral shear sense. There is also a vein offset approximately 0,5 meter below, marked with a yellow line. Unlike the vein offsets described below where the offset is perpendicular to the vein (e.g. Figure 13 and 14), this offset has an angle of 60° to the vein.

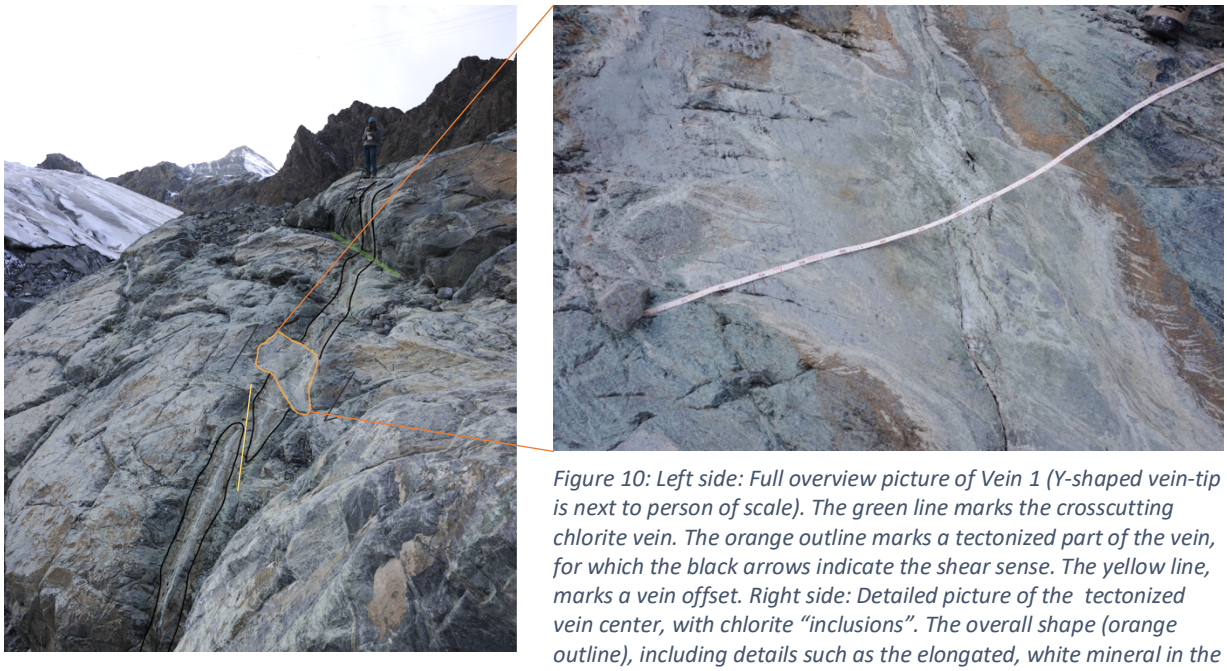

Figure 10: Left side: Full overview picture of Vein 1 (Y-shaped vein-tip is next to person of scale). The green line marks the crosscutting chlorite vein. The orange outline marks a tectonized part of the vein, for which the black arrows indicate the shear sense. The yellow line, marks a vein offset. Right side: Detailed picture of the tectonized vein center, with chlorite "inclusions". The overall shape (orange outline), including details such as the elongated, white mineral in the rusty-red reaction rim confirm the shear sense.

Vein 5 (Figure 11) has been eroded by the glacial water, and formed a shallow, 70 cm wide crack in the terrain confined by the serpentine. Within the vein, zones B3 (atg and dol) show schistosity. The schistosity exhibit a sigmoidal trend with a sinistral shear sense.

Figure 11: Vein 5. Sigmoidal schistosity in zone 3.

In Vein 6 (Figure 10) there is no foliation present, but the shear sense is marked by the magnetite lineation. The magnetite grains start off marking an orientation perpendicular to the vein, but within the vein (alteration zone) but forms a sigmoidal trace towards the central zone as found in Vein 5. It is not very easy to see the shift in magnetite orientation in the pictures, but the blue arrows in Figure 12 highlight some examples.

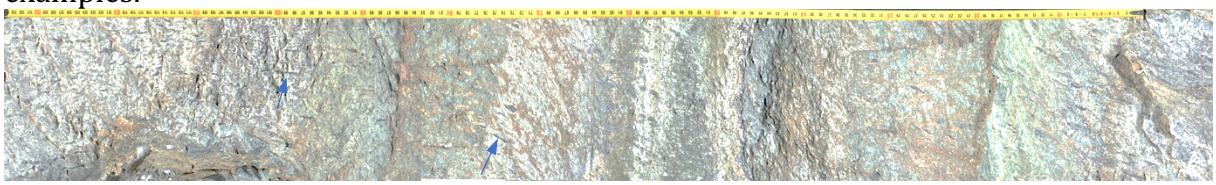

Figure 12: Picture of vein 6. Magnetite orientation indicated with blue arrows.

3.4.3 N-S oriented shear zones

The veins are generally offset by 0,1-0,5 meters (marked with shear zone indicators in the map, Figure 4). All offsets have a general N-S orientation. These "offsets" are localised on shear zones, which do not influence their internal geometry. There were two types of "offsets" found:

1) The inner zones of Vein 1 and 6 (tremolite + diopside + chlorite + magnetite) indicate an offset, but the offset is enveloped by a continuous, undisturbed outer vein-zone (rusty-red zone). This is interpreted to reflect that the initial fractures were discontinuous at the tips (Figure 13). Note that the offset is dextral.
2) In other places, the offset is sharp, and all zones are cut. These are discrete shear zones, which developed after the metasomatism (Figure 14). Note that the offset at the shear zones is always sinistral.

Figure 13: Picture of offset in Vein 6 (Figure 4). An example of crack dislocation which had no apparent effect on the outer metasomatic reaction fronts. The center/crack-infill (Tr+Di+Mt) however, is limited by the walls of the crack. The orange lines mark the orientation of magnetite grains going from host-rock and through the metasomatic reaction front, while orange arrows indicate shear sense.

Figure 14: Picture of vein-offsets in Vein 3 (Figure 4). Depicts an example of a sharp vein dislocation which affected all vein zones – both the center and the reaction front. Yellow lines mark the shear zones by which the vein was offset, arrows mark the sinistral shear sense. The orange lines mark the orientation of the magnetite grains, and orange arrows indicate the shear sense.

Within some of the shear zones marked by yellow lines, one can observe 1-4 cm sized asymmetric, isoclinal folds (Figure 15). The fold axis shows variable orientations which are listed in Table 1.

Table 1: Orientation of the fold axis within the vein offsets.

Fold axis	Orientation of fold axial plane
1	130/10
2	235/47
3	274/09

Figure 15: Small folds found in a sinistral veins offset.

Vein 9, 10 and 12 are large and have a thickness of 2-3 meters and a length of 100 meters. They have been heavily eroded, but show no particular signs of deformation (Figure 7, Figure 16). They can be up to 150 meters long (Figure 4). The veins have a width of approximately 2-3 meters. The height is approximately 2-3 meters. However, the dimension of the vein cannot be accurately evaluated, since the outcrops do not have enough relief. Nevertheless, it seems likely that their size in vertical direction is similar to that seen in the outcrop plane.

The veins dip with an angle of ~80°; hence the veins are sub-vertical. The veins exhibit a lobate pattern on the outcrop wall, nicely outlining the lobate geometry of the reaction front (Figure 16). The reaction front of the vein is sharp on the grain scale. It is marked by a 1-2 cm rusty-red rim, an oxidised carbonate richer outermost reaction zone. The amount of talc increases rapidly towards the centre .

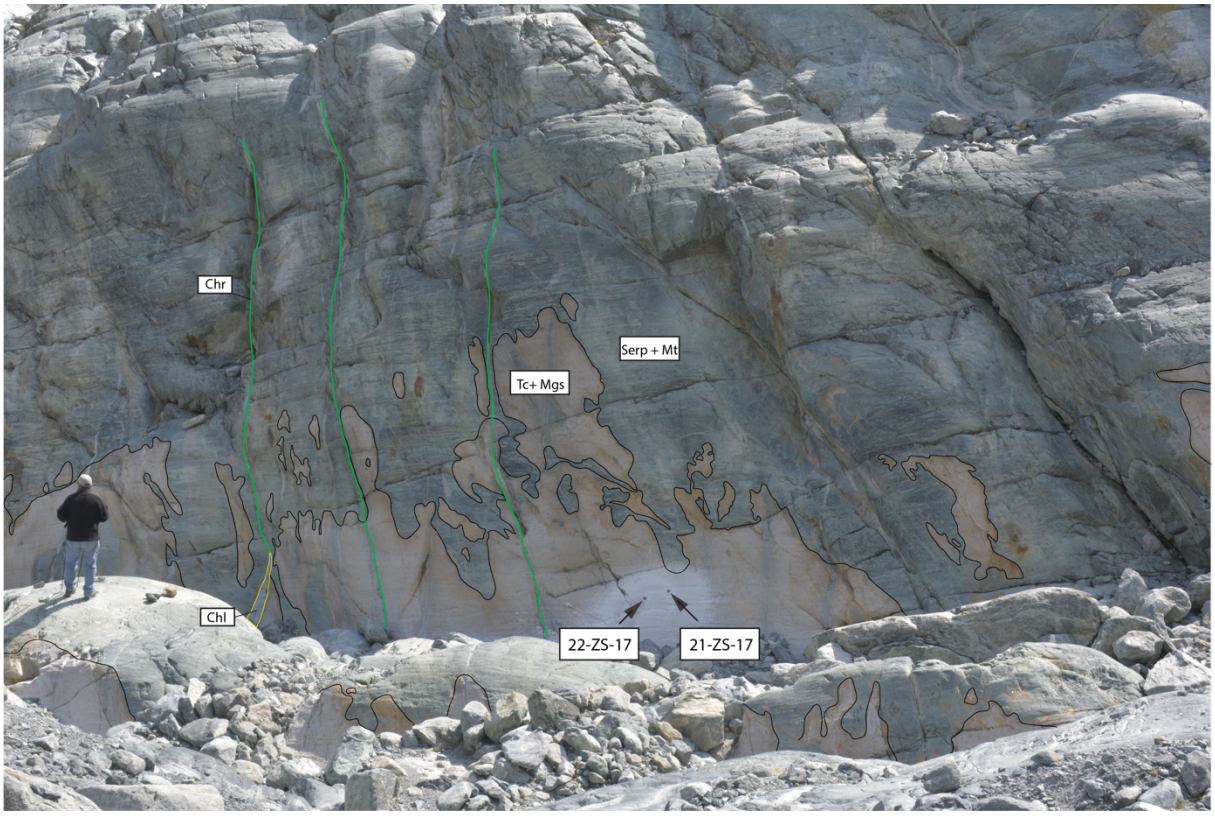

Figure 16: Vein 9 in the front. Vein 10 in the back. Arrows indicate sample- holes and names from sample site C.Person for scale.

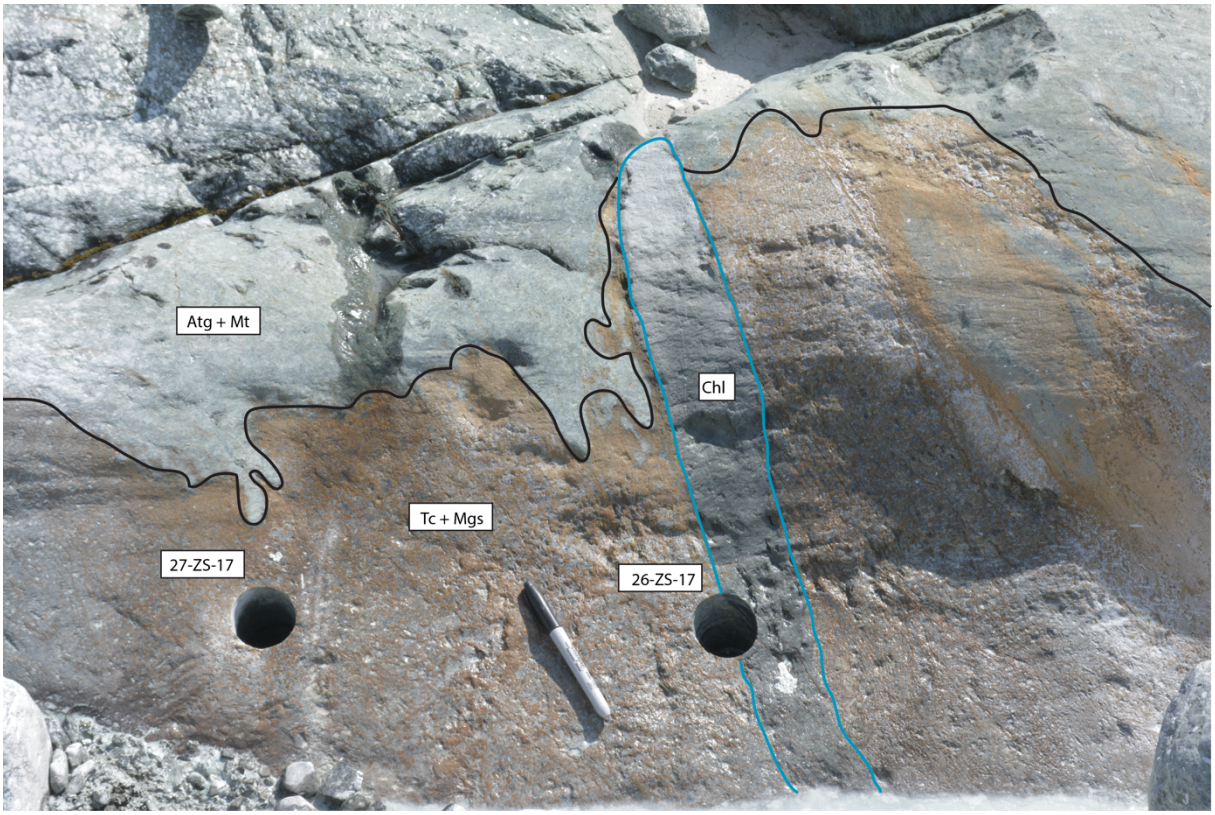

Figure 17: Vein 9, Sample site D.

4. Methods

4.1 Field work

4.1.1 Mapping

To map the veins with good precision and accuracy it was decided to use a Leica GPS with a gs14 receiver and a cs10 controller. The measuring device operates with both the American GPS-system and the Russian GLONASS-system. The two satellite systems have different constellations, and combining the two systems therefore gives a higher precision especially in mountainous environment where fewer satellites are available.

The GPS was connected through internet to the Geneva Cadastral Offices' reference antenna which provide tropospheric and ionospheric corrections to the measurements.

The measured points were recorded and converted on-the-go to swiss coordinates using *Geoid2004_03+ geoide*, and for projection the *Swiss95 projection* was used.

One geodetic control point (13481000) is available in the village of Zermatt. This point has X, Y and Z Swiss coordinates. It was measured in the morning of the first measurement day and in the afternoon after the second measurement day. This gives a good determination of the precision and accuracy of the measured points over the time span of measurements.

The precision of the X-Y coordinates is +/- 32 cm, and the precision for the Z coordinates is +/- 44 cm. The accuracy of the X-Y points measured is 16 cm, while the Z coordinates have an accuracy of 117cm. The entire set of measurement was shift based on the calculated accuracy (one translation in XY and one translation in Z to center the data set on the real position of the control point).

All the measured points were inserted in the drawing program AutoCad 2016, in which 3D-models can be created. Lines were drawn between the points to draw the veins in 3D. A satellite photo was retrieved from the webpage *map.geo.admin.ch* (© ESA / Eurimage / swisstopo, NPOC). The veins were then put as a layer on top of the satellite picture.

4.1.1 Extracting samples

Using a modified chain saw with a diamond rimmed core cutter with a diameter of 4,5 cm to extract samples.

4.2 Lab work

Sample site		Sample - ID	Thin sections	XRF	Micro Probe	SEM	Isotope
A	Host-A	19-ZS-17(T)	X	X	X		X
	A1	19-ZS-17(M)	X	X			X
	A2	19-ZS-17 (B)	X	X			X
	A3	20-ZS-17(T)	X				X
	A4	20-ZS-17(B)	X	X	X		X
B	Host-B (1)	01-ZS-17					
	Host-B (2)	02-ZS-17	X	X (T & B)	X		X
	Host-B (3)	03-ZS-17	X				
	Host-B (4)	04-ZS-17	X	X			X
		05-ZS-17	X				
	B1	06-ZS-17	X	X			X
		07-ZS-17	X		X		
		08-ZS-17	X				
	B2	09-ZS-17	X	X			X
	B3	18-ZS-17	X	X			X
	B3	10-ZS-17	X				
		11-ZS-17	X		X		
		12-ZS-17	X (T & B)				
	B4	13-ZS-17	X	X			X
		14-ZS-17	X (T & B)				
	B5	15-ZS-17	X (T & B)	X			X
	B6	16-ZS-17	X	X			X
		17-ZS-17	X				
C		21-ZS-17	X (T, M, B)				
		22-ZS-17	X				
D	Host-C,C1	23-ZS-17				X	X
		24-ZS-17	X				
		25-ZS-17					
		26-ZS-17	X				
E		27-ZS-17	X				
		28-ZS-17	X	X		X	X
		29-ZS-17	X	X		X	X
		30-ZS-17	X	X			X
		31-ZS-17	X	X			X
		32-ZS-17	X	X		X	X
		33-ZS-17	X	X			X

4.2.1 Cutting the cores

Each core was cut in three sections vertically. When cutting the cores, two aspects were taken into consideration; in the outer-most zones (1-3) it was of interest to cut the cores parallel to the magnetite orientation/lineation. For the remaining zones (4-6), it was of greater importance to cut perpendicular to the vein in order to obtain the transition zones.

4.2.2 Bulk rock chemistry

Purpose:
Whole rock chemical composition. Element transport and metasomatic pattern.

The selection of samples for the XRF-analysis was done with the aim of collecting the characteristic whole rock data from each zone. To avoid contamination between zones, only the cores extracted from the center of each zone was selected. The fact that the samples are quite heterogeneous, made it a bit challenging to select representative pieces for analysis. For analysis 4-5 cm was cut off one of the outer pieces of the cores were used.

Powder for the XRF-analysis were prepared by initially using a hydraulic press to crush the solid rock into pebbles and coarse powder. Finally, the crushed material was put into the tungsten-mill to make a fine-grained powder with an average grain size <75µm or <50µm?!. A mill of tungsten was used instead of agate to avoid contamination.

4.2.2.1 Major elements

For analysis of the major elements in the samples, 2.5 - 3.0 grams of sample material was weighted into small crucibles (using scale Mettler Toledo AG104) before performing the Loss on Ignition process (LOI). A relatively large amount of sample material was weighted, as it is expected high rates of volatile loss for carbonates during the LOI-process. The process was done by placing all the weighted samples into an oven (SOLD – Industrial Furnace) at 1050°C for 2 hours. After the LOI-process, the samples were weighed again to register the loss of volatiles. The powder tends to become a bit 'clumpy' after LOI, the samples were therefore ground in a mortar of agate in order to homogenize the powder again before proceeding.

The next step was to create fused beads for analysis of major elements. For this purpose, 6.0000 +/- 0.0002 grams of $Li_2B_4O_7$ and 1.2000 +/- 0.0002 grams of sample powder were mixed together. A mortar of glass was used to homogenize the mixture (mixing for 3 minutes). The mix was then poured carefully into a silver cup, which in turn was placed into the *Perl'X3 PANalytical*, which is the machine used to melt the powder at 1200°C for X minutes. Finally, the machine poured the melt into pellets-moulds of silver to cool down/quench.

Analysed with the XRF-machine AXios mAX (PANalytical) by Jean-Claude Lavanchy at UNIL.

4.2.2.2 Trace elements

In order to analyse the trace elements of the samples, Pressed Pallets were prepared. To make these pallets, the sample powder was mixed with *Hoechst Wax C micropowder* *($C_{38}H_{76}N_2O_2$)*, which is a tableting aid for XRF-analysis. Using a Mettler AC88 scale, 12.00 +/- 0.005 grams of sample powder and 3.00 +/- 0.005 grams of Hoechst wax was weighted into a cylindrical plastic container. Afterwards, the container was sealed and placed into the shaking-machine, Retsch MM400. The machine was programmed to shake the sample for 3 minutes with a frequency of 30 shakes/second. Finally, the powder was pressed with a Herzog press at 100kN for approx. 2-3 minutes.

4.2.2.3 Fe2+/Fe3+ ratio

First, an amount of approximately 100 +/- 20 mg sample powder (same as used for XRF) was weighted into bottles. The determination of how much powder to weigh, depends on how much Fe_{Total} each sample contains –the less Fe_{Total}, the more powder.

The powder was mixed with 10 mL ammonium-vanadate NH_4VO_3, followed by 10 mL sulphuric acid. The order of which these chemicals are mixed with the sample powder is important, as the vanadate protects the Fe^{3+} from reacting with the sulphuric acid. Further, 5 mL of concentrated fluorhydric acid was carefully added to the mix before placing all the samples into a "bain-marie". The bain-marie was set to 80°C for 1-2 hours, and 60°C during the night. The next day, the solution is neutralized with boric acid. Sodium acetate, bypyridin and water is added to form ammonium Fe^{2+} which gives a red color. The color intensity depends on the FeO content in the powder from the rock.

4.2.4 Stable Isotopes

Stable isotopes were determined for bulk rock and minerals.

4.2.4.1 Carbon- and Oxygen Isotopes for carbonates

This method was performed for both bulk rock powder and drilled grains.

Isotope analysis of bulk rock was done using the same powder as used for bulk rock chemistry, with the help of a Gas-Bench (Thermo Fisher Scientific Gas-Bench II) and a mass spectrometer (Thermo Finningan Scientific Delta Plus XL). Using a scale with high precision, between 100-200 µg was weighed in for each standard (Carrara Marble II) and between 150-250µg for each sample. The weighed material is put into glass vials and sealed with a hermetic lid. The lid has a layer of soft rubber on the top, which allows for the syringe to penetrate during the analysis. Once the samples put into the instrument, a syringe is inserted into the samples to remove all the air present in the glass vials and replace it with helium (He). Afterwards, the samples are acidified with 15 mn phosphoric acid and heated at 90°C for 1 or 24 hours. The various reaction times is due to an uncertainty of what types of carbonates were in the samples at the time of analysis. Magnesite requires longer reaction time with the acid to fully dissolve.

4.2.4.2 Oxygen Isotopes for silicates

Removing carbon from bulk rock powder

Before doing oxygen-isotope analysis, it is important to get rid of all the carbon in the samples. The samples were therefore washed with HCl -acid, which causes the carbon to react and exit the sample in form CO_2-gas. For this procedure 1 gram of sample material was mixed with 20mL HCl – acid (32%). The samples were left to react for 2 hours, at which point no bubbles of CO2-gas were ascending/visible anymore. The acidic solution was then diluted by adding 50 mL distilled water, and put away for one hour in order for the powder to precipitate. Afterwards, the liquid was carefully poured out. To ensure that as little powder as possible escapes the beaker, a small amount of liquid was retained in the bottom. The samples were then washed with water three times. Washing was done by pouring pure distilled water into the powder, let the powder settle for one hour and then pour off the water. Finally, the powder was put in the oven at 60°C to dry.

Mineral separation

The mineral separation was done by cutting the sample of interest into smaller pieces (approx. 2x3 cm). The sample was then put in a plastic bag and crushed by the use of a hammer. The crushed material was transferred into a fractionating sew to separate the different grain sizes. The sizes of sews being used in this process was 1000, 800, 500, 250 and 150. The magnetite can easily be separated from the rest of the matrix by using a hand-held magnet. And tremolite and diopside had to be separated by picking. The picking was done carefully with focus on finding pure grains with no inclusions.

Laser-Fluorination

Once the samples were washed/picked 1,5 to 2 mg of the powder/mineral was weighed for each sample. Each sample was put onto a platinum plate with holes in it for each sample. The platinum plate is put into a chamber for pre-fluorination overnight in order to remove any absorbed water. Further, the samples immersed in fluor is ablated with a CO2-laser. When the flor has completely reacted, it is removed by heated KCl salt. The pure oxygen, in the form of gas is then transferred to a spectrometer (Thermo Finnigan MAT 253 IRMS), where it is analysed and standardized with the reference gas. Depending on the type of samples being analysed, quartz or garnet standards are used. For the serpentine, quartz (Lausanne 1qtz, 30-50 mesh) was used. The data is treated in the software “Finnigan Isodat 2.0”. Based on the results of the standards, a small correction is done. The reproducibility of this method is in the order of 0.2%.

4.3 SEM

4.4 Micro probe

4.5 ISOCON method

The ISOCON method was used in order to visualize the mass transport of elements and to investigate whether the veins form at constant volume. Gresens (1967) developed an equation for estimating the gain and loss of components in relation with volume change. However, this method requires that total mass per volume unit before and after alteration is known. An alternative method was developed by Grant (1986). He rearranged the Gresens equation to create a linear relation between the concentrations of the altered and the unaltered rock. Although this method is simple and fast, it comes with the disadvantage that the components that plot far from the origin are much more important (visualy) than the ones closer to the origin.. To correct for this scale-error, Baumgartner and Olsen (1995) suggested an extension of this method where the variance for each element of the altered and unaltered rock (σ_i) is taken into account to evaluate the elements, which are compatible with being relatively unaltered.

5. Petrography

5.1 Macroscopic observations

Description of vein type A

The host rock outside vein A (Figure 18) consist of serpentine with large, elongated magnetite grains and a few carbonates just at the vein-border. The transitions between zones are often marked by brittle fractures, since they represent major weakness zones. The first zone (A1) consist of a mesh-like network of white carbonates enclosing "pockets" of serpentine inside the mesh. In zone A2, idioblastic carbonates are dispersed in a serpentine matrix. Zone A3 is quite similar to A2, but the carbonate grains become smaller in size. Zone A4 consist of fibrous, blue-grey tremolite.

Macroscopic description of vein B

The surface of the host (Figure 19) has a green matrix with elongated magnetite grains, oriented perpendicular to the vein. In the cross section of the drill-core, it becomes evident that the color of the matrix is dark-green with a mesh of bright-green veins. The large, elongated magnetite grains are also visible.

The weathering surface of Zone B1 has a green-brown matrix similar to host rock with small cavities oriented parallel to the vein. These holes formed due to weathering of carbonates at the surface. The cross section indicates that the dark green matrix with bright green veinlets is preserved, but displays a sudden increase in carbonate content. The carbonates at the surface has undergone pervasive weathering and therefore has a rust-red color. The carbonates in the lower part of the core is better preserved.

At the surface of Zone B2 it looks like the matrix has a slightly brighter green color, and somewhat less brown than the prior zones. The magnetites on the surface has undergone a small change in orientation. In cross section, the matrix has a brighter green color than prior zones. It becomes evident that this zone has a very low content of carbonates and mainly consist of massive serpentine, with a few carbonates dispersed in it.

The transition from zone B2 to B3 is fractured and oxidized. The surface of Zone B3 is brown-green. In the cross section, matrix has a dark green color. The brittle transition is confirmed by internal, oxidized cracks (the core has been glued with epoxy). The carbonates bordering the crack has been oxidised. The carbonates are concentrated in patches and, exhibit anhedral crystal shapes.

The transition from Zone B3 to B4 is sharp, at which the carbonate content increase from 20% in zone B3 to approximately 70% in zone B4. In the cross section one can observe that the carbonates in B3 are situated close to the zone-border are growing parallel to the border. Zone B4 has a grey-beige color due to the high carbonate content with some dark matrix (Oxidation). Large, lenticular oxides are dispersed in the zone.

Zone B5 consist of a blue, fibrous Tremolite which grows perpendicular to the vein. In-between the tremolite there is patches of a grey, dense mineral. There are very little oxides, if at all.

Zone B6 contains a white, fibrous mineral with no preferred orientation. Appears more dense. Oxides are present.

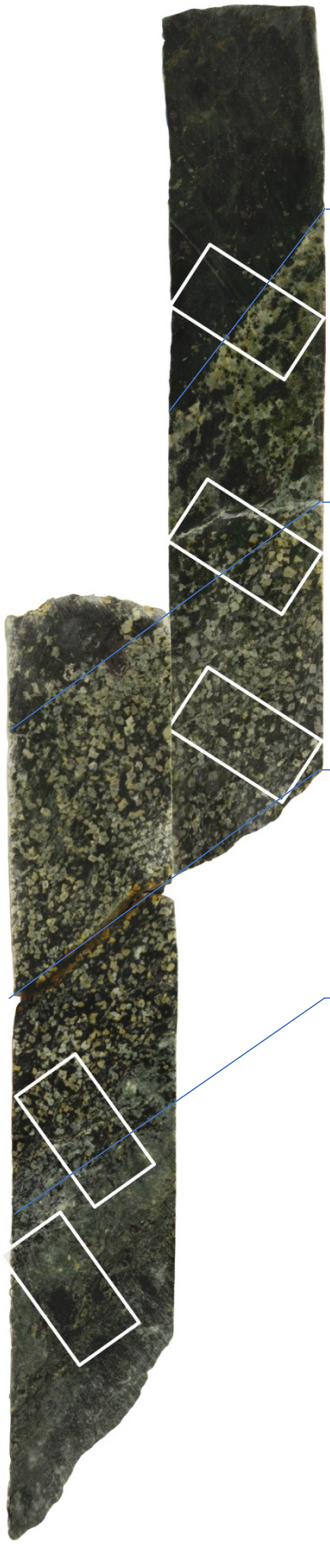

A-Host: Antigorite, magnetite, a few dolomite grains dispersed in serpentine matrix.

Zone A1: Rim. Dolomite “mesh” with pockets of antigorite.

Zone A2: Large, euhedral dolomite grains with calcite rims evenly distributed in serpentine matrix.

Zone A3: Smaller, euhedral dolomite grains evenly distributed in serpentine matrix.

Zone A4: Center of vein w/tremolite.

Figure 18: Cut cross section of vein A. White rectangles indicate where the thin sections are taken from.

5.1.2 B-type vein

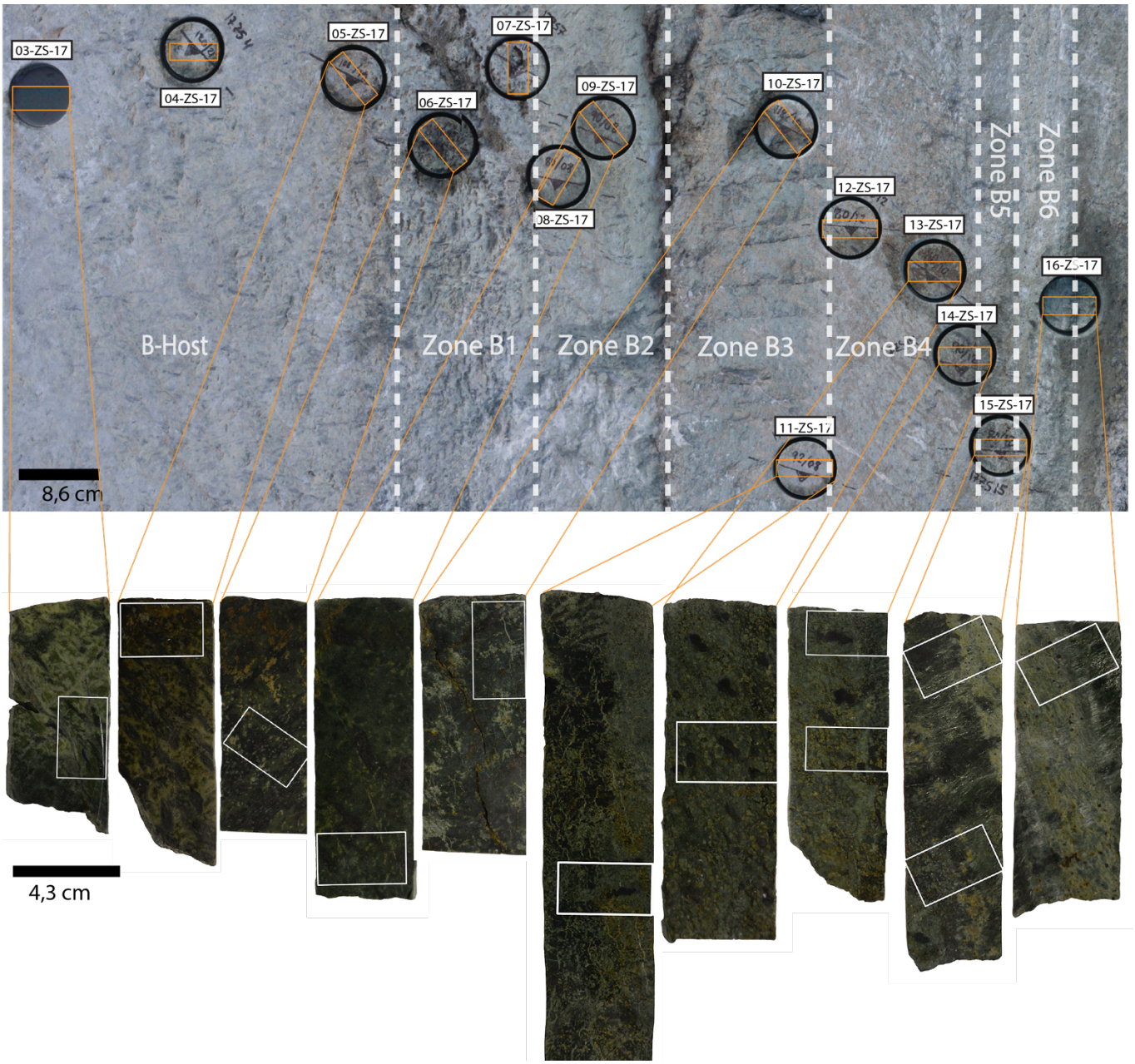

Figure 19: Above: an overview picture of vein B from rim to centre showing where the different samples are taken from. Orange rectangles indicate at which angle the cross sections were cut relative to the vein. Below: cross section of the cores. White rectangles indicate where the thin sections

Macroscopic description of vein A

The host rock outside vein A (Figure 18) consist of pure serpentine with large, elongated magnetite grains and a few carbonates just at the vein-border. The transitons between zones are often marked by brittle fractures. The first zone (A1) consist of a white network of carbonates with "pockets" of serpentine in-between. In zone A2, idioblastic carbonates are dispersed in serpentine matrix. Zone A3 is quite similar to A2, but the carbonate grains become smaller in size. Zone A4 consist of fibrous, blue/grey tremolite.

Macroscopic description of vein B

The surface of B-Host (Figure 19) has a green matrix with elongated magnetite grains oriented perpendicular to the vein. In the cross section of the drill-core, it becomes evident that the color of the matrix is dark-green with a mesh of bright-green veins. The large, elongated magnetite grains are also visible.

The surface of Zone B1 has a green-brown matrix similar to host rock with small cavities oriented parallel to the vein. These holes probably formed due to weathering of carbonates at the surface. The cross section indicates that the dark green matrix with bright green veinlets is preserved, but is differentiated by a sudden increase in carbonate content. The carbonates at the surface has undergone pervasive weathering and therefore has a rust-red color. The carbonates in the lower part is better preserved.

At the surface of Zone B2 it looks like the matrix has a slightly brighter nuance of green an less brown than the prior zones. The magnetites on the surface has undergone a small change in orientation. In cross section, the matrix has a brighter green color than prior zones. It becomes evident that this zone has a very low content of carbonates and mainly consist of massive serpentine, with a few carbonates dispersed in it.

The transition from zone B2 to B3 is brittle and oxidised. The surface of Zone B3 is brown-green. In the cross section, matrix has a dark green color. The brittle transition is confirmed by internal, oxidised cracks (the core has been glued with epoxy). The carbonates bordering to the crack has been oxidised. The carbonates are concentrated in clusters/patches and, exhibit anhedral crystal shape.

The transition from Zone B3 to B4 is sharp, at which the carbonate content increase from 20% in zone B3 to approximately 70% in zone B4. In the cross section one can observe that the carbonates in B3 that are situated close to the absolute zone-border are growing parallel to the border. Zone B4 has a grey/beige colour due to the high carbonate content with some dark matrix. Oxidation. Large, elongated /lenticular oxides are dispersed in the zone.

Zone B5 consist of a blue, fibrous mineral which grows perpendicular to the vein. In-between the tremolite there is patches of a grey, dense mineral. There's no/little oxides.

Zone B6 contains a white, fibrous mineral with no preferred orientation. Appears more dense. Oxides are present.

5.1.3 C-type vein

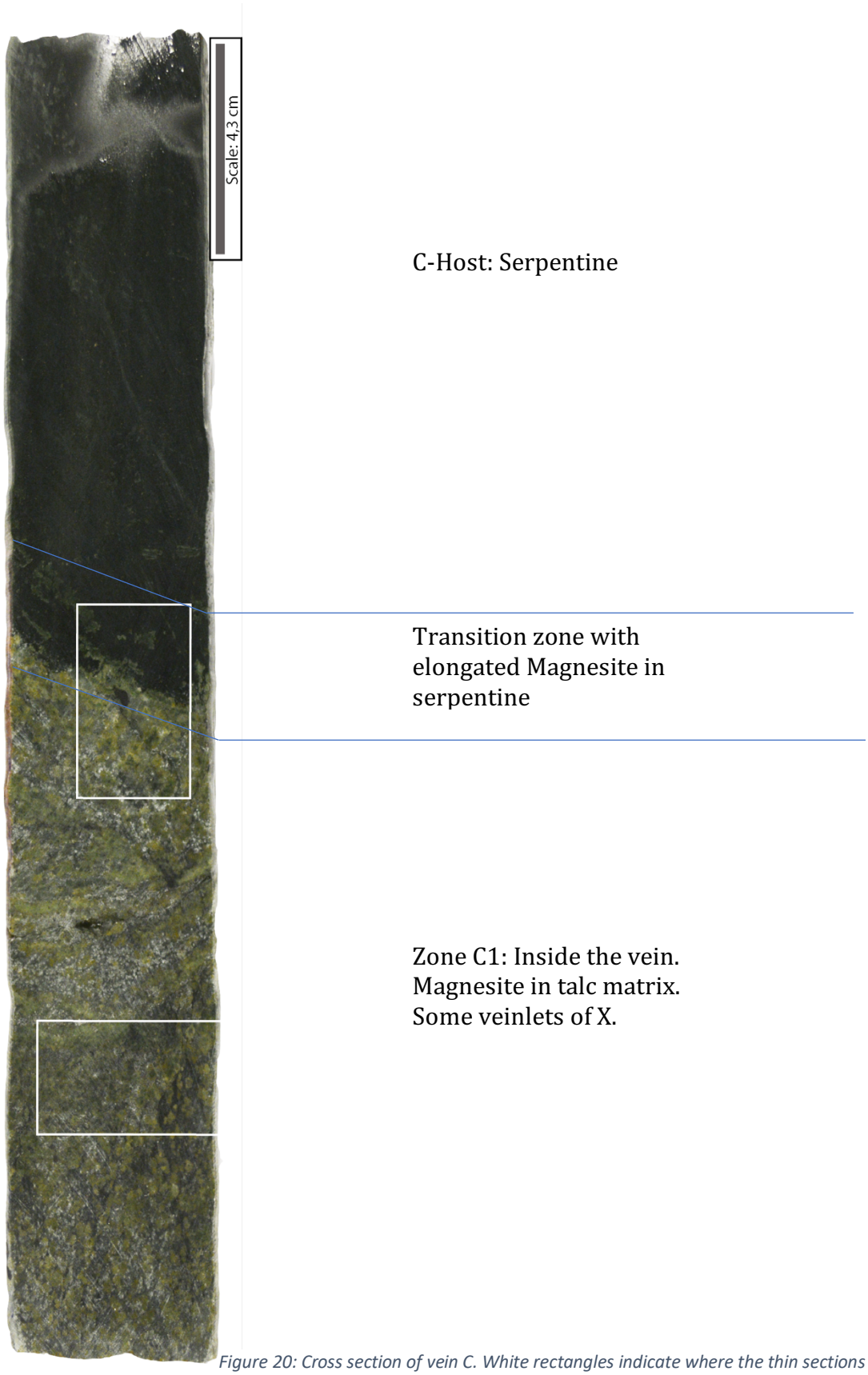

Figure 20: Cross section of vein C. White rectangles indicate where the thin sections are taken from.

5.2 Microscopic observations

Microprobe and SEM was used to determine what types of carbonates are present in the veins.

5.2.1 A-type vein

5.2.1.1 Host-A

The host rock (Figure 21) is composed of antigorite (Atg) with a fine grained texture. No pseudomorphs were detected. The Atg- grains are xenoblastic and interlocking. There are some elongated magnetite grains (~5mm) dispersed in the Atg. The texture of the antigorite generally remains the same through the vein as well (Figure 1).

5.2.1.2 Zone A1

Zone A1 (Figure 21) marks the transition from host rock to vein. It consists of a fine-grained antigorite-matrix with large anhedral dolomite grains in it. The dolomite forms a network of aggregates, while antigorite concentrate in "pockets" in-between. Antigorite is also found within the dolomite grains. A couple of thin dolomite veins are also present in this zone (Image 1).

5.2.1.3 Zone A2

The transition from zone A1 – A2 (Figure 21) is marked by a brittle crack. The dolomite grains in this zone exhibit large, idioblastic to subidioblastic shape and are evenly dispersed in a matrix of serpentine. The texture of the dolomite is poikiloblastic with Atg grains growing inside. The concentration of Atg inside the grains is highest in the center of the grain. The magnetite grains are concentrated in the matrix between the dolomite grains.

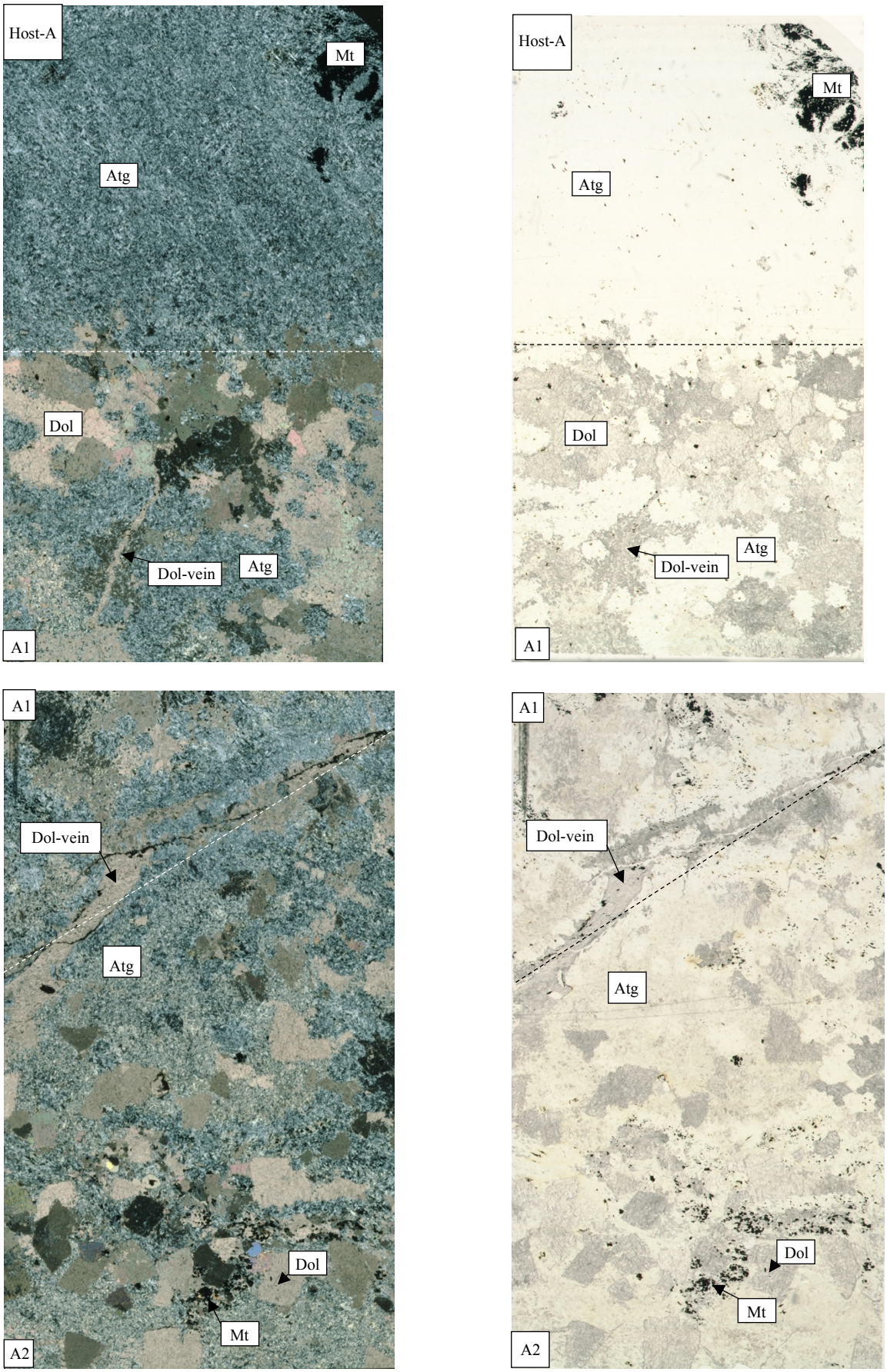

Figure 21:Pictures of thin sections from Vein A.

5.2.1.4 Zone A3

From zone A2 to A3 (Figure 23) there is a decrease in dolomite grains size, but the idioblastic shape is maintained. The matrix is still composed of antigorite. The dolomite show a poikiloblastic texture with antigorite grains dispersed within the grain (Figure 22). The concentration of antigorite within the dolomite grain is highest in the center. In optical microscopy the idioblastic grains often have a rim with a different extinction angle than the center. The rim has a "granular" texture. Analyzed with the micro probe, it became evident that the rim and core show two different compositions – the rim consist of calcite, while the center is composed of dolomite. Elongated antigorite grains grow in the center of the carbonate crystals. Amongst all the dolomite grains in the thin section, one of the grains contained Talc.

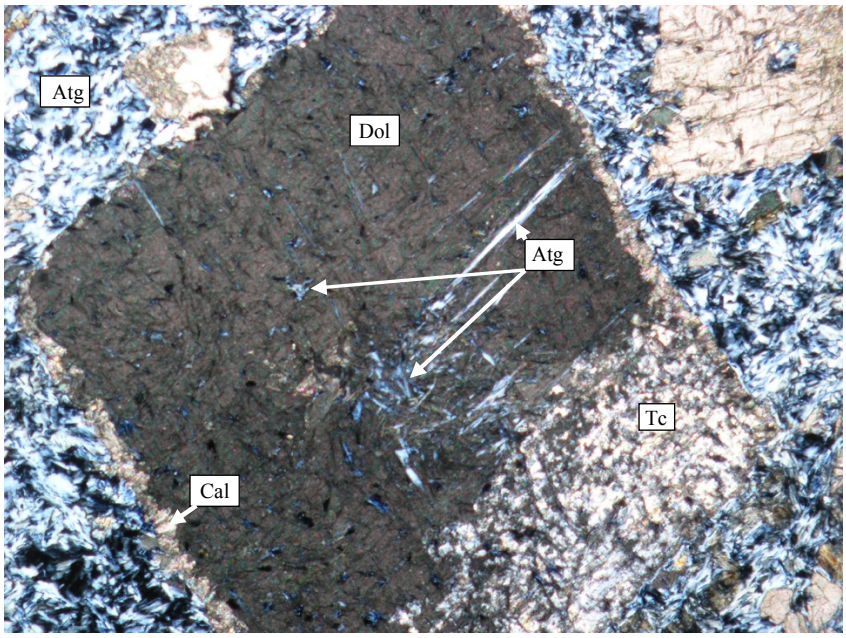

Figure 22: Picture of dolomite grain with calcite rim and traces of talc inside. Antigorite in the centre of the grain.

5.2.1.5 Zone A4

The transition from A3 to Zone A4 (Figure 23) is marked by yet another fracture and a slight decrease of the number of carbonate grains. It is uncertain if this crack is a former carbonate vein. Zone 4 consist of tremolite, and is interpreted to represent the center of the vein. The tremolite grains are fine grained in the transition zone, but become better developed (longer) as one approaches the center of the vein. It is most likely an open vein fill.

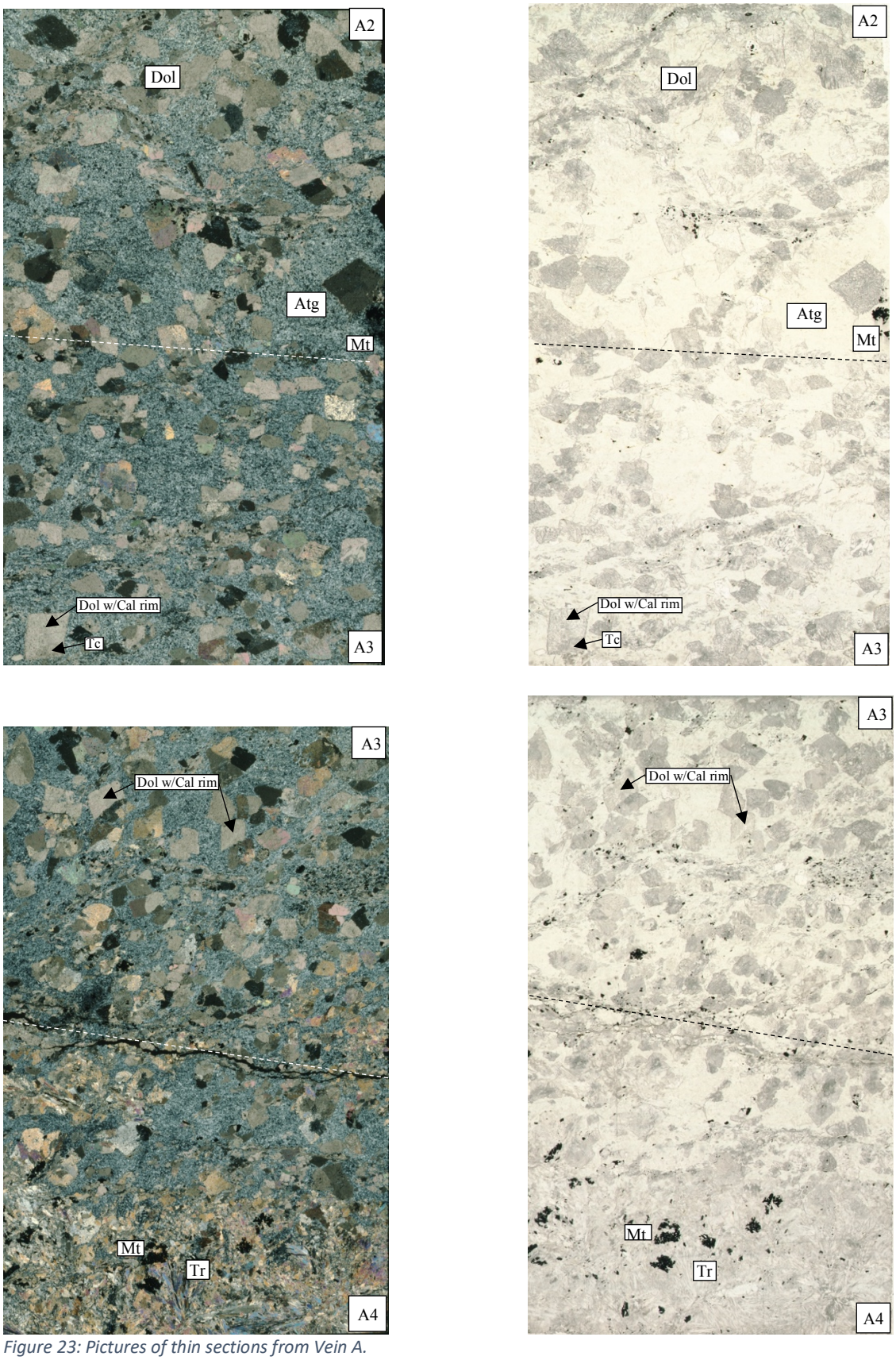

Figure 23: Pictures of thin sections from Vein A.

5.2.2 B-type vein

5.2.2.1 B-Host

This sample (Figure 24) consist of a fine-grained antigorite matrix with olivine veins, magnetite, and accessory dolomite. The olivine veins show two different orientations; the larger ol-veins (20-30 μm(?)) are crosscut by smaller ol-veins (Figure X). The Ol-grains in the large veins are large, euhedral and cracked, whereas the Ol-grains in the smaller veins are more anhedral and "fragmented". The Atg-grains bordering to the ol-veins are sometimes elongated and oriented parallel to the veins. The magnetite grains are often concentrated in the veins or nearby. In other part of the zone one can observe concentrated areas with "dissolved"/small grains of olivine. Patches of fine-grained serpentine (new generation of serp?) "overlap" olivine in some places.

Larger grains of olivine are deformed. Oxides grains are included in the olivine grains. Elongates serpentine grains are inside and between the olivine grains. Dolomite is exhibiting the shape of relict olivine grains and form veins. Dolomites show lamellae.

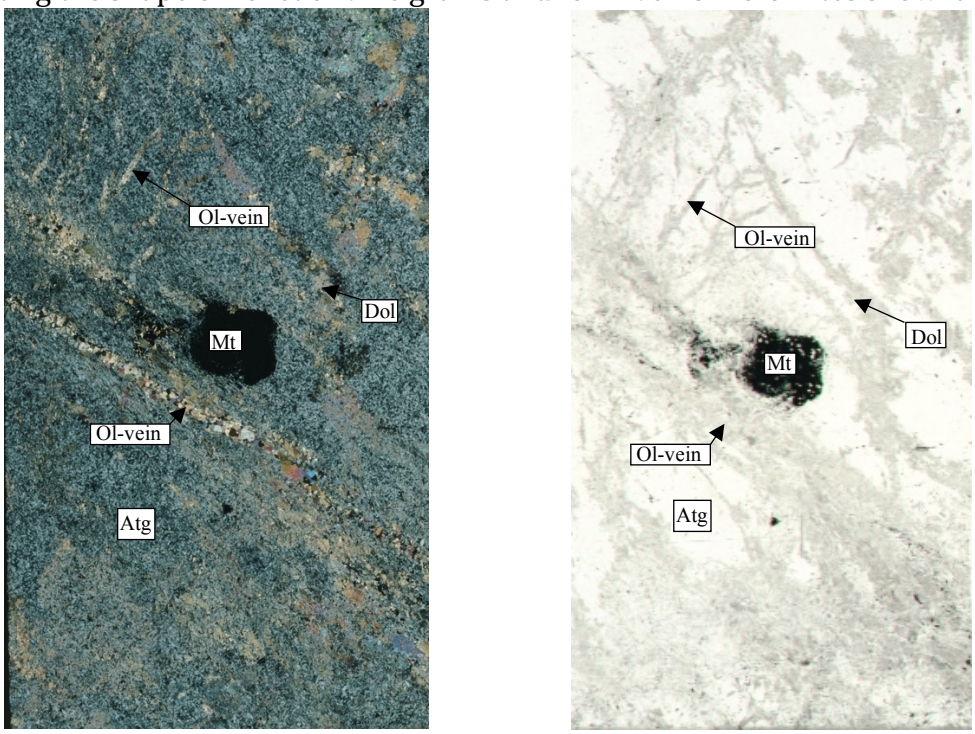

Figure 24: Thin section from Host-B (02-ZS-17)

5.2.2.2 Zone B1

The matrix in zone B1 (Figure 25) consists of interpenetrative antigorite with dolomite grains. The dolomites form slightly elongated aggregates. The dolomite grains are classified as poikiloblastic as they have inclusions of serpentine and oxides. In some places the serpentine and/or chlorite grains are oriented in the same direction.

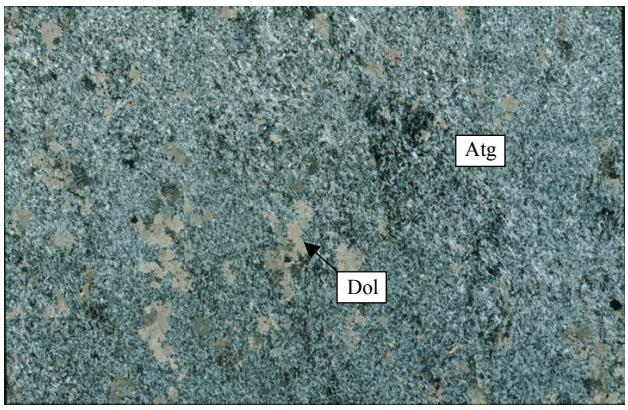

Figure 25: Thin section from zone B1 (06-ZS-17).

5.2.2.3 Zone B2

The transition from zone B1 to B2 is sharp, as the dolomite content decrease quite suddenly in this zone. The matrix in zone B2 (Figure 26) consists of interpenetrative serpentine grains. Carbonate content decrease quite suddenly in this zone. The remaining carbonates are small grained and often surrounded by fine grained serpentine and or chlorite. Large magnetite are, elongated, and lens shape. Larger serpentine grains are often associated with areas with higher concentrations of magnetite.


Figure 26: Thin section from zone B2 (09-ZS-17).

5.2.2.4 Zone B3

The matrix in zone B3 (Figure 27) consist of interpenetrative serpentine grains. The amount of dolomite increase to 30% in this zone. The shape of the dolomite grains is subhedral, and they form aggregates. Elongated serpentine grain inclusions seem to grow along the cleavage planes of the dolomite grains.

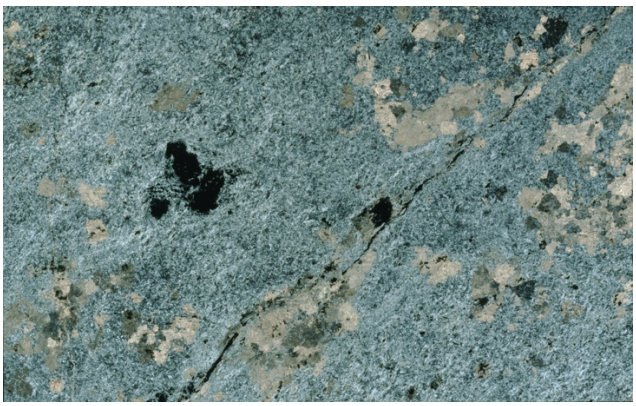

Figure 27: Thin section from zone B3 (10-ZS-17).

5.2.2.5 Transition B3-B4

From zone B3 to B4, there is a gradual transition, by which the dolomite content increase significantly (Figure 28). The matrix still consist of antigorite, but chlorite is also present. In this transition, small veinlets of calcite were identified with the electron microanalyser (EMPA) (Figure 29). The magnetite grains are large, brittle and have a lenticular shape. Even the magnetite has a poikiloblastic texture with serpentine inclusions. Clinopyroxene is also present (Diopside?).

Figure 28: Thin section from the transition between zone B3 (left)and B4 (right)(11-ZS-17).

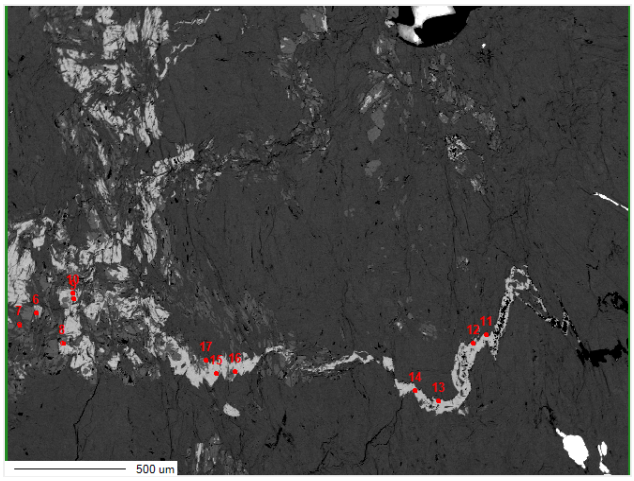

Figure 29: Calcite veinlet in the transition between zone B3 and B4.

5.2.2.6 Zone B4

The matrix consist of interpenetrative serpentine grains. The dolomite content is estimated to approximately 70% (Figure 30). The dolomite grains (Figure 31) exhibit a subhedral grain shape, and form aggregates. Elongated serpentine grains grow along the cleavage planes of the dolomite. The serpentine inclusions in carbonates in the poikiloblastic grains is fully pervasive. The matrix consist of both antigorite and chlorite.

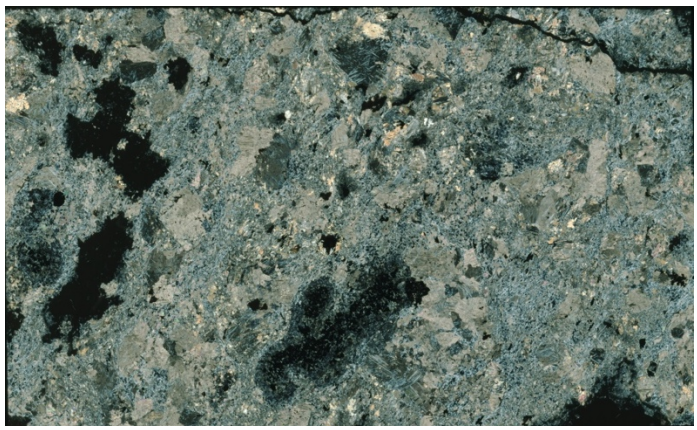

Figure 30: Thin section from zone B4 (13-ZS-17).

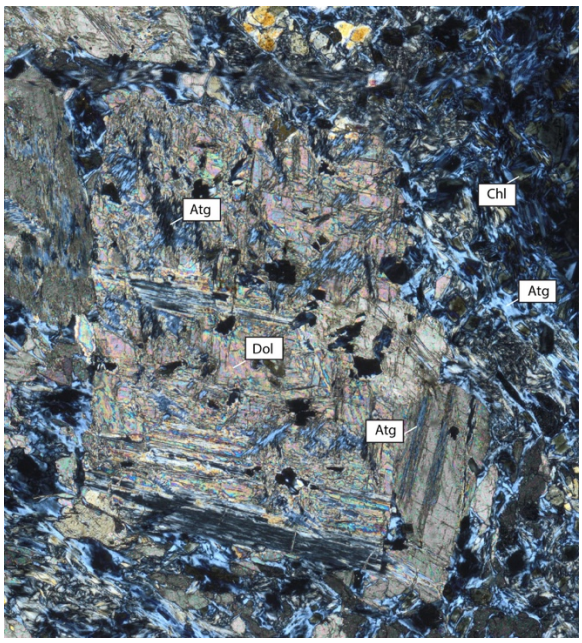

Figure 31: Picture of a typical dolomite grain in zone B4.

5.2.2.7 Zone B5 and B6

Zone B5 (left, Figure 32) consists of fibrous tremolite with chlorite inclusions and some magnetite. The tremolite grains are long, fibrous and oriented paralell. Small magnetite grains are situated in the center of chlorite aggregates, which indicates chloritization of magnetite. The chlorite aggregates exhibit the shape of relict, elongated magnetite grains. Zone B6 (right, Figure 32)consists of tremolite, diopside, and magnetite. The tremolite grains have no preferred orientation and vary in size (Filiform grainshape?). The magnetite grains are idioblastic.

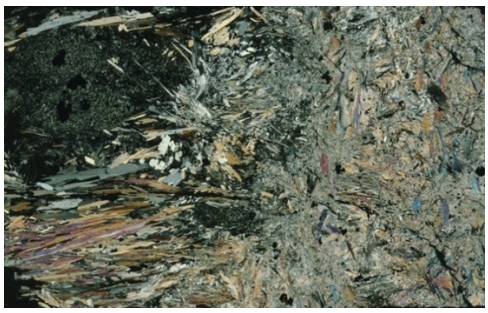

Figure 32: Zone B5(left) and B6 (right).

5.2.3 C-type Vein

5.2.3.1 C-Host and C1

This zone consists of fine-grained, interlocking antigorite grains with a couple of magnesite grains in it close vicinity of the vein-border and some magnetite. Lepidoblastic Atg.

The transition from host rock to vein is sharp (Figure 33a). The Atg was replaced by magnesite, talc and some magnetite. There is almost no Atg inside the vein, except for a few grains inside the magnesite grains and cause a poikiloblastic texture. The magnesite grains are densely packed at the border. Some of the magnesite grains show lamellae. The talc appears as fine-grained matrix, but also as larger blades.

Further inside the vein (Figure 33b), the talc content increase and form a matrix in which the magnesite grains are more widely dispersed. The magnesite varies between aggregates and single grains, and exhibit a framboidal to idioblastic shape. The magnesite grains still have a poikiloblastic texture with mostly talc and some serpentine inside. The talc in the matrix shows two different textures, one fine- and one coarse-grained. The overall talc-matrix is fine-grained with no specific growth orientation, whereas the coarser type has a preferred orientation and grows perpendicular to the vein.

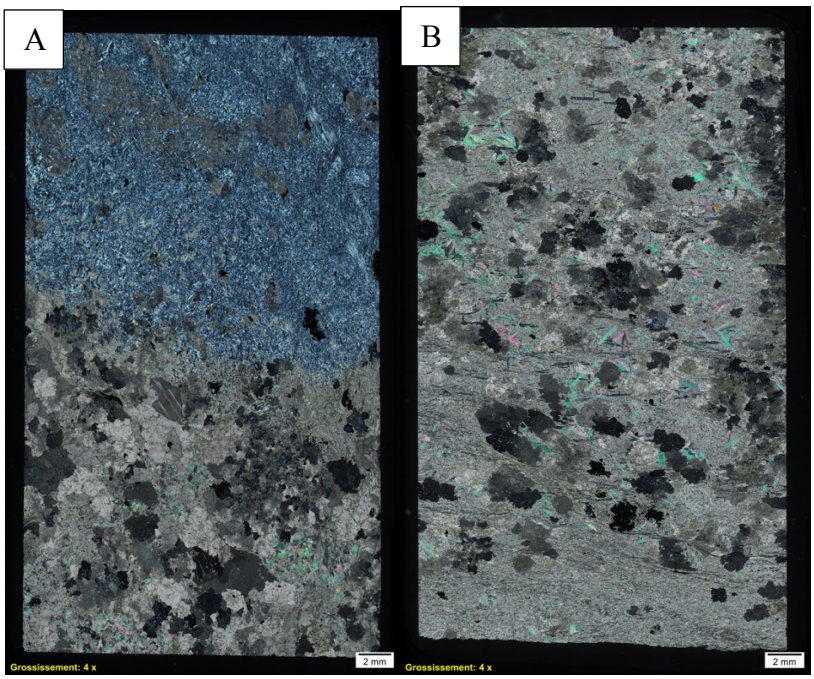

Figure 33: Host rock-vein transition(a); talc matrix with magnesite grains(b).

Within the Talc matrix there are Magnesite aggregates. The grains in the aggregate have Iron-poor rims and cores (Figure 34). The texture of the magnesite is poikiloblastic with Tc and Atg inclusions. High concentration of Atg in the center.

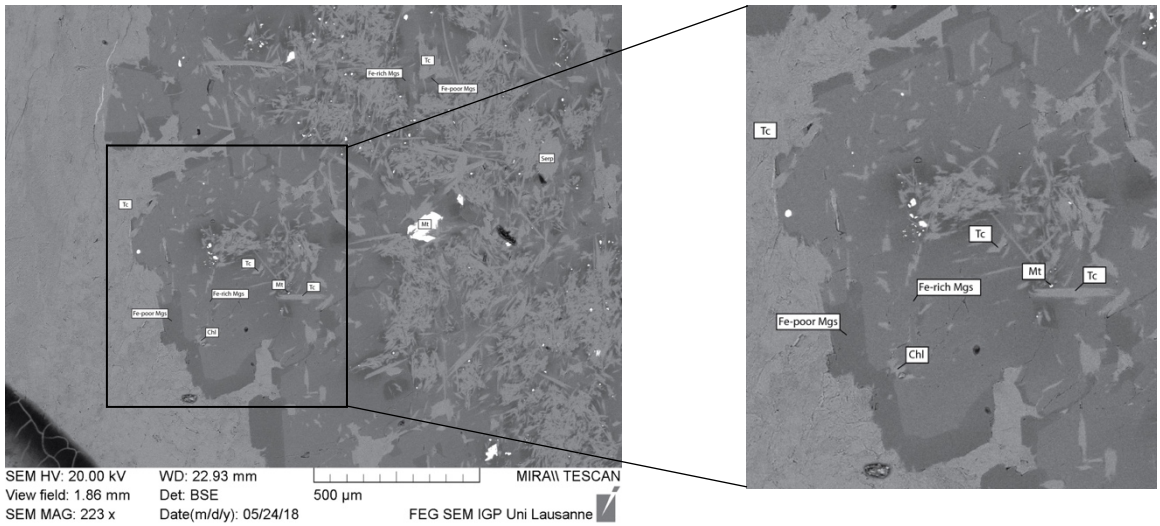

Figure 34: BSE image of magnesite aggregate in talc matrix.

Sample site E

At sample site E, a couple of host rock samples were taken in order to investigate whether carbonates are present in the host rock as well as the vein.

The matrix consist of interpenetrative coarse-grained antigorite. The texture of the Atg is variable as it appears to have undergone some deformation. Shear zones can be recognized by elongated Atg grains oriented in the same direction. In some places, the antigorite form patches with a more fine-grained texture, which seem to resemble the shape of relict olivine and/or carbonates (and cpx?). In some cases, these fine grained patches form aggregates with different extinction angles. The different texture in serpentine may indicate two different generations of antigorite.

Aggregates of carbonates (different extinctions) are widely dispersed. The dolomite contain intragranular serpentine. In sample 28-ZS-17 (Figure 35), the dol aggregates are elongated. The center of the aggregate has a different extinction angle than the outer part. Magnetite grains are present both in the carbonates and in the serpentine, but there's a higher concentration in the carbonates.

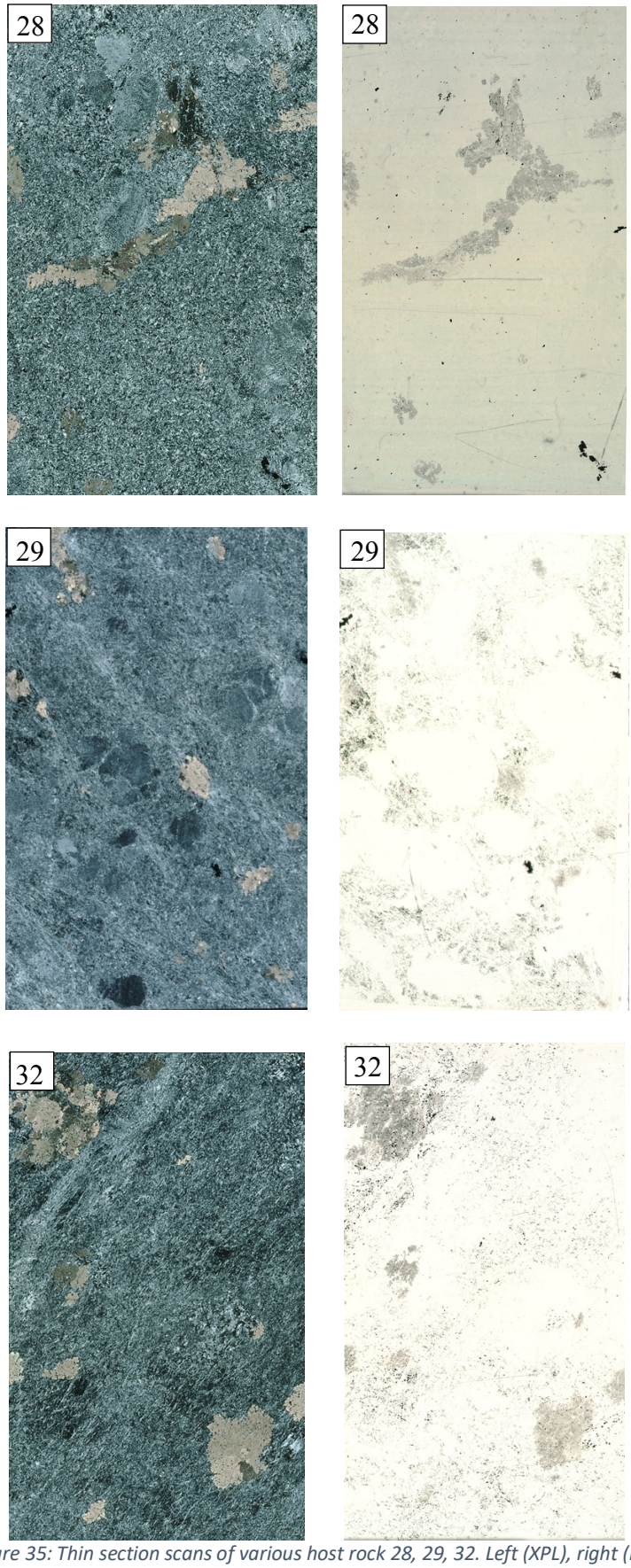

Figure 35: Thin section scans of various host rock 28, 29, 32. Left (XPL), right (PPL)

6. Bulk Rock

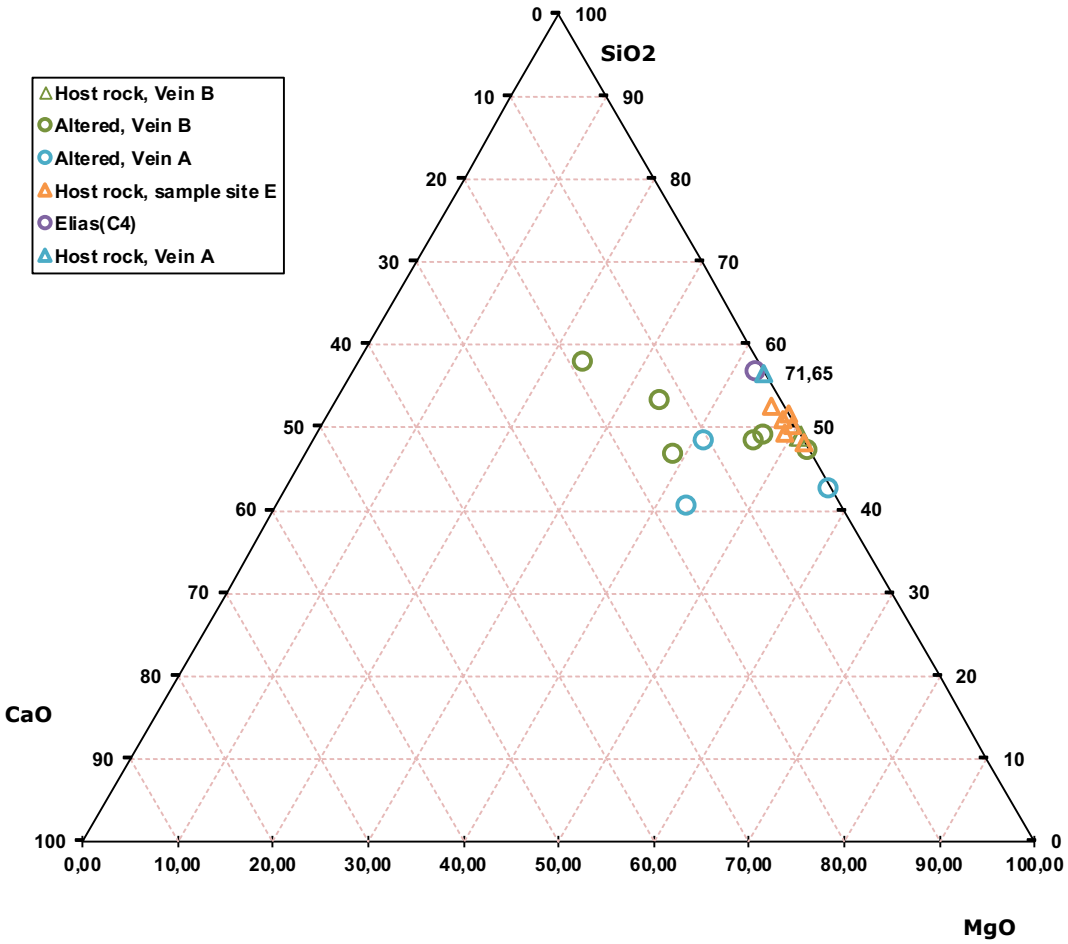

Bulk rock analysis were done for the veins A and B, as well as the neighboring host rocks. The results are shown in the CaO-MgO-SiO2 diagram (Figure X), and supplemented with Kempf (2014) bulk rock analysis for the Tc-Mgs vein from sample site C.

The host rocks (triangles) are especially high in Mg and Si, but almost Ca-free (<1,5%). Within the veins (circles), the Ca-content increase, while the Mg-content decrease. There is also a slight variation in Si-content within the veins.

The most Ca-rich samples (50%) was extracted from zone B6, which consist of tremolite, diopside and magnetite. Tremolite and diopside contain CaO. This is fracture fill, and hence the fluids precipitated this. Since MgO and SiO2 could be extracted from the host rock, the fluids need to be quite CaO rich.

Moving from the rim towards the core, the Fe^{2+}-content increase relative to the Fe^{3+}-content. It is not a very large increase, but there is no overlap between the error bars in Host-B versus B4, which indicates that it is a true change. The host rock contain antigorite, olivine and magnetite. Amongst these minerals, magnetite is the mineral that contains Fe3+ in its structural formula. The magnetite content decrease from rim to core of Vein B.

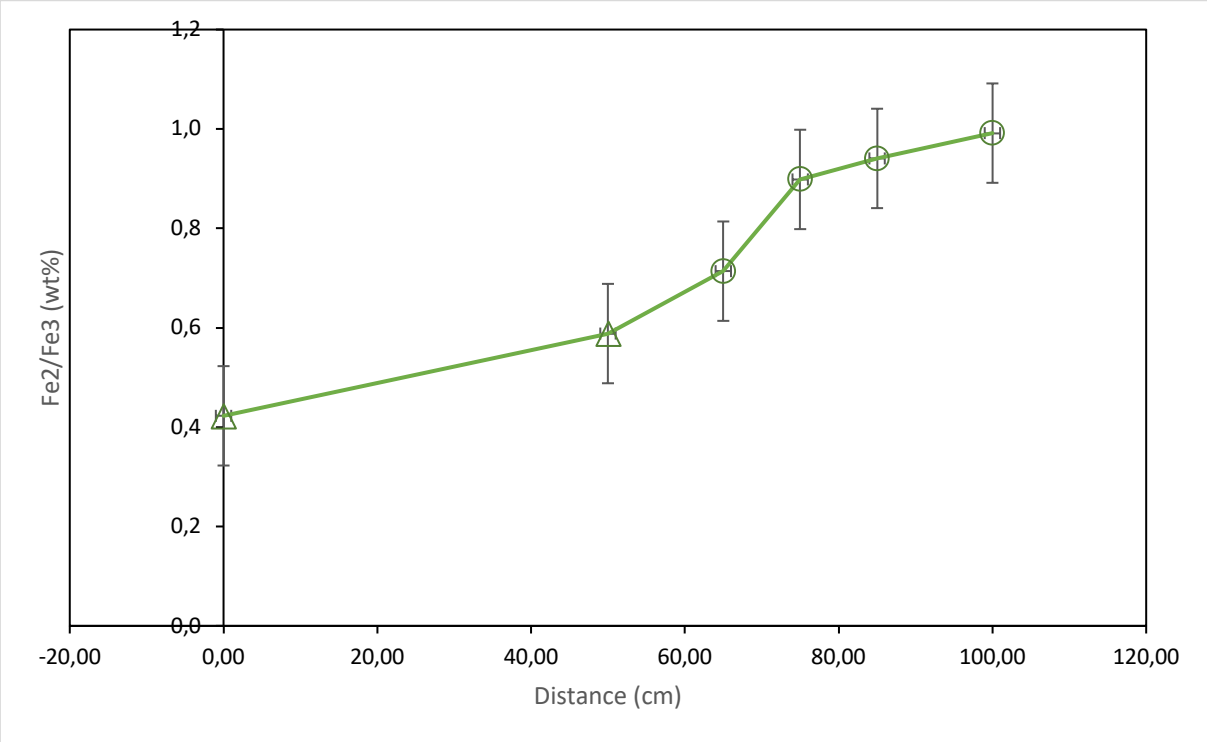

6.1 Element Transport in the veins

In this part the goal is to get a more detailed understanding of the element transport and to assess if the veins form at constant volume or not.

The slope of the ISOCON determines whether mass was lost or gained during the metasomatic alteration. If the slope has a value greater than one (>1) it indicates a mass decrease, whereas a value less than one (<1) indicates mass increase (Grant, 1986). Where the elements plot relative to the line, indicates whether there has been an enrichment or depletion in concentration. If the elements plot above, they are enriched.

The diagrams below(FigureX and Figure X) illustrate the element transport for each of the vein zones in Vein A and Vein B (ref. to the veins described in Petrography). To see the evolution of alteration from zone to zone, one diagram for each vein zone is constructed separately. Note that the center of the vein representing a vein fill is not plotted (tremolite and diopside zone). The zones are plotted as "altered rock" on the y-axis, and "unaltered rock" on the x-axis. Each of the zones are plotted against the average composition of the surrounding host rock.

The average composition of the unaltered rock for Vein B was calculated based on two samples (02-ZS17(T) and 04-ZS-17, see Table X). Sample 02-ZS-17(B) was not included in the calculation because it contained too much Ca to be considered a "true" unaltered rock. The variability/standard deviation (σ) was also calculated based on these two samples (TS2T and TS4). For Vein A, only one sample (Host-A, (19-ZS-17(T)) was done for the unaltered, and therefore the standard deviation of Vein B was applied for ISOCON calculations for Vein A as well.

For the altered zones, only one sample from each zone was available, and one cannot calculate the variability based on only one sample. Therefore, the variability for unaltered rock was also applied for all the zones assuming that the altered rock inherited the variability of the unaltered rock. The data has been corrected for LOI by re-normalization.

Ideally, more samples should have been obtained to calculate a more accurate average composition and variability, as it is not statistically significant to calculate standard deviation based on only two samples. Especially since the rocks are very heterogeneous. However, this was not possible due to lack of sample material and time. Due to these limitations it is likely that some features are missed. Nevertheless, a first evaluation of mass transport is possible.

		Host-B (1)		Host-B (2)	Unaltered Avg. Host-B	Variability	Altered B1	Altered B2	Altered B3	Altered B4	B5	B6
Major Elements		Serpentinite 02-ZS-17(T)	Serpentinite 02-ZS-17(B)	Serpentinite 04-ZS-17	(02-ZS-17+ 04-ZS-17)/2	σ	Serp+Dol 06-ZS-17	Serp+Dol 09-ZS-17	Serp+Dol 18-ZS-17	Dol+Serp 13-ZS-17	Trem 15-ZS-17	Trem+Diop 16-ZS-17
Si	wt%	37.74	36.22	35.48	36.61	1.60	37.08	36.17	35.98	34.46	45.47	47.19
Ti	wt%	0.02	0.03	0.02	0.02	0.00	0.02	0.03	0.02	0.02	0.04	0.03
Al	wt%	1.12	5.35	0.63	0.87	0.34	0.59	0.66	1.30	2.03	4.01	0.55
Fe3+	wt%	7.39	4.84	9.03	8.21	1.16	6.15	6.95	6.03	4.28	2.88	2.69

Fe2+	wt%	3.12	3.98	5.31	4.22	1.55	4.39	6.24	5.67	4.24	3.88	3.12
Mg	wt%	5.60	33.40	49.24	49.92	0.97	51.49	45.58	44.88	37.87	29.46	23.79
Ca	wt%	0.00	15.61	0.27	0.14	0.19	0.26	4.36	6.11	16.90	13.02	21.71
Na	wt%	0.00	0.49	0.00	0.00	0.00	0.00	0.00	0.00	0.16	1.12	0.82
K	wt%	0.00	0.07	0.00	0.00	0.00	0.00	0.00	0.00	0.03	0.12	0.09
P	wt%	0.01	0.01	0.01	0.01	0.00	0.01	0.01	0.01	0.01	0.01	0.01
Trace Elements												
Sc	ppm	4.30	3.40	4.40	4.35	0.07	4.00	5.00	4.10	6.10	7.00	10.40
V	ppm	23.60	25.50	26.80	25.20	2.26	16.90	21.00	22.10	17.80	40.70	26.40
Cr	ppm	2268.00	2045.60	2898.10	2583.05	445.55	1453.20	2013.40	2044.40	1792.50	1081.10	526.60
Mn	ppm	663.20	726.70	883.00	773.10	155.42	700.50	725.60	786.90	868.50	558.60	605.70
Co	ppm	114.10	116.00	121.40	117.75	5.16	104.60	92.00	99.70	92.60	66.60	66.00
Ni	ppm	2068.40	2040.70	2176.60	2122.50	76.51	1884.10	1572.20	1753.90	1530.10	1138.40	724.10
Cu	ppm	11.20	10.30	11.80	11.50	0.42	8.00	8.50	15.80	13.50	4.90	5.00
Zn	ppm	31.60	28.40	43.70	37.65	8.56	24.50	38.00	39.50	26.70	30.10	22.10
Ga	ppm	1.20	1.50	1.00	1.10	0.14	0.00	1.00	1.50	1.90	3.00	0.00
Ge	ppm	0.00	0.00	0.00	0.00	0.00	0.00	0.00	0.00	0.00	1.40	1.30
As	ppm	20.30	16.40	16.00	18.15	3.04	15.80	8.00	6.10	0.00	0.00	0.00
Rb	ppm	0.00	0.00	0.00	0.00	0.00	0.00	0.00	0.00	1.30	0.00	0.00
Sr	ppm	0.00	0.00	1.40	0.70	0.99	1.30	86.60	140.10	259.00	21.10	50.50
Y	ppm	0.00	0.00	0.00	0.00	0.00	0.00	0.00	0.00	0.00	0.00	1.50
Zr	ppm	0.00	0.00	0.00	0.00	0.00	0.00	0.00	0.00	0.00	0.00	1.10
Cs	ppm	2.40	0.00	0.00	1.20	1.70	0.00	0.00	0.00	2.30	0.00	3.00
Hf	ppm	0.00	0.00	0.00	0.00	0.00	0.00	0.00	4.00	0.00	3.00	0.00
W	ppm	105.50	111.30	130.00	117.75	17.32	63.30	59.50	59.90	55.00	87.30	105.10
Th	ppm	0.00	0.00	0.00	0.00	0.00	0.00	0.00	0.00	1.10	0.00	0.00

		Host-A	Variability	A1	A2	A3
Major Elements		19-ZS-17(T)	σ (veinB)	19-ZS-17(M)	19-ZS-17(B)	20-ZS-17
Si	wt%	39.99	1.60	30.23	27.35	36.58
Ti	wt%	0.02	0.00	0.03	0.03	0.02
Al	wt%	1.60	0.34	1.95	2.51	1.14
Fe3+	wt%	5.42	1.16	7.13	4.61	7.93
Fe2+	wt%	5.43	1.55	5.99	6.06	4.43
Mg	wt%	47.37	0.97	41.91	41.21	49.78
Ca	wt%	0.16	0.19	12.76	18.21	0.12
Na	wt%	0.00	0.00	0.00	0.00	0.00
K	wt%	0.00	0.00	0.00	0.00	0.00
P	wt%	0.01	0.00	0.01	0.01	0.01
Trace Elements						
Sc	ppm	2.50	0.07	6.00	8.00	11.60
V	ppm	26.90	2.26	30.40	28.10	33.60
Cr	ppm	1991.40	445.55	1992.50	1941.50	1529.50
Mn	ppm	627.70	155.42	995.10	1028.20	783.40
Co	ppm	93.80	5.16	95.90	100.20	70.50
Ni	ppm	1697.40	76.51	1756.40	1738.60	1295.70
Cu	ppm	16.40	0.42	21.50	19.20	9.70
Zn	ppm	44.60	8.56	34.70	28.70	27.60
Ga	ppm	1.70	0.14	1.50	2.00	3.00
Ge	ppm	0.00	0.00	0.00	0.00	0.00
As	ppm	3.30	3.04	5.20	4.70	0.00
Rb	ppm	0.00	0.00	0.00	1.60	0.00
Sr	ppm	2.30	0.99	272.10	300.40	131.10
Y	ppm	0.00	0.00	0.00	1.00	0.00
Zr	ppm	0.00	0.00	0.00	0.00	0.00
Cs	ppm	0.00	1.70	3.40	2.40	2.80
Hf	ppm	0.00	0.00	0.00	0.00	0.00
W	ppm	61.20	17.32	62.50	60.80	59.10
Th	ppm	0.00	0.00	0.00	1.50	0.00

Vein A

The host rock (Host-A (19-ZS-17(T)))as described in the Petrography chapter, is comprised of atg, mag, and a few dolomite grains. Relative to the host rock, Si and Mg is depleted in the most distal zone (A1) and in A2, whereas Ca is being enriched at approximately the same rate. Si is depleted in bot A1 and A2. Fe^{2+} and $Fe^{3+}$are immobile in A1. Fe^{2+} remains immobile, while Fe^{3+} is depleted in A2. Aluminum plots on the ISOCON line and is immobile in all zones. Cr and Ni are immobile in A1 but undergo depletion in A2. Mn is depleted in A1 and A2. Sr is enriched in both zone A1 and A2.

The gradual enrichment of Ca correlates well with a significant increase in dolomite in the vein zones. Like mentioned above (Figure X), the CaO is added to the system by the infiltrating fluid. The gradual depletion of Si and Mg is interpreted to be linked to the decrease in antigorite, which is a Mg-and Si-bearing mineral. Apparently the fluids were Mg- and Si-undersaturated but Ca oversaturated. The depletion in Fe3+ is seen in correlation with a decrease of magnetite as the zones become more carbonated. Al is immobile in all zones. Aluminum has a quite low solubility, due to its high charge and small ionic radius (Eugster and Baumgartner, 1987) it is not so easily transported by the fluids. Elements that plot on the line are based on the model – immobile. In reality they are "much less mobile". Al is present in the form of spinel, chlorite, and serpentine in the serpentine protolith. Two Al ions substitutes for MgSi in the mineral structure of antigorite. Clinochlore contains Al and is also found inside the vein. The decrease in Ni is interpreted to be linked to olivine freaction to form serpentine.

The ISOCON line for Zone A1, A2 and A3 does not yield a 1:1 line, and according to this model, the metasomatic reaction is therefore not isovolumetric. The slope for A1 is 1.05, which indicates a mass decrease of 5%. For zone A2, the slope is 1.23, which indicates an even higher mass decrease (23%). However, zone A3 has a slope of 1, which indicates isovolumetric conditions. One should nevertheless not forget that this apparent mass decrease is partially compensated by the gain of volatile elements.

Zone	Mg	Si	Fe3	Fe2	Al	Cr	Ni	Ca	Mn	Sr
A1	<	<	-	-	-	-	-	>	<	>
A2	<	<	<	-	-	<	<	>	<	>

Vein B

The host rock (Host-B, (02+04)-ZS-17) as described in the Petrography chapter, is comprised of atg, ol, mag and a few dolomite grains. In zone B1, Mg, Si, Fe 2+, Al, Ca, Mn and Sr are immobile. The only elements that change are Cr, Ni and Fe3+ which are being depleted. In zone B2, Mg is depleted, whereas Ca is being enriched at approximately the same rate. Fe^{2+} is immobile in all zones, while Fe^{3+} is depleted in almost all zones. In zone B3 and B4, the same enrichment/depletion pattern is seen, but with enrichment of Sr.

Interpretation:

The fact that almost no elements were enriched/depleted in zone B1, indicate a small change in mass transport from from Host-B to B1. The depletion in Ni is seen in correlation with olivine being removed in B1. Depletion of Cr might be due to reduced chromium content. However, there is a significant change in mineralogy based on Petrographic observations. From Host-B to B1 olivine disappears and there is a significant increase in dolomite content. It is therefore strange that Ca is not enriched in B1.

In zone B2, gradual enrichment of Ca and Sr is seen in correlation with a zone of atg with a significant decrease in dolomite -which is strange as one would assume an decrease in Ca and Sr.

In zone B3 and B4, the Mg continues to decrease while Ca and Sr increase, which correlates nicely to a decrease in antigorite and increase in dolomite. The gradual depletion of Mg is interpreted to be linked to the decrease in antigorite and olivine which both are Mg-bearing minerals. The depletion in Fe3+ is seen in correlation with a decrease in magnetite as the zones become more carbonated. The decrease in Ni is interpreted to be linked to "removal" of the olivine (in Host-B) from the system.

The ISOCON lines for all zones in Vein B are approximately 1:1. The slopes variates between 0.98-1.01, which only gives an insignificant volume change of 1-2%. The vein is considered to be isovolumetric.

Zone	Mg	Si	Fe3	Fe2	Al	Cr	Ni	Ca	Mn	Sr
B1	-	-	<	-	-	<	<	-	-	-
B2	<	-	-	-	-	<	<	>	-	-
B3	<	-	<	-	-	<	<	>	-	>
B4	<	-	<	-	>	<	<	>	-	>

Elements > 0.3 wt%

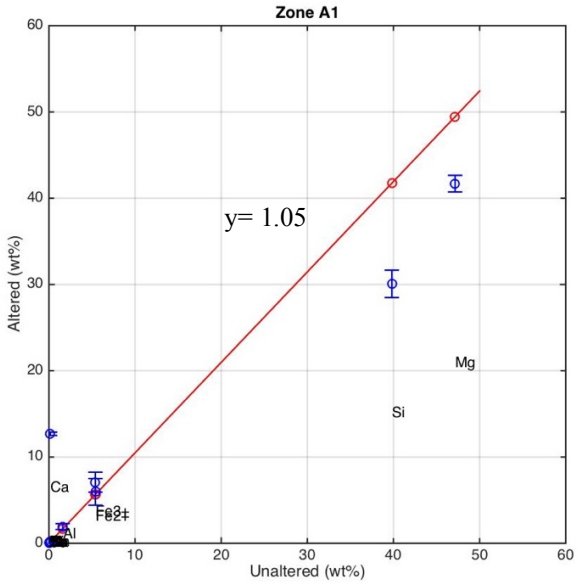

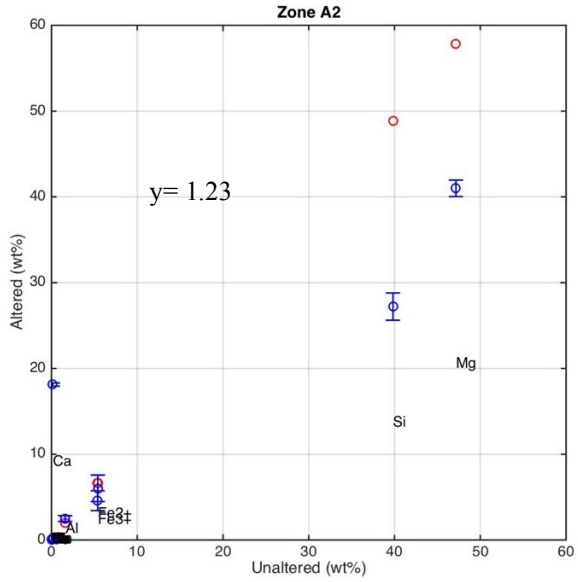

Elements < 0.3 wt%

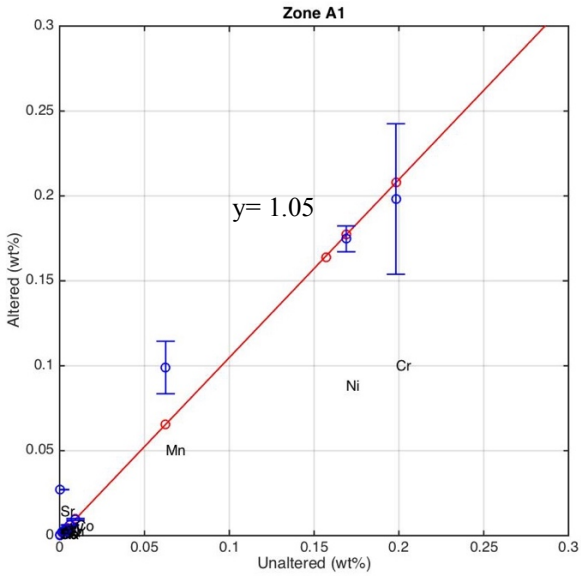

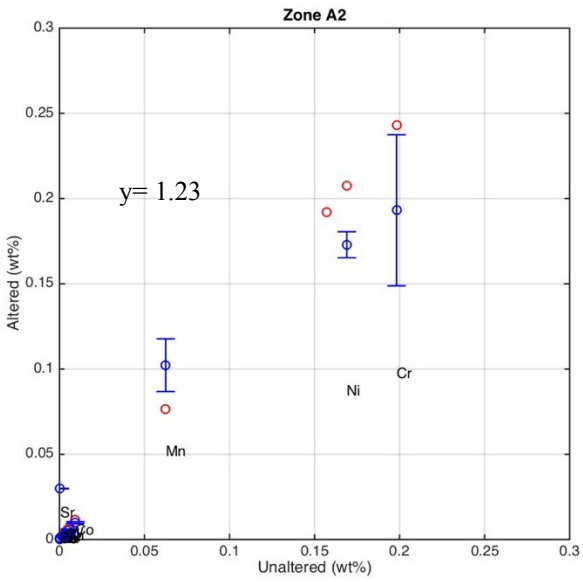

Elements > 0.3 wt%

Elements < 0.3 wt%

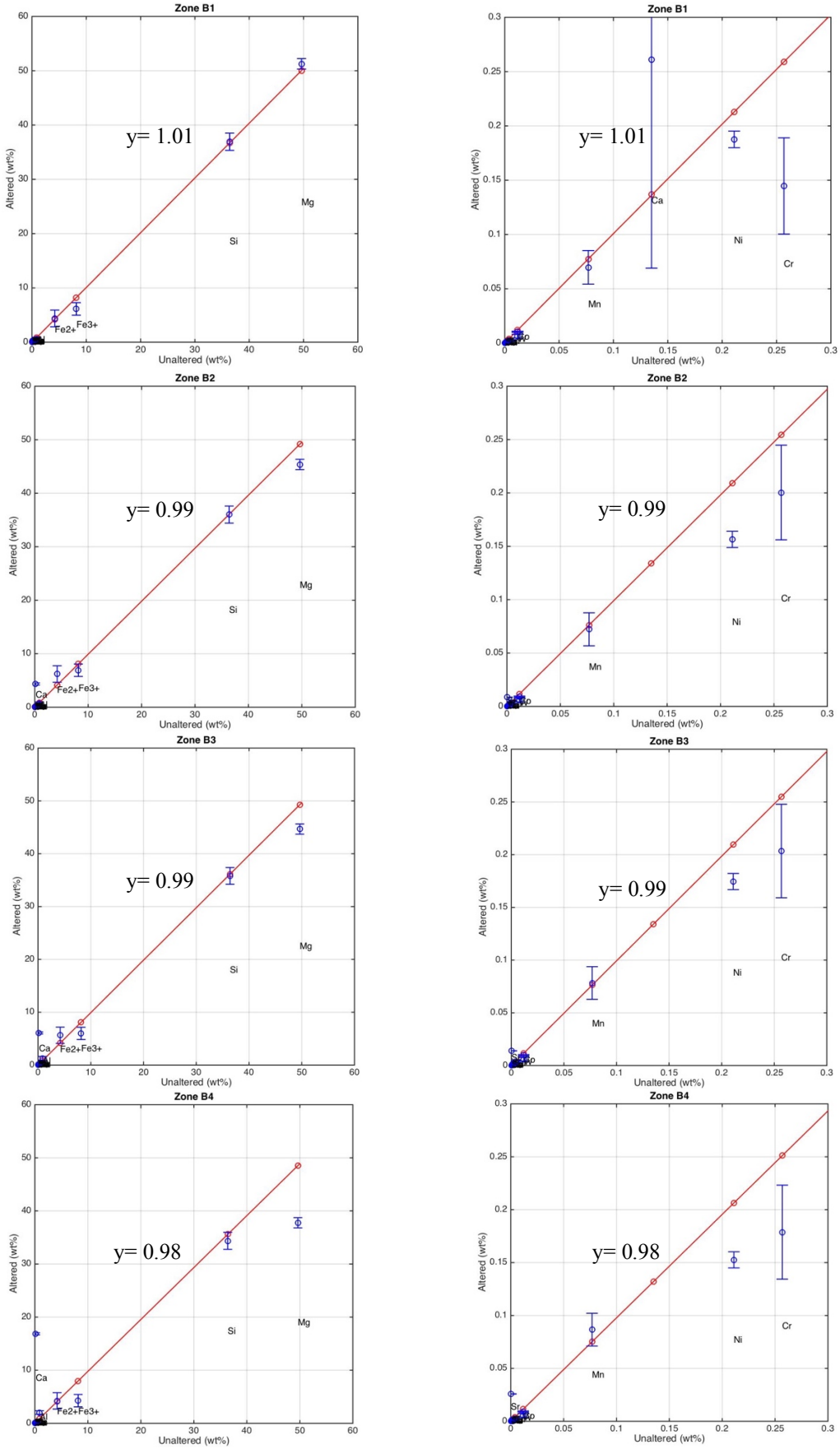

Figure 36: The graphs above illustrate element transport for each zone in Vein A.

7. Stable Isotopes

7.1 Oxygen Isotope Thermometry

In an attempt to determinine the temperature at which the Atg-Dol veins formed, the center (zone B6, sample 16-ZS-17) from Vein B was chosen for oxygen isotope thermometry (Figure X). The reason for selecting B6 for this purpose is that it is considered to be "crack-infill", hence it contains only precipitated minerals from the fluid phase, and it contains minerals like tremolite, diopside and magnetite, which can be used for O-isotope thermometry. Co-precipitation of the phases should result in an equilibration of the phases, and no inherited magnetite or silicate minerals should be present. Tremolite and diopside were easy to separate, while the magnetite was more challenging. The magnetite grains variated in texture -some were idioblastic, massive and clean, while others were more "fuzzy" with small amounts of attached Tr and/or Di on the surface. The diopside and tremolite residue was removed as good as possible.

The three minerals ca be combined to 3 isotope thermometers: Mag-Tr, Mag-Di, and Di-Tr. The last combination, Di-Tr has a relatively small temperature dependence, and hence resulting uncertainties would be large due to analytical, uncertainties. Hence only the combinations with Mag were used. The two mineral combinations were used to make δ–δ plots for all measured mineral pairs. If the minerals are in equilibrium they should plot within the same temperature range. The isotope fractionation factors (1000 ln α) utilized in these thermometry calculations were derived by Zheng (1993) for tremolite and diopside, and Simon and Zheng (1991) for magnetite.

In Figure X, δ18O Magnetite is plotted against δ18O Tremolite. Two of the measurements plot within the temperature range of 350-400°C, whereas the third one plots within the range of 500-600°C. In the case where δ18O Magnetite is plotted against δ18O Diopside (Figure X) two of the measurements plot within the temperature range of 350-450°C. Again, the third measurement plots at significantly higher temperatures; 600°C.

Stable Isotope values for minerals in Zone B6		
Sample name	δ18O, VSMOW (‰)	Mineral
16_M_B	7.05	Diopside
16_M_T	7.06	Diopside
16_L_M	6.99	Diopside
16_M_B	7.76	Tremolite
16_M_T	7.73	Tremolite
16_L_M	7.82	Tremolite
16_M_B	0.90	Magnetite
16_M_T	0.60	Magnetite
16_L_M	2.72	Magnetite

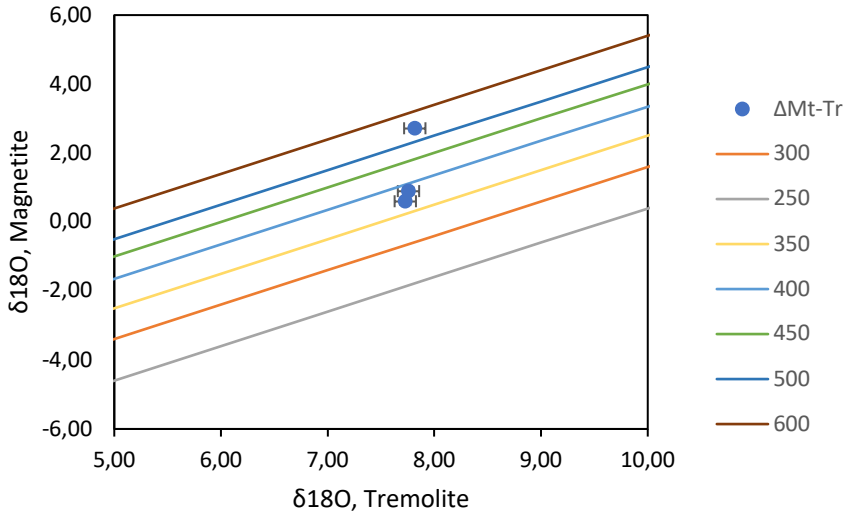
6,00
4,00
2,00
0,00
-2,00
-4,00
-6,00
5,00
6,00
7,00
8,00
9,00
10,00
δ18O, Magnetite
δ18O, Tremolite
ΔMt-Tr
300
250
350
400
450
500
600

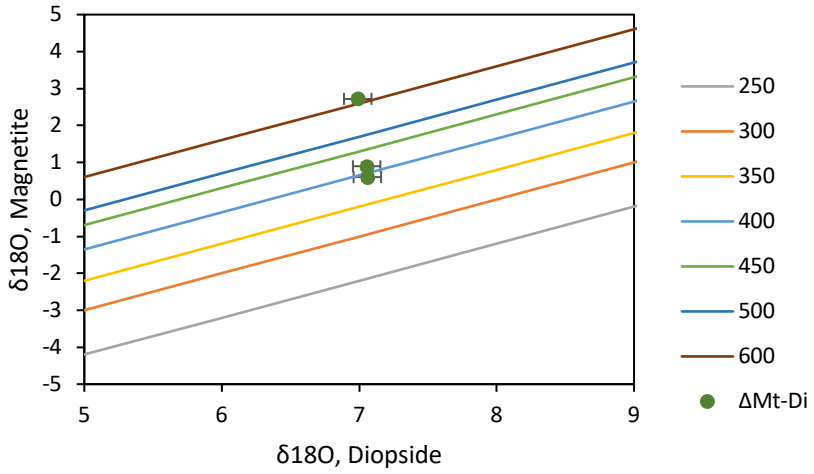
5
4
3
2
1
0
-1
-2
-3
-4
-5
5
6
7
8
9
δ18O, Magnetite
δ18O, Diopside
250
300
350
400
450
500
600
ΔMt-Di

7.2 Bulk Rock Isotope Analysis

To observe if there is any isotopic compositional gradient in Vein A and B, $\delta^{13}C$ and $\delta^{18}O$ were measured for the bulk rock carbonates, and $\delta^{18}O$ for bulk rock silicates.

7.2.1 Sample site A

The results are listed in Table X and X. Zone A2 had too low CO_2 amounts to be measured accurately (peak hight <300 during the isotope analysis) and was therefore excluded from the results. In Figure X the results are plotted as a function of position in the vein.

Stable Isotope values for carbon (Bulk-rock) in Vein A		
Sample	δ13C, VPDB	δ18O, VSMOW
19-ZS-17(Host-A)	-1.06	10.13
19ZS17(A1)	-0.87	10.49
20ZS17(A4)	-1.21	11.35

Stable Isotope values for silicates (bulk rock) in Vein A	
Sample	δ18O, VSMOW (‰)
19-ZS-17 (Host-A)	6.87
19-ZS-17 (A1)	6.74
19-ZS-17 (A3)	7.24

The carbon (Figure x) from Host-A and A1 measures $\delta^{18}O$-isotopes values between 10.13 and 10.49‰, respectively, with $\delta^{13}C$-isotope values measure at -1.06 and -0.87‰, respectively. For the silicates, the $\delta^{18}O$ measure are 6.87 and 6.74‰. In zone A4, which represents the tremolite-center of the vein, the $\delta^{18}O$ for carbonates is increasing by 0.86‰ and $\delta^{13}C$ decrease by 0.34‰. The $\delta^{18}O$ for the silicates show the inverse trend than that for $\delta^{13}C$ of carbonates.

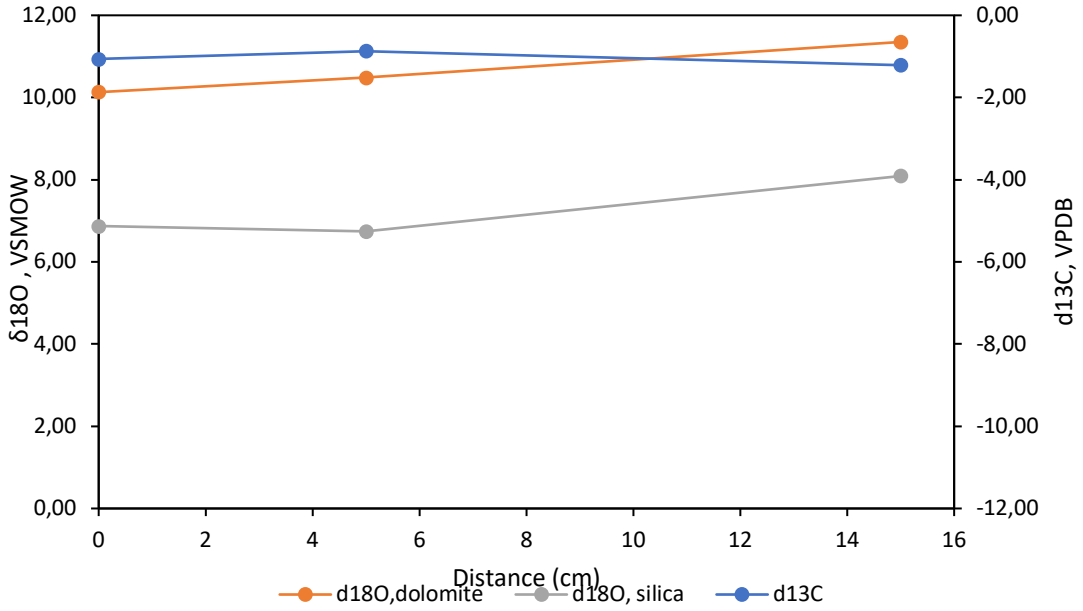

7.2.2 Sample site B

Starting from the host rock (B-Host), going toward the first zone (B1), there is a sharp increase in $\delta^{13}C$ (VPDB) from respectively -7.07‰ to -0.50‰. The smaller compositional change obtained in B-Host (2) indicates, that it is too close to the vein to be considered a "true" host rock. From B-Host (2) (-2.99‰) to zone B1 (-0.50‰), there is an increase of 2.49‰. The values stabilize from B1 to B3 (-0.50 +/- 0.20‰). Approaching B4, which is the zone with the highest carbonate content, the $\delta^{13}C$ value decrease to -1.64‰. In the tremolite zones in the center ("crack-infill") the $\delta^{13}C$ decrease to -3.26‰ in B5, followed by an increase in B6 (-1.82‰). In general, there is a clear increase in $\delta^{13}C$ from B-Host to the vein (-7.07‰) to B4 (-1.64‰).

Bulk rock stable isotope-values for carbon in Vein B			
Sample	δ13C, VPDB (‰)	δ18O, VSMOW (‰)	Zone
02-ZS-17 (T)	-7.07	11.59	B-Host (1)
04-ZS-17	-2.99	11.60	B-Host (2)
06-ZS-17	-0.50	12.60	B1
09-ZS-17	-0.30	12.05	B2
18-ZS-17(10)	-0.69	12.44	B3
13-ZS-17	-1.64	12.19	B4
15-ZS-17	-3.26	12.28	B5
16-ZS-17	-1.82	12.26	B6

Bulk rock stable isotope-values for silicates in Vein B		
Sample	δ18O, VSMOW (‰)	Zone
02-ZS-17 (T)	6.59	Host 1
04-ZS-17	5.99	Host 2
06-ZS-17	7.49	B1
09-ZS-17	7.26	B2
18-ZS-17(10)	7.07	B3
13-ZS-17	7.42	B4
15-ZS-17	8.82	B5
16-ZS-17	7.81	B6

The variations in $\delta^{18}O$ (VSMOW) isotope values in carbonates are smaller. Nevertheless, there are some slight changes. In B-Host (1 and 2) the $\delta^{18}O$ -values seem to be very stable (~11.60‰). In B1, it increases by 1‰ (12.60‰) followed by a small decrease in B2 (12.05‰). Generally, the $\delta^{18}O$ values are fluctuating between 12.0 +/- 0.3‰.

The $\delta^{18}O$ (VSMOW) isotope-values for silica, show a clear increase from Host-B to the center of the vein (B6). The most distal host rock (Host-B(1)) measure 6.59‰, whereas the closest host (Host-B (2)) 5.99‰. Within the first zone (B1), there is an increase of 1.5‰, but from zone B1 to B3 the isotope values remains stable (the error

bars overlap) at approximately 7‰ +/- 0.20‰. In zone B4, the value increase to 7.42‰. The $\delta^{18}O$ reach the peak in the tremolite zone(B5) at 8.82‰. In the center (B6), the value decrease by 1‰ (7.81‰).

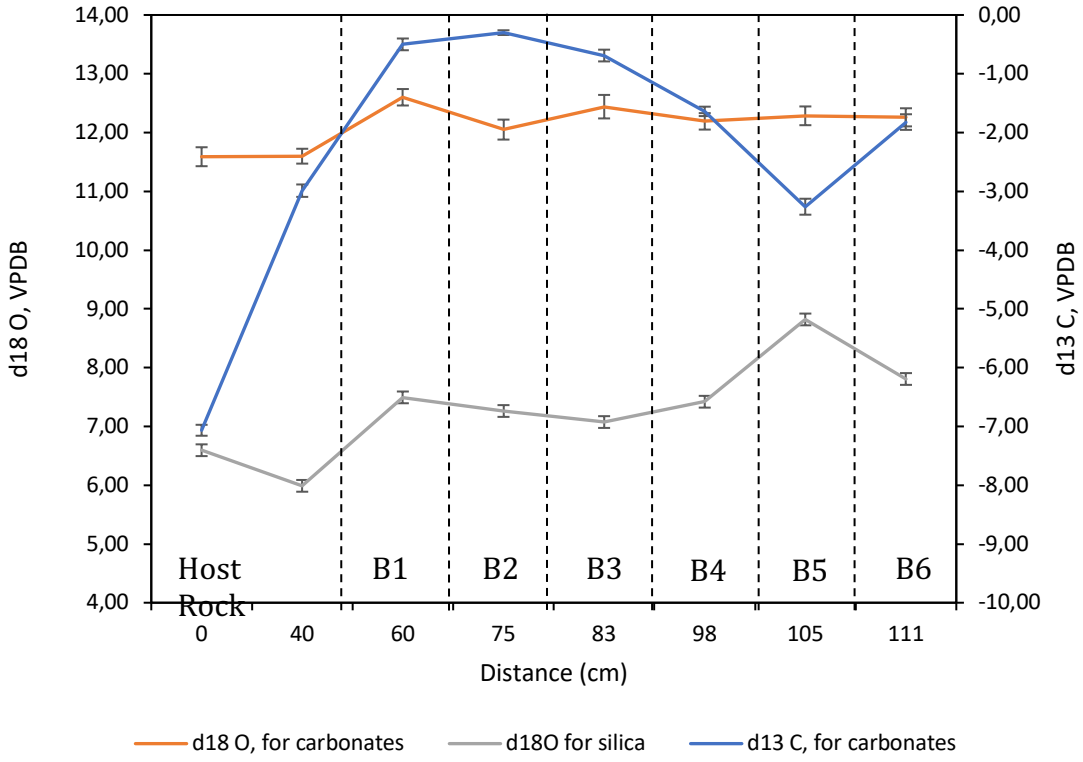

In Figure X, a coupled C-O trend based on data from Table X show increasing δ18O - and d13C with increasing metasomatism. The non-metasomatised Host-B (triangle) has the lowest δ18O and d13C isotope-values, whereas the metasomatic vein (circles) measures show a significant increase in both d13C and d18O. Different zones are marked by different colors in the plot. There is no specific "sub-pattern" for how the separate zones increase/decrease.

The d13C values for Host-B is -6.59 and -5.99‰, which is typical values for mantle carbon (-5.5‰). Whereas the zones that are affected by the fluids (e.g. B1-B4) have d13C values between -0.30 to -1.64‰, which are quite close to the typical values for marine sediments 0‰ (Hoefs, 2015). Overall, these variations support a possible fluid origin from the surrounding marine sediments.

7.3 Stable Isotopes – small scale sampling by drilling Carbonate grains

7.3.1 Sample site A

Stable Isotope values for dolomite in Vein A			
Sample	δ13C, VPDB (‰)	δ18O, VSMOW (‰)	Zone
19-ZS-17	-2.16	11.50	A 1.1
19-ZS-17	-3.74	11.22	A 1.2
19-ZS-17	-0.87	10.90	A 2.1
19-ZS-17	-1.13	11.13	A 2.2
19-ZS-17	-1.46	11.18	A 2.3
20-ZS-17	-1.12	10.99	A 2.4
20-ZS-17	-1.22	11.33	A 3.1
20-ZS-17	-1.30	11.37	A 3.2
20-ZS-17	-1.15	11.38	A 3.3
20-ZS-17	-1.55	11.49	A 4.1
20-ZS-17	-1.76	12.33	A 4.3
20-ZS-17	-1.89	11.27	A 4.4
20-ZS-17	-1.43	11.68	A 4.2
20-ZS-17	-1.06	11.13	A 5.1
20-ZS-17	-1.39	11.29	A 5.2

Small aliquots of dolomite was drilled from the slabs. The dolomite drilled within the host rock (grain A1.1 and A1.2) yield a lower d13C value (-2.16‰ and -3.74‰) than the ones inside the vein. However, the variation from -2.16 to -3.74 indicates that the variation in d13C is quite high only within the first zone. It has been observed that Vein A contains idioblastic dolomite grains with calcite rims. However, these findings are based on microprobe analysis in the central part of the vein (A3 and A4). Whether this variation is caused by a different type of carbonate, is difficult to say as no micro probe analysis was obtained in this part of the vein.

Right on the border of the vein (A2.1), there is a sharp increase to -0.87‰, which is correlated to a significant increase in carbonate. The values stay more or less stable within zone A2 and A3 with d13C values around -1.13‰ +/- 0.25. In zone 4, there is a significant decrease in d13C. This might be linked to the transition from reaction rim to crack-infilll tremolite (zone A5). The same trend is seen in bulk rock for vein B at the transition from zone B4 to B5.

A general observation is that the bulk rock stable isotope analysis (Table X) of the same vein zones show slightly lower stable isotope values than the small-scale drilling. This might be caused by the fact that the vein contains dolomite grains with calcite rim, and as bulk rock powder it is not possible to separate these two. Whereas for the drilling, mostly the center (dolomite) was drilled. The original goal was to drill/sample the rim and the core separately to see if the stable isotope values showed any trend, but as the calcite rims were so thin, it was not possible to obtain enough material from the rim.

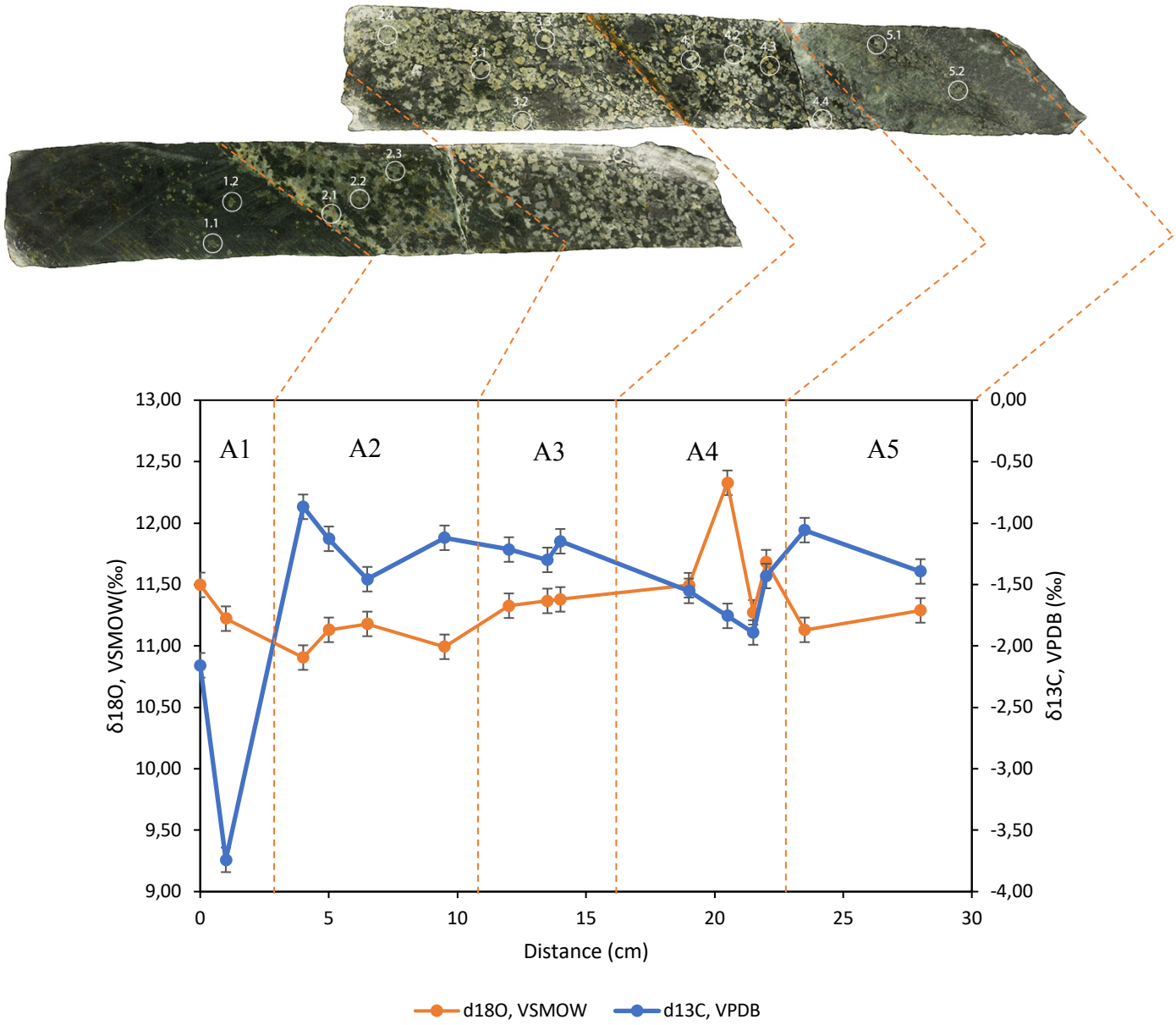

In Figure X, a coupled C-O trend based on data from Table X shows increasing δ18O - and a small decrease d13C with increasing alteration by the vein fluids.

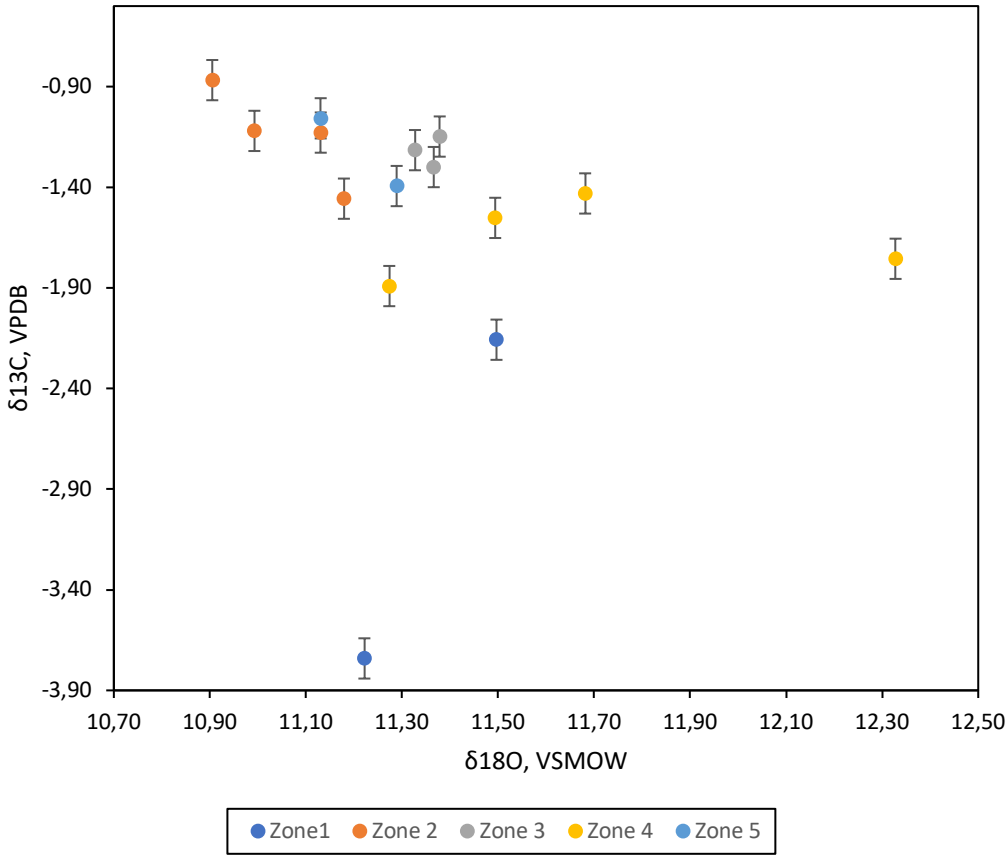
-0,90
-1,40
-1,90
-2,40
-2,90
-3,40
-3,90
δ13C, VPDB
10,70
10,90
11,10
11,30
11,50
11,70
11,90
12,10
12,30
12,50
δ18O, VSMOW
Zone1
Zone 2
Zone 3
Zone 4
Zone 5

7.3.2 Sample site C

A Talc-Magnesite vein was sampled. At location C. In this core, the carbonate grains seemed to exhibit a rim and a core. To see if there was any isotopic variation from rim to core, it was decided to drill them separately. However, the d13C values does not show any clear pattern -some grains have an increase towards the rim, while others have a decrease. The d18O values are quite constant from core to rim and only vary with a few percentages. Most of the d18O values increase slightly towards the rim. The drilled sample from Host-C (grain nr 6, see Figure X) contained too little CO2 to be measured accurately (peak hight <300 during the isotope analysis).

δ13C (‰) for magnesite grains in Vein C			
Sample	Core	Rim	Difference (‰)
23m-1	-0.91	-0.19	-0.73
23m-2	-0.31	-0.06	-0.24
23s-5-2	-0.12	-1.08	0.95
23s-5-1	-1.16	-0.58	-0.58
23s-1	-0.14	0.05	-0.19
23s-2	-0.14	-0.25	0.12
23s-3	0.06	-0.36	0.42

δ18O (‰) for magnesite grains in Vein C			
Sample	Core	Rim	Difference (‰)
23m-1	11.37	11.73	-0.36
23m-2	12.11	11.95	0.16
23s-5-2	12.00	11.72	0.27
23s-5-1	11.76	11.61	0.14
23s-1	12.12	12.10	0.02
23s-2	11.86	11.32	0.54
23s-3	12.29	10.03	2.26

The equation for Magnesite ←→H2O by Zheng (1999) (eq. 6) was used to calculate the isotopic composition of the infiltrating water at the calculated temperature (T ~400°C) for the vein formation. The calculations yield an isotopic composition of d18O ca. 8‰ for the water.

$$1000\ ln\ \alpha = 4.070\frac{(10^6)}{T^2} + (-4.640)\frac{(10^3)}{T} + 1.720$$

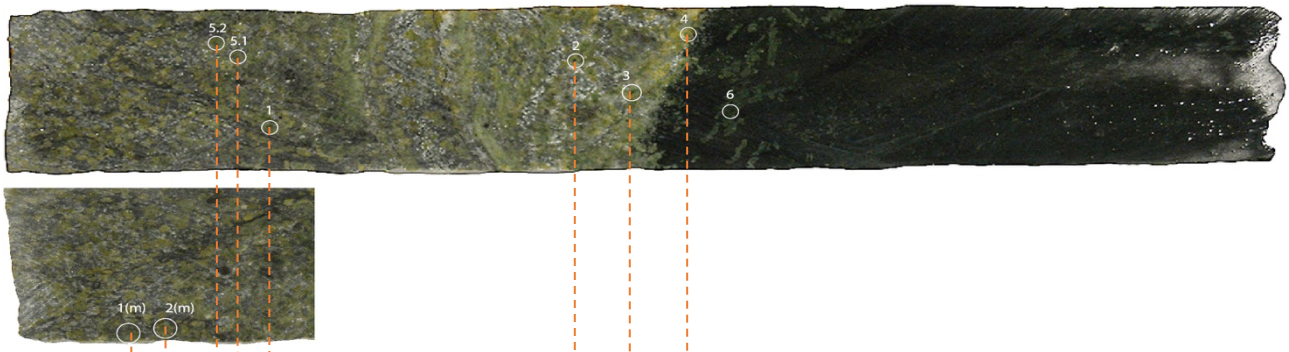
5.2
5.1
1
2
3
4
6

1(m)
2(m)

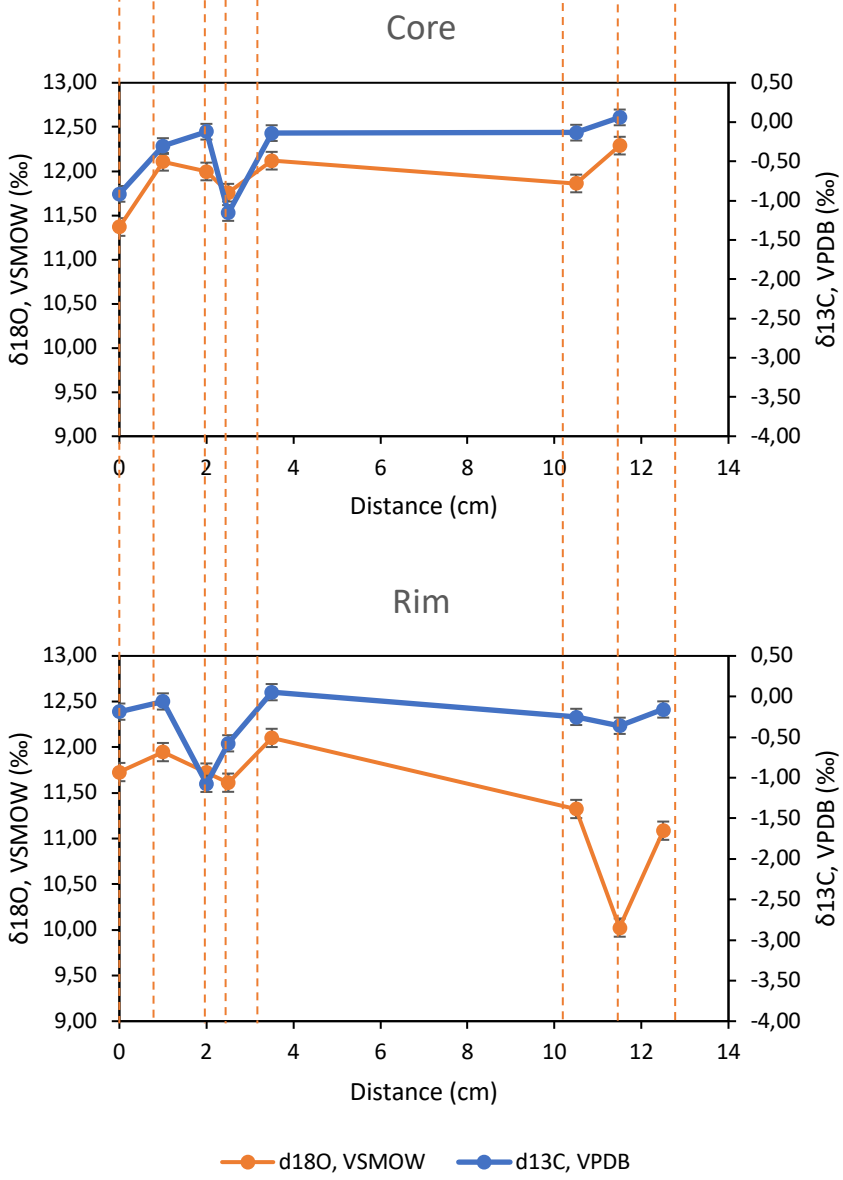
Core
δ18O, VSMOW (‰)
δ13C, VPDB (‰)
Distance (cm)
Rim
δ18O, VSMOW (‰)
δ13C, VPDB (‰)
Distance (cm)
d18O, VSMOW
d13C, VPDB

9. Discussion

Vein geometry

The veins studied above tend to exhibit a zonation pattern within the reaction rim (e.g. Vein A and Vein B). The process which forms such zones is called bi-metasomatism, and has been modeled by Frantz and Mao (1979). However, their model is based on mass transfer by diffusion in a closed system, whereas in this case the mass transfer happens by infiltration in an open system.

9.1 Temperature of the vein formation

Temperature estimations based on $\Delta^{18}O$ for magnesite-tremolite and magnesite-diopside for two samples indicate temperatures between 350-450°C. The third sample plots at 500-600°C. The $\delta^{18}O$ for tremolite and diopside is approximately the same for all three pairs. It is an increase of the $\delta^{18}O$ -value of one of the three magnetite samples that cause this variation in temperature. There are several possible explanations the $\delta^{18}O$ change of magnetite: 1) the magnetite could have preserved the d18O-values from previous event (mantle or high-P metamorphism); 2) the magnetite might have crystallized and stopped "exchanging" with the other minerals and is hence not fully equilibrated with the silicates; 3) during picking it was noted that the shape of the Mt-grains varied - some were nicely euhedral, and others were more aggregate-like; or 4) the vein actually formed over a ca. 100°C interval. Case 1) does not seem to be very probable, since the vein fill is used for determination of the temperature, which is filling in an empty space. Hence inheritance seems excluded. Case 3 is also not very likely, despite the fact that anhedral magnetites are interpreted that not all silicate was removed during picking. Contamination of magnetite by silicate would require roughly 30% (by volume) of silicate to change the magnetite composition to the one measured. While this is possible, it is not likely, since care was taken to obtain as pure as possible separates. Case 2 is difficult to evaluate, since equilibrium can not be proven. Finally, case 4) could be possible, since there are indications that the serpentine veins were once talc veins (see inclusion of talc in carbonate), that hence the talc vein was re-activated at lower temperatures when the antigorite replaced talc.

Nevertheless, we believe that the temperatures of ca. 350-450°C indicates that the antigorite-carbonate veins formed at middle to lower greenschist facies conditions. This correlates well with the low degree of deformation observed in the field. The mineral phases, as described above, are also typical for greenschist facies metamorphism.

9.2 Fluid origin

Originally, it was assumed that all the veins observed in the field had the same mineralogy, and that the only characteristics distinguishing them were the size and the preservation of the vein center in the smaller veins. However, petrographic studies reveal that they can be divided into three different categories depending on their mineralogy. The uppermost vein (A) is comprised of Atg and Dol grains with Cal-rims, the middle vein (B) Atg and Dol grains with a few Cal-veinlets, whereas the bottom vein (C) is comprised mainly of Tc and Mgs grains. Some of the grains have iron-depleted rims. Elias Kempf (2014) observed dolomite rims on the magnesite grains and a few small calcite grains in vein C as well.

9.2.1 Element Transport

From the compositional CaO-MgO-SiO2 diagram (Figure X) it becomes evident that the host rock is CaO-poor. The Tc-Mgs vein measured by Kempf (2014) is also CaO-poor, whereas the Atg-Dol veins show an enrichment in CaO. During the modelling of the mass transport in the veins, it was observed that Ca and Sr are enriched, whereas Mg, Fe3+, Si, Ni and Cr are depleted. Also, the ISOCON lines indicate that the veins form approximately at constant volume. The enrichment of Ca and Sr are helpful clues when it comes to determining the source of the fluid. Indeed, as the host rock does not contain a lot of calcium, strontium, or carbon originally (see Figure X), it is evident that the calcium and carbon is derived from an external source. Rocks that are abundant in Ca, Sr, and CO_2 are typical Bündnerschiefer , also called schist lustre. They are sedimentary rocks, formed by turbidite-like deposits of carbonatious material with variable amounts of clastic silicate minerals.

9.2.2 Stable isotope characteristics

The characteristics of the stable isotopes in the veins and host rock can help determine where the Ca-and CO2 rich fluid is derived from. The $\delta^{13}C$ values for Host-B is -7.07‰ which plots within the range of typical values for mantle carbonates (-5.5‰) (Hoefs, 1997). Whereas the zones that are affected by the fluids (e.g. B1-B4) have $\delta^{13}C$ values between -0.30 to -1.64‰, which are quite close to the typical values for marine carbonates 0‰ (Hoefs, 2015). The $\delta^{18}O$ values for the carbonates plots slightly higher than the typical range for magmatic carbonate, and significantly lower than the typical $\delta^{18}O$ range for marine carbonates. During metasomatism the $\delta^{18}O$ composition usually only change by a few percent, as rocks in general have a high oxygen concentration. Considering that the unaltered rock is ultramafic serpentinite, it is logic that the metasomatized rock has a $\delta^{18}O$ slightly higher than typical mantle carbonates. However, ultramafic rocks are very poor in carbon and will therefore be highly affected by the carbon in the fluid. The individual metasomatic vein profiles described earlier in this work show that $\delta^{13}C$ increase towards the center of the vein. All the values from the vein profiles (A, B, C and Host Rock from sample site E) are compiled in Figure X. The carbonate values start at -7.07‰ and gradually increase until they reach values close to 0‰ which are typical for marine carbonates.

What is worth noticing, is how the whole rock samples from Sample site E plot close to $\delta^{13}C$ 0‰, compared to the host rock next to Vein B which plots at -7.07‰. The host rock in sample site E contain separate dolomite aggregates that are dispersed in the serpentinite (see FigureX). This might indicate that the massive host rock serpentinite has undergone a pervasive carbonization with the same type of fluid.

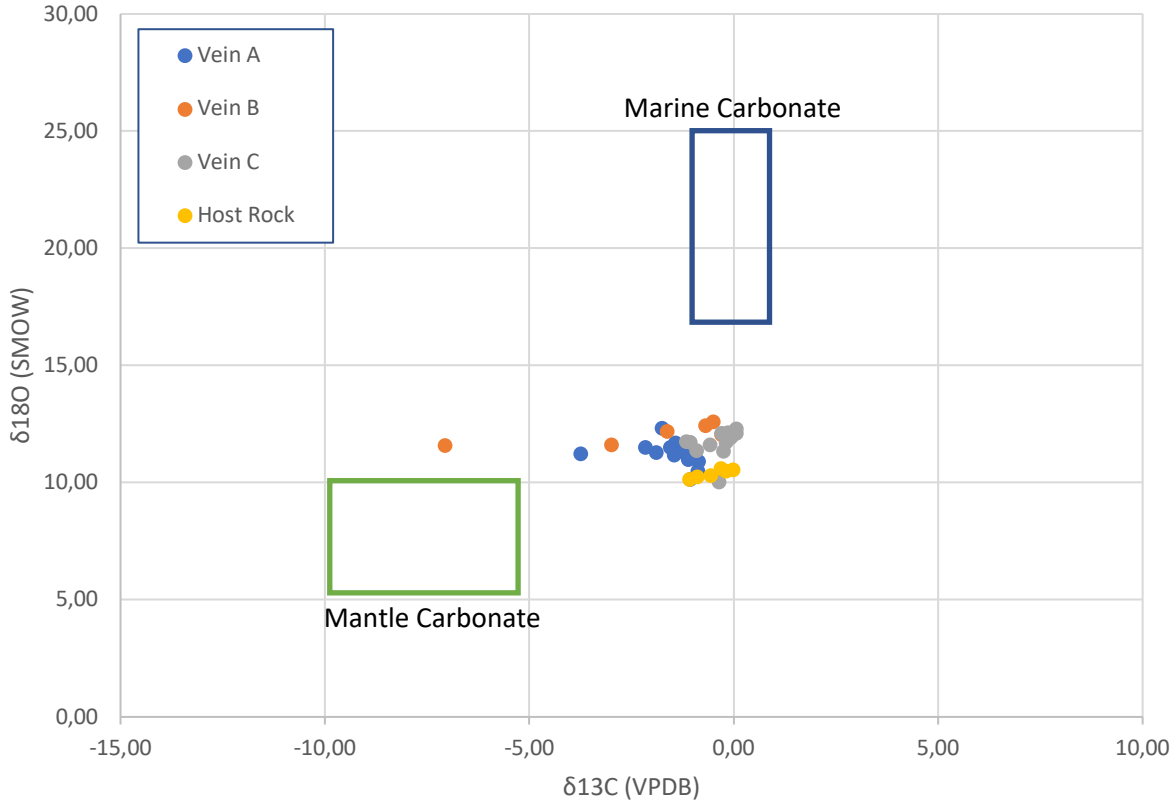

In Figure X, $\delta^{18}O$ values from the carbonate veins A, B and C (highlighted with blue) plotted together with the δ^{18} from Seydoux (2013) analysis of calcschist, calc-silicates from the Bündnerschiefer and serpentinite. The $\delta^{18}O$ values for Vein A, B and C plots between serpentinite and the metasediments. The calc-silicates partly overlaps with the vein values.

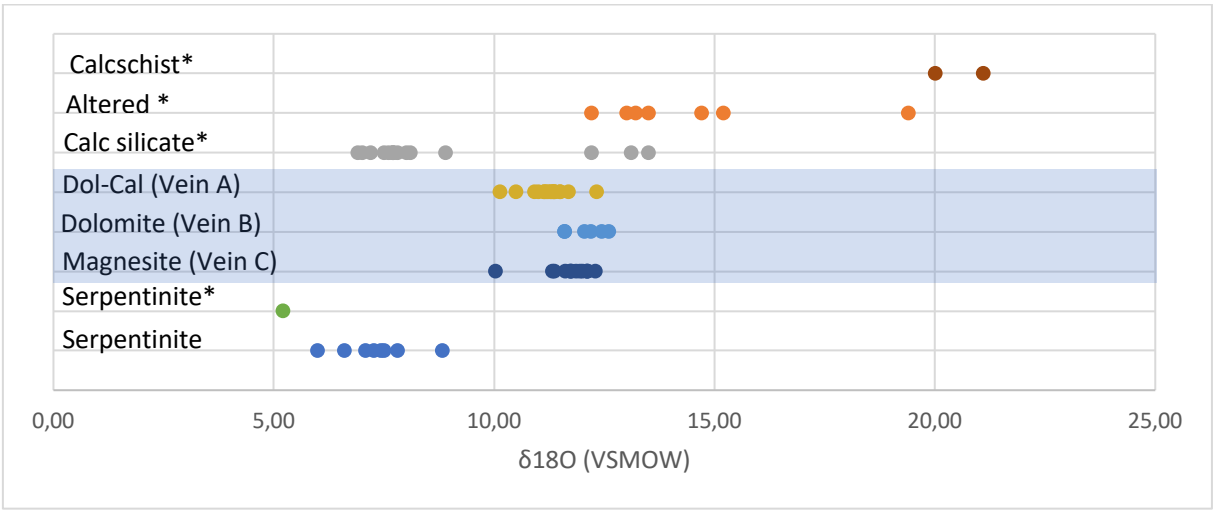

*Seydoux (2013)

9.3 What causes the difference in mineralogy

Originally, it was assumed that all the veins observed in the field had the same mineralogy, and that the only things distinguishing them were the size and the preservation of the vein center in the smaller veins. However, petrographic studies reveals that they can be divided into 3 different categories depending on their mineralogy. The uppermost vein (A) is comprised of Atg and Dol grains with Cal-rims, the middle vein (B) Atg and Dol grains with a few Cal-veinlets, whereas the bottom vein (C) is comprised mainly of Tc and Mgs grains Some of the grains have iron-depleted rims. Elias Kempf (2014) observed dolomite rims on the magnesite grains and a few small calcite grains in vein C as well.

Traces of talc inside dolomite grain were found and represent a preserved former Tc-Mgs border. This would suggest that initially all the veins were comprised of Tc-Mgs, and that a later fluid event rich in Ca would cause a back-reaction and form Atg-Dol with traces of talc. While texturally this seems reasonable, the stable isotope values do not vary significantly between Atg-Dol and Tc-Mgs veins.

Another theory that might explain the difference in mineralogy and thickness of reaction rim depends on the width of the crack, fluid flow direction and the relative content of CaO/H2O that is flowing through the cracks.

Fluid flow is driven by pressure gradients, which could be due to dehydration/decarbonation reactions, by density variations due to temperature, or by tectonic pressure gradients. The reaction fronts (or mineral zones) grow outward, perpendicular to the crack. Depending on how long fluid percolated through the crack, the thickness of the reaction front will vary. Nevertheless, as long as the same fluid is flowing through the cracks, with velocities large enough to impose the composition in the fluid in the vein, the same zonation will develop around the vein (see e.g. Frantz and Mao, 1976). Hence the most plausible mechanism is that the initial veins were all talc veins.

9.4 Timing of the vein formation

Metasomatic carbonate veins can form in serpentinites at the ocean floor during seafloor hydration ( ). However, if this was the case, the veins would be highly deformed due to the alpine subduction. As seen in the outcrop (Figure 4), the Atg-Dol and Tc-Mgs veins are the least deformed veins observed in the area. It is therefore not very likely that these veins formed at seafloor before the subduction of the oceanic lithosphere. Also, the phase mineralogy of the veins are estimated formation at low-P conditions at ca. 5 kbar (estimated by Kempf, 2014).

The veins also crosscut all other veins in the field (including the subduction related veins, Kempf (2014)), and are oriented in SW-NE direction. The veins are interpreted to initially being extensional fissures which formed due to compressional forces from SW and NE. The sinistral strike-slip offsets observed in the field are oriented NW-SE (e.g. Figure 14) might be shear fractures that most likely happened during the same compressional event (Figure X). The internal dextral SW-NE shear sense (indicated by the Mt-trend, Figure X) within the Atg-Dol veins are interpreted to have formed during the opening of the veins.

The backfolding during the late stage of the alpine orogeny fits the orientation of the SW-NE compressional forces. This folding event happened around 31-25 Ma years ago at lower amphibolite to higher greenschist facies (Steck, 2008). As the temperature for vein

formation is estimated to be at low P-T conditions at ca. 350-450°C and 5kbar, it might be possible that these veins formed during the late stages of the backfolding.

Conclusions

- The temperature calculations based on isotope fractionation suggest that the veins formed at temperatures between 350-450°C at middle- to lower greenschist facies conditions, which suggest that the veins formed during or shortly after the backfolding event.

- Vein A and B mainly contain antigorite and dolomite, whereas Vein C contain talc and magnesite. Mass transport indicates that the fluids are not only enriched in CO2, but also CaO.

- It is assumed that the veins formed during the same fluid event, and that the changes in mineralogy is caused by local variations in the concentration of Ca and CO2 within the fluid.

- The d13C values from the center of the veins correlates well with the d13C values for the Bündenerschiefer. In addition, these metasediments are also rich in CaO and CO2, which suggests that the fluids are very likely to derive from this lithological sequence.

- The zonations in the veins form by the process bi-metasomatism.

- According to the ISOCON models, the veins formed with little/no change in volume.

- The stable isotope values for d13C show large variation from host rock to center of the vein. The d13C values goes from typical mantle carbonate outside the vein to marine carbonate inside the vein.

- Dolomite aggregates are dispersed in the massive host rock, and might indicate light, pervasive carbonation of the serpentinite.

10. References

Barnicoat, A. (1988) : "Zoned high-pressure assemblages in pillow lavas of the Zermatt-Saas ophiolite zone, Switzerland," *Lithos*, 21, 227-236.

Barnicoat, A. and Fry, N. (1986). High-pressure metamorphism of the Zermatt-Saas Fee ophiolite zone, Switzerland. Journal of the Geological Society, 143, 607-618.

Bearth, P. (1953) : Blatt Zermatt, Geologischer Atlas der Schweiz. Nr. 29. Schweiz Geol. Kommision, Basel.

(1959) : "Über Eklogite, Glaukophanschiefer und metamorphe Pillowlaven," Schweiz Mineral Petrogr Mitt, 39, 267-286.

Bigeleisen, J. (1965) Chemistry of isotopes. Science, 147: 463-471.

Bosquet, R. (2008). Metamorphic heterogeneities within a single HP-unit: Overprint effect or metamorphic mix?. Lithos, 103, 46-69.

Compagnoni, R. (1977). The Sesia-Lanzo zone: high pressure – low temperature metamorphism in the Austroalpine continental margin. Rendiconti della Società italiana di Mineralogia e Petrologia, 33, 281-334.

Dal Piaz, G. (1999). The Austroalpine-Piedmont nappe stack and the puzzle of Alpine Tethys. Memorie di Scienze Geologiche, 51, 155-176.

Dewey, J., Helman, M., Knott,S., Turco, E. and Hutton, D. (1989): "Kinematics of the western Mediterranean," *Geological Society*, *London, Special Publications,* 45, 265-283.

Dietz, R. S. and Holden, J. C. (1970). *The Breakup of Pangea.* Scientific American, vol. 223, no. 4, 1970, pp. 30–41., www.jstor.org/stable/24927634.

Duchêne, S., Lardeaux, J., and Albarède, F., (1997a). Exhumation of eclogites: Insights from depth-time path analysis: Tectonophysics, 280, 125-140.

Escher, A. & Beaumont, C. (1997). Formation and evolution of basement nappes at crustal scale: geometric model based on the Western Apls. Journal of Structural Geology 19/7, 955-974.

Eugster, HP, Baumgartner, LP (1987). Mineral solubilities and speciation in supercritical metamorphic fluids. Reviews in Mineralogy 17, 367 - 404

Frantz, J. and Mao, H. (1979). Bimetasomatism resulting from intergranular diffusion; II, Prediction of multimineralic zone sequences. American Journal of Science, 279, 301-323.

Garcia, B., Beaumont, V., Perfetti, E., Rouchon, V., Blanchet, D., Oger, P., Dromart, G., Huc, A.Y., and Haeseler, F. (2010). Experiments and geochemical modelling of CO2 sequestration by olivine: Potential, quantification. Applied Geochemistry, 25, 1383-1396.

Grant, J. A., The isocon diagram; a simple solution to Gresens' equation for metasomatic alteration, Economic Geology, 81, 1976-1982.

Hoefs, J. (2015). Stable Isotope Geochemistry (7th Edition). Springer, p. 69 and 88.

Hunziker, J.C. (1974) Rb-Sr and K-Ar age determination and the alpine tectonic history of the Western Alps. Memorie Degli Instituti Di Geologia E Mineralogia Dell' Universita Di Padovia, 1-55.

Kempf, E. (2014). Reactive transport in serpentinites (Zermatt, Switzerland). Unpublished data. Department of Earth Sciences, ETH Zürich.

Labhart, T.P. (1992) Geologie der Schweiz. 211 p. Ott Verlag, Thun.

Meyer, J. (1983) : "Mineralogie und Petrologie des Allalingabbros".

Oberhänsli, R. (1982) : "The PT history of some pillow lavas from Zermatt," *Ofioliti*, 7.

Keith, M.L. and Weber, J.N. (1964). Carbon and oxygenisotopic composition of selected limestones and fossils. Geochim. Cosmochim. Acta, 28, 1787-1816.

Li, X.P., Rahn, M. and Bucher, K. (2004b) : "Serpentinites of the Zermatt-Saas ophiolite complex and their texture evolution," *Journal of Metamorphic Geology*, 22(3), 159-177.

Marthaler, M. (2001) *Le Cervi est-il africain?* 96 p. L.E.P. Loisirs et Pédagogie S.A., Lausanne.

Marthaler, M. and Stampfli, G (1989). Les schistes lustrés à ophiolites de la nappe du Tsaté: Un ancien prisme d'accrétion issu de la marge active apulienne?. Schweizerische Mineralogische und Petrograpische Mitteilungen, 69, 211-216.

O'Hanley, D. S., and Wicks, J. F. (1995). *Conditions of formation of lizardite, chrysotile and antigorite*, Cassiar, British Columbia: Canadian Mineralogist, v. 33, p. 753–774.

Putnis, A. and Austrheim, H. (2010). *Fluid-induced processes: metasomatism and metamorphism.* Geofluids, 10: 254-269.

Reinecke, T. (1991). Very high-pressure metamorphism and uplift of coesite-bearing metasediments from the Zermatt-Saas Zone, Western Alps. European Journal of Mineralogy, 3, 7-17.

(1998). Prograde high- to ultrahigh-pressure metamorphism and exhumation of oceanic sediments at Lago di Cignana, Zermatt-Saas Zone, western Alps. Lithos, 42, 147-189.

Rubatto, D., Gebauer D. and Fanning, M. (1998) : "Jurassic formation and Eocene subduction of the Zermatt-Saas Fee ophiolites : Implications for the geodynamic evolution of the Central and Western Alps," *Contributions to Mineralogy and Petrology*, 132, 269-287.

Sartori, M. (1987). Structure de la zone du Combin entre les Diablons et Zermatt (Valais). Eclogae Geologicae Helveticae, 80, 789-814.

Seydoux, L. (2013). *Interactions fluide-roche dans les ultramafiques de la zone de Zermatt Saas Fee.*(Unpublished data). Université de Lausanne, Institut des sciences de la Terre.

Skora, S., Mahlen, N.J., Johnson, C.M, Baumgartner, L.P., Lapen, T.J., Beard, B.L. and Szilvagyi, E.T. (2015). Evidence for protracted prograde metamorphism followed by rapid exhumation of the Zermatt-Saas Fee ophiolite.

Stampfli, G. and Borel, G. (2002). Metamorphic phase equilibria and pressure temperature-time paths, Washington, D.C.: Mineralogical Society of America.

Spear, F.S. (1995). Metamorphic phase equilibria and pressure-temperature -time paths. Washington, D.C. : Mineralogical Society of America.

Steck, A. (2008) Tectonics of the Simplon massif and Lepontine gneiss dome: deformation structures due to collision between the underthrusting European plate and the Adriatic indenter. Swiss Journal of Geosciences, 101(2): 515-546.

Trümpy, R. (1960). Paleotectonic evolution of the Central and Western Alps. 860 p. Bulletin of The Geological Society of America, 71, 843-908.

(1980). Geology of Switzerland a guide book. 104 p. Wepf & Co, Basel.

Valley, J.W. (1986). Stable isotope geochemistry of metamorphic rocks. Reviews in Mineralogy 16: 445-489.

Venturini, G. (1995). Geology, Geochemistry and Geochronology of the inner central Sesia Zone (Western Alps – Italy). 148 p. Université de Lausanne, Lausanne.

Zharikov, V.A., Pertsev, N.N., Rusinov, V.L., Callegari, E. and Fettes, D.J. (2007). *9.Metasomatism and metasomatic rocks*. A classification of metamorphic rocks and glossary of terms. Recommendations of the International Union of Geological Sciences Subcommission on the Systematics of Metamorphic Rocks.

Appendix

Sample site	Sample - ID	Rock	Thin sections	XRF	Micro Probe	Isotope
A.1	01-ZS-17	Atg + Ol + Mt + Mgs/Dol				
	02-ZS-17	Atg + Ol+ Cpx + Mt + Mgs/Dol	X	X (T & B)	X	X
	03-ZS-17		X			
	04-ZS-17		X	X		X
	05-ZS-17	Atg + Dol + Mt	X			
	06-ZS-17	Atg + Dol + Mt	X	X		X
	07-ZS-17	Atg + Dol + Mt	X		X	
	08-ZS-17	Atg + Dol + Mt	X			
	09-ZS-17	Atg + (Dol) + Mt	X	X		X
	18-ZS-17	Atg + Dol + Mt	X	X		X
	10-ZS-17	Atg + Dol + Mt	X			
	11-ZS-17	Atg + ? + Ol + Mt + ? + Dol	X		X	
	12-ZS-17	Atg +? + Ol + Mt + Dol	X (T & B)			
	13-ZS-17	Atg + ? + Ol + Mt + Dol +Chl	X	X		X
	14-ZS-17	Atg + ? +Ol + Mt + Dol + Chl + Tr	X (T & B)			
	15-ZS-17	Atg + Mt + Dol + Chl + Tr	X (T & B)	X		X
	16-ZS-17	Tr + Mt	X	X		
	17-ZS-17		X			
A.2	19-ZS-17(T)	Atg + Dol	X	X	X	X
	19-ZS-17(M)	Atg + Dol	X	X		X
	19-ZS-17 (B)	Atg + Dol	X	X		X
	20-ZS-17(T)	Atg + Dol + Tr	X			X
	20-ZS-17(B)		X	X	X	X
B	21-ZS-17	Tc + Mgs	X (T, M, B)			
	22-ZS-17	Tc + Mgs	X			
C	23-ZS-17	Tc + Mgs				X
	24-ZS-17	Tc + Mgs	X		X	
	25-ZS-17	Tc + Mgs				
	26-ZS-17	Tc + Mgs	X			
D	27-ZS-17	Tc + Mgs	X			
	28-ZS-17	Atg + Dol	X	X		
	29-ZS-17	Atg + Dol	X	X		
	30-ZS-17		X	X		
	31-ZS-17		X	X		
	32-ZS-17	Atg + Mgs	X	X		
	33-ZS-17		X	X		

Microprobe analysis of serpentine (Vein B)

Micro probe was used to measure the composition of antigorite and dolomite throughout to study how the mineral chemistry change across the vein. Measurements were done for antigorite and dolomite in the Host-B (02-ZS-17), in zone B1 (07-ZS-17) and from the transition between zone B3 and B4 (11-ZS-17). The serpentine in the host rock (blue points, Figure Xa) is zone B1 (orange) and B3-B4 (grey).

In Figure Xa the FeTot/Si-relation is plotted. Si plots horizontally, but is divided in three groups due to the increase in FeTot. There is no substitution between FeTot and Si, but it is evident that the FeTot content in antigorite increase towards the center of the vein.

In Figure Xb, the Fe_{Tot}/Mg-relation displays a 1:1 line. The negative slope indicates a decrease in Mg and an enrichment in Fe_{Tot}. The color of the plot indicates that Mg is gradually being replaced by Fe_{Tot} as one approaches the center of the vein.

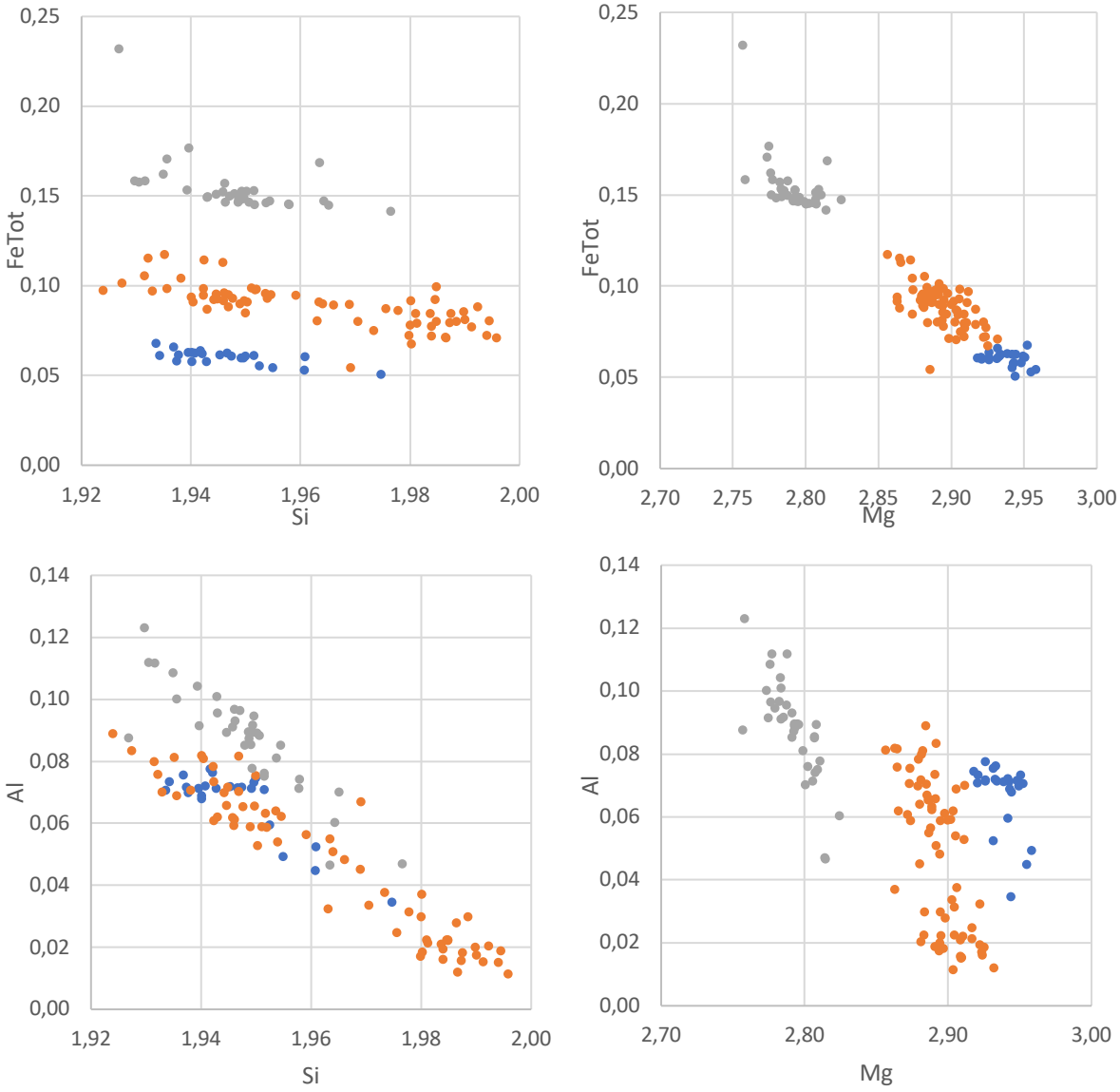

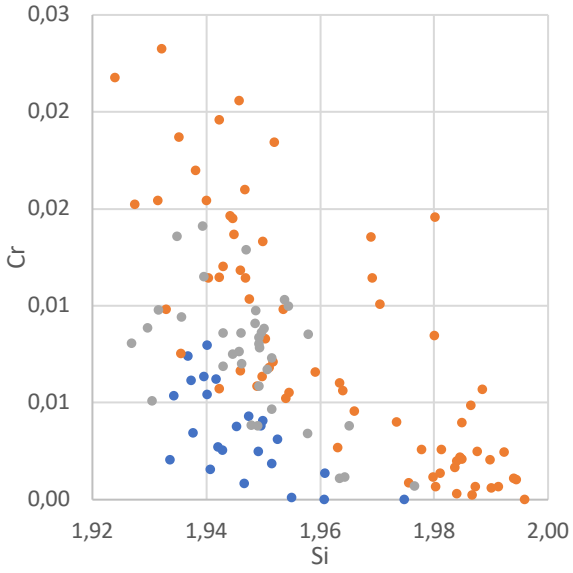
0,03
0,02
0,02
0,01
0,01
0,00
Cr
1,92
1,94
1,96
1,98
2,00
Si

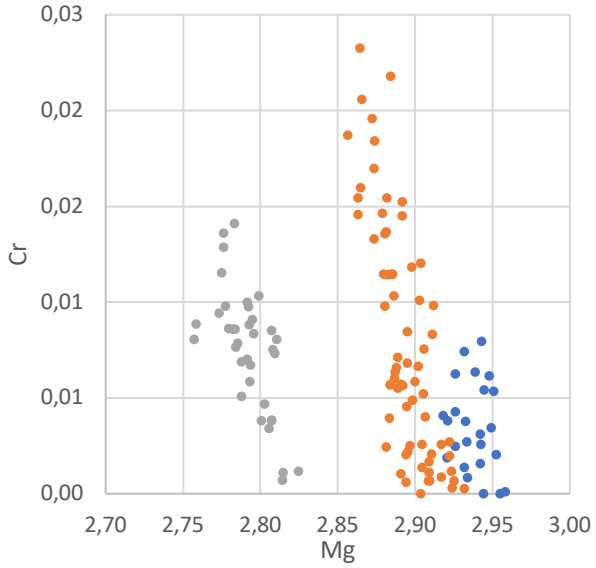
0,03
0,02
0,02
0,01
0,01
0,00
Cr
2,70
2,75
2,80
2,85
2,90
2,95
3,00
Mg

Microprobe analysis of dolomite (Vein B)

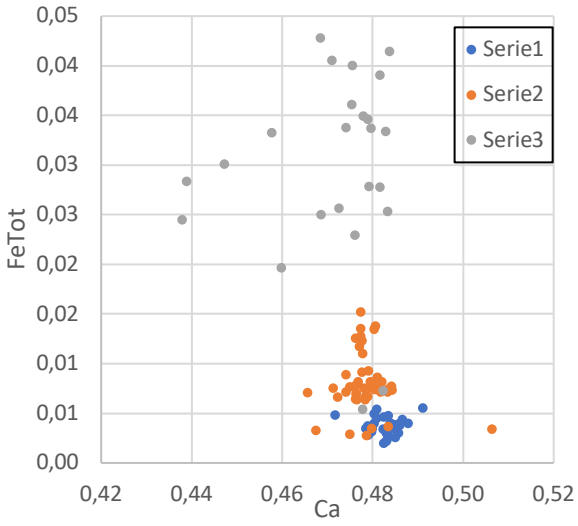

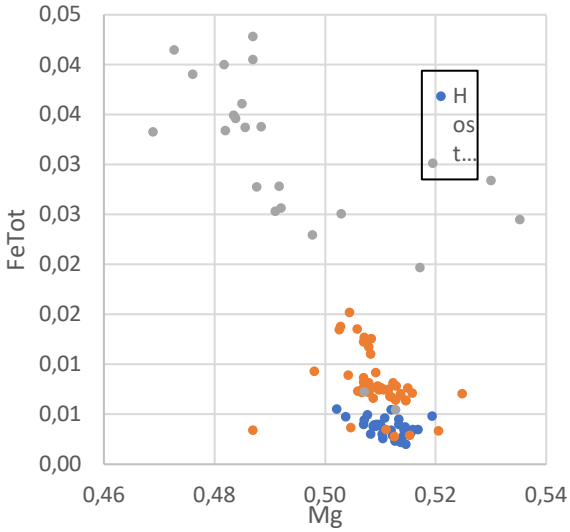

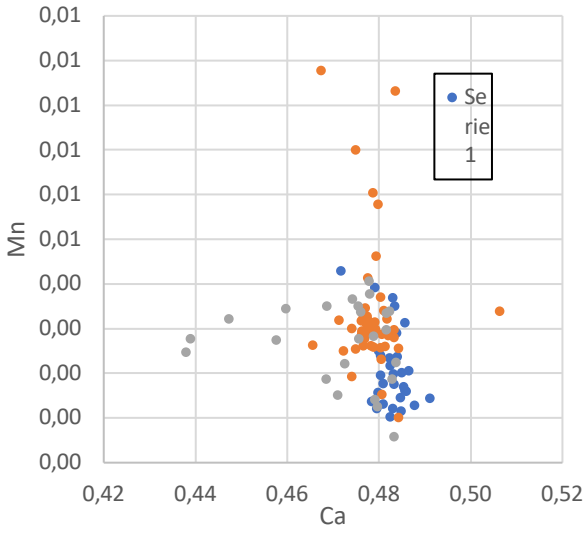

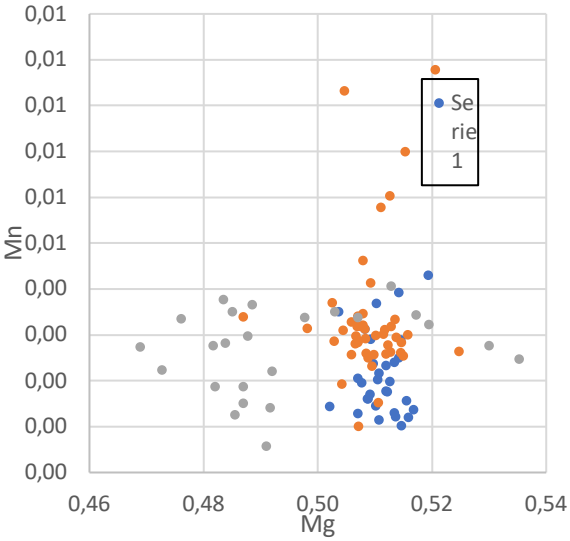

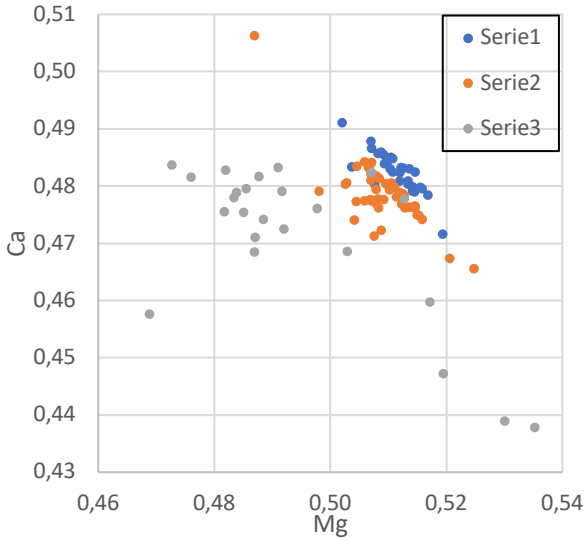

T1

	T1_c7_carb41	T1_c7_carb42	T1_c7_carb43	T1_c7_carb44	T1_c7_carb45	T1_c7_carb46	T1_c7_carb47	T1_c7_carb48	T1_c7_carb49	T1_c7_carb50	T1_c7_carb51	T1_c7_carb52	T1_c7_carb53
FeO	0.29	0.37	0.27	0.35	0.22	0.27	0.39	0.37	0.30	0.44	0.30	0.36	0.35
MnO	0.22	0.33	0.10	0.16	0.30	0.19	0.15	0.27	0.11	0.11	0.12	0.17	0.10
MgO	22.37	22.36	22.40	22.51	22.45	22.59	22.57	22.32	22.53	22.21	22.50	22.56	22.46
CaO	28.97	28.25	28.85	30.05	29.10	29.33	29.71	29.80	29.78	30.22	29.90	29.65	29.27
0.514	0.00	0.00	0.00	0.00	0.00								
Total	51.85	51.30	51.62	53.07	52.07	52.38	52.82	52.77	52.72	52.98	52.82	52.74	52.18

Cations all Fe2+ (Cations = Input)

Al	0.00	0.00	0.00	0.00	0.00	0.00	0.01	0.00	0.00	0.00	0.00	0.00	0.00
Fe	0.00	0.00	0.00	0.00	0.00	0.00	0.00	0.00	0.00	0.01	0.00	0.00	0.00
Mn	0.00	0.00	0.00	0.00	0.00	0.00	0.00	0.00	0.00	0.00	0.00	0.00	0.00
Mg	0.51	0.52	0.52	0.51	0.51	0.51	0.51	0.50	0.51	0.50	0.51	0.51	0.51
Ca	0.48	0.47	0.48	0.49	0.48	0.48	0.48	0.48	0.48	0.49	0.49	0.48	0.48
Add Ele	0.00	0.00	0.00	0.00	0.00	0.00	0.00	0.00	0.00	0.00	0.00	0.00	0.00
C	1.00	1.00	1.00	1.00	1.00	1.00	1.00	1.00	1.00	1.00	1.00	1.00	1.00
Total	2.00	2.00	2.00	2.00	2.00	2.00	2.00	2.00	2.00	2.00	2.00	2.00	2.00

	T1_c7_carb54	T1_c7_carb55	T1_c7_carb56	T1_c8_carb57	T1_c8_carb58	T1_c8_carb59	T1_c8_carb60	T1_c8_carb61	T1_c8_carb62	T1_c9_carb64	T1_c9_carb65	T1_c9_carb66	T1_c9_carb67
FeO	0.24	0.22	0.31	0.27	0.30	0.23	0.20	0.31	0.18	0.16	0.30	0.31	0.42
MnO	0.29	0.14	0.10	0.18	0.13	0.24	0.16	0.18	0.15	0.08	0.12	0.18	0.14
MgO	22.44	22.68	22.48	22.52	22.55	22.22	22.52	22.59	22.49	22.93	22.38	22.50	22.49
CaO	29.55	29.77	30.09	29.52	29.91	29.54	29.77	29.84	29.49	29.91	29.72	29.29	29.39
0.510													
Total	52.51	52.81	52.98	52.49	52.89	52.23	52.65	52.93	52.31	53.08	52.53	52.28	52.44

Cations all Fe2+ (Cations = Input)

Al	0.00	0.00	0.00	0.00	0.00	0.00	0.00	0.00	0.00	0.00	0.00	0.00	0.00
Fe	0.00	0.00	0.00	0.00	0.00	0.00	0.00	0.00	0.00	0.00	0.00	0.00	0.01
Mn	0.00	0.00	0.00	0.00	0.00	0.00	0.00	0.00	0.00	0.00	0.00	0.00	0.00
Mg	0.51	0.51	0.51	0.51	0.51	0.51	0.51	0.51	0.51	0.51	0.51	0.51	0.51
Ca	0.48	0.48	0.49	0.48	0.49	0.49	0.48	0.48	0.48	0.48	0.49	0.48	0.48
Add Ele	0.00	0.00	0.00	0.00	0.00	0.00	0.00	0.00	0.00	0.00	0.00	0.00	0.00
C	1.00	1.00	1.00	1.00	1.00	1.00	1.00	1.00	1.00	1.00	1.00	1.00	1.00
Total	2.00	2.00	2.00	2.00	2.00	2.00	2.00	2.00	2.00	2.00	2.00	2.00	2.00

T5

	T1_c9_carb68	T1_c9_carb69	T1_c9_carb70	T1_c9_carb71	T1_c9_carb72	T5_c1_dol1	T5_c1_dol2	T5_c1_dol3	T5_c1_dol4	T5_c1_dol5	T5_c1_dol6	T5_c1_dol7	T5_c1_dol8
FeO	0.27	0.26	0.31	0.17	0.25	0.56	0.63	0.59	0.61	0.55	0.50	0.52	0.59
MnO	0.09	0.09	0.22	0.09	0.12	0.23	0.21	0.19	0.24	0.23	0.22	0.19	0.25
MgO	22.50	22.30	22.44	22.32	22.49	22.56	22.22	22.40	22.32	22.45	22.49	22.48	22.41
CaO	29.10	29.45	29.66	29.20	29.12	28.85	28.77	28.74	28.83	28.96	28.95	29.03	28.95
0.516				0.00	0.00								
Total	51.96	52.10	52.64	51.78	51.98	52.20	51.83	51.93	52.00	52.18	52.16	52.23	52.20

Cations all Fe2+ (Cations = Input)

Al	0.00	0.00	0.00	0.00	0.00	0.00	0.00	0.00	0.00	0.00	0.00	0.01	0.01
Fe	0.00	0.00	0.00	0.00	0.00	0.01	0.01	0.01	0.01	0.01	0.01	0.01	0.01
Mn	0.00	0.00	0.00	0.00	0.00	0.00	0.00	0.00	0.00	0.00	0.00	0.00	0.00
Mg	0.52	0.51	0.51	0.51	0.52	0.52	0.51	0.51	0.51	0.51	0.51	0.51	0.51
Ca	0.48	0.48	0.48	0.48	0.48	0.47	0.48	0.47	0.48	0.48	0.48	0.47	0.47
Add Ele	0.00	0.00	0.00	0.00	0.00	0.00	0.00	0.00	0.00	0.00	0.00	0.00	0.00
C	1.00	1.00	1.00	1.00	1.00	1.00	1.00	1.00	1.00	1.00	1.00	1.00	1.00
Total	2.00	2.00	2.00	2.00	2.00	2.00	2.00	2.00	2.00	2.00	2.00	2.00	2.00

	T5_c1_dol9	T5_c1_dol20	T5_c1_dol21	T5_c2_dol22	T5_c2_dol23	T5_c2_dol24	T5_c2_dol25	T5_c2_dol36	T5_c2_dol37	T5_c4_dol26	T5_c4_dol27	T5_c4_dol28	T5_c4_dol29
FeO	0.53	0.95	0.64	0.28	0.26	0.26	0.27	0.22	0.23	0.55	0.50	0.86	1.05
MnO	0.24	0.24	0.22	0.64	0.67	0.26	0.45	0.47	0.54	0.20	0.20	0.24	0.25
MgO	22.38	22.06	22.11	22.01	22.72	21.27	22.36	22.59	22.57	22.92	22.37	22.19	21.99
CaO	29.11	28.92	29.25	29.34	28.38	30.77	29.20	29.35	28.94	28.29	29.03	29.02	28.87
0.512													
Total	52.26	52.17	52.21	52.27	52.03	52.56	52.28	52.62	52.28	51.96	52.10	52.31	52.16

Cations all Fe2+ (Cations = Input)

Al	0.00	0.00	0.00	0.00	0.00	0.00	0.00	0.00	0.00	0.00	0.00	0.00	0.00
Fe	0.01	0.01	0.01	0.00	0.00	0.00	0.00	0.00	0.00	0.01	0.01	0.01	0.01
Mn	0.00	0.00	0.00	0.01	0.01	0.00	0.01	0.01	0.01	0.00	0.00	0.00	0.00
Mg	0.51	0.51	0.51	0.50	0.52	0.49	0.51	0.51	0.52	0.52	0.51	0.51	0.51
Ca	0.48	0.48	0.48	0.48	0.47	0.51	0.48	0.48	0.47	0.47	0.48	0.48	0.48
Add Ele	0.00	0.00	0.00	0.00	0.00	0.00	0.00	0.00	0.00	0.00	0.00	0.00	0.00
C	1.00	1.00	1.00	1.00	1.00	1.00	1.00	1.00	1.00	1.00	1.00	1.00	1.00
Total	2.00	2.00	2.00	2.00	2.00	2.00	2.00	2.00	2.00	2.00	2.00	2.00	2.00

	T5_c4_dol30	T5_c4_dol31	T5_c4_dol32	T5_c4_dol33	T5_c4_dol34	T5_c4_dol35	T2_c5_carb4	T2_c5_carb6	T2_c5_carb9	T2_c5_carb15	T2_c6_carb20	T2_c6_carb23	T2_c6_carb24
FeO	0.53	0.60	0.98	0.91	0.50	0.97	0.54	0.64	0.61	0.58	0.59	0.59	0.56
MnO	0.20	0.23	0.22	0.27	0.20	0.22	0.26	0.36	0.08	0.12	0.22	0.23	0.25
MgO	22.50	22.51	21.95	22.14	22.51	22.09	22.87	22.54	22.60	22.62	22.47	22.60	22.47
CaO	29.28	29.42	28.75	28.93	29.00	28.79	29.51	29.60	30.02	29.62	29.82	29.39	29.65
0.512													
Total	52.51	52.76	51.90	52.24	52.21	52.07	53.19	53.14	53.31	52.94	53.10	52.81	52.93

Cations all Fe2+ (Cations = Input)

Al	0.00	0.00	0.00	0.00	0.00	0.00	0.00	0.00	0.00	0.00	0.00	0.00	0.00
Fe	0.01	0.01	0.01	0.01	0.01	0.01	0.01	0.01	0.01	0.01	0.01	0.01	0.01
Mn	0.00	0.00	0.00	0.00	0.00	0.00	0.00	0.00	0.00	0.00	0.00	0.00	0.00
Mg	0.51	0.51	0.51	0.51	0.51	0.51	0.51	0.51	0.51	0.51	0.51	0.51	0.51
Ca	0.48	0.48	0.48	0.48	0.48	0.48	0.48	0.48	0.48	0.48	0.48	0.48	0.48
Add Ele	0.00	0.00	0.00	0.00	0.00	0.00	0.00	0.00	0.00	0.00	0.00	0.00	0.00
C	1.00	1.00	1.00	1.00	1.00	1.00	1.00	1.00	1.00	1.00	1.00	1.00	1.00
Total	2.00	2.00	2.00	2.00	2.00	2.00	2.00	2.00	2.00	2.00	2.00	2.00	2.00

													T2
	T2_c6_carb25	T2_c7_carb26	T2_c7_carb27	T2_c7_carb28	T2_c7_carb29	T2_c7_carb30	T2_c7_carb31	T2_c7_carb32	T2_c7_carb33	T2_c8_carb36	T2_c8_carb37	T2_c8_carb39	T2_c2_carb20
FeO	0.68	0.70	0.73	0.58	0.56	1.18	1.08	1.05	0.57	0.60	0.72	0.61	0.42
MnO	0.27	0.15	0.25	0.20	0.23	0.24	0.22	0.29	0.20	0.20	0.32	0.18	0.31
MgO	22.44	22.32	22.15	22.37	22.33	22.04	22.12	22.03	22.25	22.55	22.60	22.45	22.31
CaO	29.62	29.20	29.64	29.32	29.63	29.01	29.41	29.29	29.63	29.70	29.49	29.45	28.92
0.507													0.00
Total	53.01	52.37	52.77	52.47	52.75	52.47	52.83	52.66	52.65	53.06	53.14	52.69	51.96

Cations all Fe2+ (Cations = Input)

Al	0.00	0.01	0.01	0.00	0.00	0.00	0.00	0.00	0.00	0.00	0.00	0.00	0.00
Fe	0.01	0.01	0.01	0.01	0.01	0.02	0.01	0.01	0.01	0.01	0.01	0.01	0.01
Mn	0.00	0.00	0.00	0.00	0.00	0.00	0.00	0.00	0.00	0.00	0.00	0.00	0.00
Mg	0.51	0.50	0.50	0.51	0.51	0.50	0.50	0.50	0.51	0.51	0.51	0.51	0.51
Ca	0.48	0.47	0.48	0.48	0.48	0.48	0.48	0.48	0.48	0.48	0.48	0.48	0.48
Add Ele	0.00	0.00	0.00	0.00	0.00	0.00	0.00	0.00	0.00	0.00	0.00	0.00	0.00
C	1.00	1.00	1.00	1.00	1.00	1.00	1.00	1.00	1.00	1.00	1.00	1.00	1.00
Total	2.00	2.00	2.00	2.00	2.00	2.00	2.00	2.00	2.00	2.00	2.00	2.00	2.00

	T2_c5_carb54	T2_c5_carb55	T2_c5_carb56	T2_c5_carb58	T2_c6_carb34	T2_c6_carb35	T2_c6_carb36	T2_c6_carb37	T2_c6_carb39	T2_c8_carb46	T2_c8_carb47	T2_c8_carb48	T2_c9_carb49
FeO	2.58	2.12	2.64	2.56	3.08	1.98	2.65	1.50	3.26	1.76	1.91	2.97	2.17
MnO	0.28	0.22	0.21	0.14	0.11	0.17	0.22	0.26	0.14	0.26	0.26	0.25	0.21
MgO	20.95	20.91	20.72	20.73	20.77	21.30	20.95	22.14	20.82	21.41	21.54	20.32	22.76
CaO	28.29	28.73	28.53	28.89	27.95	28.46	28.45	27.38	27.87	28.49	27.92	28.60	26.22
0.482	0.00												
Total	52.10	51.98	52.10	52.32	51.91	51.91	52.27	51.28	52.09	51.92	51.63	52.14	51.36

Cations all Fe2+ (Cations = Input)

Al	0.00	0.00	0.00	0.00	0.00	0.01	0.04	0.00	0.00	0.00	0.00	0.00	0.00
Fe	0.03	0.03	0.03	0.03	0.04	0.03	0.03	0.02	0.04	0.02	0.03	0.04	0.03
Mn	0.00	0.00	0.00	0.00	0.00	0.00	0.00	0.00	0.00	0.00	0.00	0.00	0.00
Mg	0.49	0.49	0.48	0.48	0.49	0.49	0.47	0.52	0.49	0.50	0.50	0.48	0.53
Ca	0.47	0.48	0.48	0.48	0.47	0.47	0.46	0.46	0.47	0.48	0.47	0.48	0.44
Add Ele	0.00	0.00	0.00	0.00	0.00	0.00	0.00	0.00	0.00	0.00	0.00	0.00	0.00
C	1.00	1.00	1.00	1.00	1.00	1.00	1.00	1.00	1.00	1.00	1.00	1.00	1.00
Total	2.00	2.00	2.00	2.00	2.00	2.00	2.00	2.00	2.00	2.00	2.00	2.00	2.00

	T2_c9_carb50	T2_c9_carb51	T2_c9_carb52	T2_c9_carb53	T2_c11_carb6	T2_c11_carb7	T2_c11_carb8	T2_c11_carb9	T2_c11_carb16	T2_c11_carb17
FeO	2.66	0.56	3.18	1.94	3.04	2.57	2.12	2.74	1.86	2.27
MnO	0.28	0.26	0.17	0.04	0.21	0.09	0.11	0.26	0.19	0.24
MgO	20.67	21.89	20.34	21.12	20.54	20.76	21.03	20.65	22.81	21.99
CaO	28.43	28.97	28.96	28.92	28.21	28.53	28.51	28.16	25.96	26.34
0.483										
Total	52.04	51.68	52.65	52.02	52.00	51.95	51.77	51.81	50.82	50.84

Cations all Fe2+ (Cations = Input)

Al	0.00	0.00	0.00	0.00	0.00	0.00	0.00	0.00	0.00	0.00
Fe	0.03	0.01	0.04	0.03	0.04	0.03	0.03	0.04	0.02	0.03
Mn	0.00	0.00	0.00	0.00	0.00	0.00	0.00	0.00	0.00	0.00
Mg	0.48	0.51	0.47	0.49	0.48	0.49	0.49	0.48	0.54	0.52
Ca	0.48	0.48	0.48	0.48	0.48	0.48	0.48	0.48	0.44	0.45
Add Ele	0.00	0.00	0.00	0.00	0.00	0.00	0.00	0.00	0.00	0.00
C	1.00	1.00	1.00	1.00	1.00	1.00	1.00	1.00	1.00	1.00
Total	2.00	2.00	2.00	2.00	2.00	2.00	2.00	2.00	2.00	2.00

	T1								
Serpentine	T1_c2_serp84	T1_c2_serp85	T1_c2_serp86	T1_c2_serp87	T1_c2_serp88	T1_c2_serp89	T1_c2_serp90	T1_c2_serp91	T1_c2_serp92
SiO2	41.34	42.68	41.54	41.73	41.89	41.77	41.71	42.41	41.59
TiO2	0.00	0.01	0.02	0.01	0.01	0.02	0.02	0.00	0.01
Cr2O3	0.14	0.00	0.09	0.04	0.00	0.22	0.17	0.00	0.17
Al2O3	1.33	0.63	1.27	1.31	0.89	1.26	1.30	0.82	1.30
FeO	1.56	1.31	1.58	1.61	1.39	1.49	1.62	1.37	1.49
MnO	0.01	0.04	0.04	0.02	0.04	0.02	0.01	0.03	0.03
NiO	0.03	0.06	0.02	0.04	0.04	0.03	0.04	0.06	0.03
MgO	42.31	42.69	42.42	42.44	42.53	42.51	42.40	42.88	42.46
CaO	0.00	0.00	0.00	0.01	0.00	0.00	0.01	0.00	0.00
Total	86.73	87.42	86.99	87.22	86.80	87.32	87.27	87.58	87.08
Cation									
Si	1.93	1.97	1.94	1.94	1.95	1.94	1.94	1.96	1.94
Ti	0.00	0.00	0.00	0.00	0.00	0.00	0.00	0.00	0.00
Cr	0.01	0.00	0.00	0.00	0.00	0.01	0.01	0.00	0.01
Al	0.07	0.03	0.07	0.07	0.05	0.07	0.07	0.04	0.07
Fe3+	0.00	0.00	0.00	0.00	0.00	0.00	0.00	0.00	0.00
Fe2+	0.06	0.05	0.06	0.06	0.05	0.06	0.06	0.05	0.06
Mn	0.00	0.00	0.00	0.00	0.00	0.00	0.00	0.00	0.00
Ni	0.00	0.00	0.00	0.00	0.00	0.00	0.00	0.00	0.00
Mg	2.95	2.94	2.95	2.94	2.96	2.94	2.94	2.95	2.95
Ca	0.00	0.00	0.00	0.00	0.00	0.00	0.00	0.00	0.00
Total Cations	5.03	5.01	5.02	5.02	5.02	5.02	5.02	5.02	5.02
XMg	0.98	0.98	0.98	0.98	0.98	0.98	0.98	0.98	0.98

Serpentine	T1_c2_serp93	T1_c2_serp94	T1_c2_serp95	T1_c2_serp96	T1_c2_serp97	T1_c2_serp98	T1_c2_serp99	T1_c2_serp100	T1_c9_serp1
SiO2	42.22	41.96	41.70	41.86	41.89	41.73	42.46	42.05	41.64
TiO2	0.01	0.03	0.01	0.01	0.01	0.02	0.01	0.02	0.01
Cr2O3	0.08	0.07	0.20	0.02	0.10	0.06	0.04	0.08	0.15
Al2O3	1.09	1.30	1.38	1.30	1.31	1.29	1.09	1.10	1.24
FeO	1.43	1.49	1.70	1.61	1.58	1.75	2.64	2.73	1.61
MnO	0.05	0.03	0.02	0.02	0.02	0.04	0.01	0.02	0.02
NiO	0.05	0.02	0.09	0.02	0.03	0.01	0.02	0.06	0.03
MgO	42.68	42.64	42.35	42.33	42.37	42.75	42.89	42.65	42.40
CaO	0.00	0.01	0.00	0.00	0.00	0.00	0.00	0.00	0.00
Total	87.61	87.54	87.45	87.17	87.31	87.65	89.17	88.71	87.10
Cation									
Si	1.95	1.94	1.94	1.95	1.95	1.93	1.94	1.94	1.94
Ti	0.00	0.00	0.00	0.00	0.00	0.00	0.00	0.00	0.00
Cr	0.00	0.00	0.01	0.00	0.00	0.00	0.00	0.00	0.01
Al	0.06	0.07	0.08	0.07	0.07	0.07	0.06	0.06	0.07
Fe3+	0.00	0.00	0.00	0.00	0.00	0.00	0.00	0.00	0.00
Fe2+	0.06	0.06	0.07	0.06	0.06	0.07	0.10	0.11	0.06
Mn	0.00	0.00	0.00	0.00	0.00	0.00	0.00	0.00	0.00
Ni	0.00	0.00	0.00	0.00	0.00	0.00	0.00	0.00	0.00
Mg	2.94	2.94	2.93	2.93	2.93	2.95	2.92	2.93	2.94
Ca	0.00	0.00	0.00	0.00	0.00	0.00	0.00	0.00	0.00
Total Cations	5.02	5.02	5.02	5.02	5.02	5.03	5.03	5.03	5.02
XMg	0.98	0.98	0.98	0.98	0.98	0.98	0.97	0.97	0.98

Serpentine	T1_c9_serp2	T1_c9_serp3	T1_c9_serp4	T1_c9_serp5	T1_c9_serp6	T1_c9_serp7	T1_c9_serp8	T1_c9_serp9	T5 T5_c1_serp1
SiO2	41.89	41.74	41.67	42.32	42.02	41.84	41.94	42.08	42.72
TiO2	0.02	0.00	0.03	0.01	0.01	0.02	0.01	0.01	0.02
Cr2O3	0.10	0.17	0.05	0.04	0.07	0.07	0.11	0.12	0.05
Al2O3	1.33	1.41	1.28	0.96	1.30	1.39	1.36	1.31	0.38
FeO	1.54	1.64	1.56	1.56	1.54	1.60	1.56	1.57	2.18
MnO	0.04	0.02	0.05	0.02	0.02	0.01	0.03	0.02	0.05
NiO	0.02	0.01	0.02	0.06	0.01	0.02	0.04	0.00	0.06
MgO	42.11	42.20	41.84	42.45	42.32	42.40	42.11	42.42	42.03
CaO	0.02	0.01	0.04	0.03	0.08	0.00	0.01	0.06	0.01
Total	87.07	87.20	86.54	87.46	87.36	87.35	87.17	87.60	87.48

Cation									
Si	1.95	1.94	1.95	1.96	1.95	1.94	1.95	1.95	1.98
Ti	0.00	0.00	0.00	0.00	0.00	0.00	0.00	0.00	0.00
Cr	0.00	0.01	0.00	0.00	0.00	0.00	0.00	0.00	0.00
Al	0.07	0.08	0.07	0.05	0.07	0.08	0.07	0.07	0.02
Fe3+	0.00	0.00	0.00	0.00	0.00	0.00	0.00	0.00	0.00
Fe2+	0.06	0.06	0.06	0.06	0.06	0.06	0.06	0.06	0.08
Mn	0.00	0.00	0.00	0.00	0.00	0.00	0.00	0.00	0.00
Ni	0.00	0.00	0.00	0.00	0.00	0.00	0.00	0.00	0.00
Mg	2.92	2.93	2.92	2.93	2.93	2.93	2.92	2.93	2.91
Ca	0.00	0.00	0.00	0.00	0.00	0.00	0.00	0.00	0.00
Total Cations	5.01	5.02	5.01	5.01	5.01	5.02	5.01	5.01	5.00
XMg	0.98	0.98	0.98	0.98	0.98	0.98	0.98	0.98	0.97

Serpentine	T5_c1_serp2	T5_c1_serp3	T5_c1_serp4	T5_c1_serp5	T5_c1_serp6	T5_c1_serp60	T5_c1_serp61	T5_c1_serp62	T5_c1_serp63
SiO2	42.84	42.81	41.21	41.82	41.26	43.05	42.99	42.79	43.36
TiO2	0.00	0.03	0.02	0.01	0.01	0.01	0.01	0.00	0.03
Cr2O3	0.01	0.07	0.42	0.18	0.27	0.02	0.06	0.02	0.00
Al2O3	0.29	0.33	1.45	1.07	1.27	0.28	0.37	0.32	0.21
FeO	2.00	2.18	2.69	2.53	2.48	1.99	2.21	2.09	1.84
MnO	0.08	0.15	0.08	0.06	0.05	0.05	0.05	0.11	0.07
NiO	0.07	0.11	0.07	0.08	0.07	0.06	0.05	0.15	0.09
MgO	42.36	41.86	41.25	41.63	41.70	42.20	41.95	41.75	42.32
CaO	0.01	0.01	0.00	0.00	0.01	0.04	0.06	0.16	0.18
Total	87.67	87.56	87.18	87.39	87.11	87.71	87.75	87.38	88.10

Cation									
Si	1.98	1.99	1.93	1.95	1.93	1.99	1.99	1.99	2.00
Ti	0.00	0.00	0.00	0.00	0.00	0.00	0.00	0.00	0.00
Cr	0.00	0.00	0.02	0.01	0.01	0.00	0.00	0.00	0.00
Al	0.02	0.02	0.08	0.06	0.07	0.02	0.02	0.02	0.01
Fe3+	0.00	0.00	0.00	0.00	0.00	0.00	0.00	0.00	0.00
Fe2+	0.08	0.08	0.11	0.10	0.10	0.08	0.09	0.08	0.07
Mn	0.00	0.01	0.00	0.00	0.00	0.00	0.00	0.00	0.00
Ni	0.00	0.00	0.00	0.00	0.00	0.00	0.00	0.01	0.00
Mg	2.92	2.90	2.88	2.89	2.91	2.91	2.89	2.89	2.90
Ca	0.00	0.00	0.00	0.00	0.00	0.00	0.00	0.01	0.01
Total Cations	5.01	5.00	5.02	5.02	5.03	5.00	5.00	5.00	5.00
XMg	0.97	0.97	0.96	0.97	0.97	0.97	0.97	0.97	0.98

Serpentine	T5_c1_serp64	T5_c1_serp65	T5_c1_serp66	T5_c1_serp67	T5_c1_serp68	T5_c1_serp69	T5_c1_serp70	T5_c1_serp71	T5_c1_serp72
SiO2	42.78	42.80	42.96	42.91	43.01	41.04	41.43	41.75	41.34
TiO2	0.00	0.00	0.01	0.02	0.01	0.03	0.04	0.01	0.01
Cr2O3	0.03	0.02	0.11	0.06	0.07	0.63	0.53	0.56	0.51
Al2O3	0.34	0.29	0.41	0.41	0.37	1.36	1.10	1.12	1.47
FeO	2.06	2.05	2.57	2.39	2.28	2.93	2.92	2.90	3.00
MnO	0.04	0.07	0.07	0.05	0.08	0.04	0.06	0.07	0.05
NiO	0.09	0.07	0.15	0.08	0.22	0.10	0.10	0.09	0.08
MgO	41.60	42.03	41.87	42.00	41.73	40.82	41.10	41.25	40.94
CaO	0.12	0.15	0.00	0.01	0.00	0.00	0.00	0.00	0.01
Total	87.05	87.48	88.14	87.92	87.77	86.95	87.27	87.75	87.41

Cation									
Si	1.99	1.99	1.98	1.98	1.99	1.93	1.94	1.95	1.94
Ti	0.00	0.00	0.00	0.00	0.00	0.00	0.00	0.00	0.00
Cr	0.00	0.00	0.00	0.00	0.00	0.02	0.02	0.02	0.02
Al	0.02	0.02	0.02	0.02	0.02	0.08	0.06	0.06	0.08
Fe3+	0.00	0.00	0.00	0.00	0.00	0.00	0.00	0.00	0.00
Fe2+	0.08	0.08	0.10	0.09	0.09	0.12	0.11	0.11	0.12
Mn	0.00	0.00	0.00	0.00	0.00	0.00	0.00	0.00	0.00
Ni	0.00	0.00	0.01	0.00	0.01	0.00	0.00	0.00	0.00
Mg	2.89	2.91	2.88	2.90	2.88	2.86	2.87	2.87	2.86
Ca	0.01	0.01	0.00	0.00	0.00	0.00	0.00	0.00	0.00
Total Cations	5.00	5.00	5.00	5.00	5.00	5.02	5.02	5.01	5.01
XMg	0.97	0.97	0.97	0.97	0.97	0.96	0.96	0.96	0.96

Serpentine	T5_c1_serp73	T5_c1_serp74	T5_c2_serp7	T5_c2_serp8	T5_c2_serp9	T5_c2_serp81	T5_c2_serp82	T5_c2_serp83
SiO2	42.46	41.62	42.69	41.34	42.49	42.59	42.17	42.37
TiO2	0.00	0.02	0.00	0.01	0.00	0.00	0.01	0.02
Cr2O3	0.40	0.50	0.06	0.32	0.07	0.01	0.02	0.04
Al2O3	0.67	1.06	0.40	1.10	0.39	0.22	0.45	0.40
FeO	2.35	2.50	2.06	2.44	2.03	1.82	2.23	2.16
MnO	0.08	0.06	0.06	0.06	0.04	0.06	0.05	0.06
NiO	0.12	0.14	0.03	0.04	0.08	0.09	0.10	0.22
MgO	41.19	41.11	42.00	41.30	41.97	42.17	41.77	41.68
CaO	0.01	0.00	0.00	0.01	0.02	0.00	0.01	0.03
Total	87.27	87.01	87.30	86.61	87.09	86.95	86.80	86.98

Cation								
Si	1.98	1.95	1.98	1.95	1.98	1.99	1.98	1.98
Ti	0.00	0.00	0.00	0.00	0.00	0.00	0.00	0.00
Cr	0.01	0.02	0.00	0.01	0.00	0.00	0.00	0.00
Al	0.04	0.06	0.02	0.06	0.02	0.01	0.02	0.02
Fe3+	0.00	0.00	0.00	0.00	0.00	0.00	0.00	0.00
Fe2+	0.09	0.10	0.08	0.10	0.08	0.07	0.09	0.08
Mn	0.00	0.00	0.00	0.00	0.00	0.00	0.00	0.00
Ni	0.00	0.01	0.00	0.00	0.00	0.00	0.00	0.01
Mg	2.86	2.87	2.91	2.90	2.92	2.93	2.92	2.90
Ca	0.00	0.00	0.00	0.00	0.00	0.00	0.00	0.00
Total Cations	4.99	5.01	5.00	5.02	5.01	5.01	5.01	5.01
XMg	0.97	0.97	0.97	0.97	0.97	0.98	0.97	0.97

Serpentine	T5_c3_serp10	T5_c3_serp75	T5_c3_serp76	T5_c3_serp77	T5_c3_serp78	T5_c3_serp79	T5_c3_serp80	T5_c4_serp27	T5_c4_serp28
SiO2	41.87	42.12	41.89	42.62	42.14	41.74	41.91	41.46	40.98
TiO2	0.01	0.02	0.02	0.00	0.02	0.01	0.02	0.01	0.00
Cr2O3	0.23	0.15	0.16	0.15	0.14	0.31	0.19	0.39	0.41
Al2O3	0.96	0.92	0.99	0.54	0.99	1.28	1.15	1.19	1.50
FeO	2.34	2.31	2.32	2.05	2.40	2.44	2.51	2.43	2.58
MnO	0.08	0.03	0.04	0.04	0.05	0.03	0.02	0.05	0.05
NiO	0.05	0.07	0.04	0.11	0.05	0.04	0.05	0.03	0.04
MgO	41.93	41.61	41.32	41.47	42.04	41.50	41.62	41.36	41.25
CaO	0.00	0.00	0.01	0.01	0.00	0.00	0.01	0.01	0.02
Total	87.47	87.24	86.79	87.00	87.83	87.36	87.49	86.92	86.83
Cation									
Si	1.95	1.96	1.96	1.99	1.95	1.95	1.95	1.94	1.93
Ti	0.00	0.00	0.00	0.00	0.00	0.00	0.00	0.00	0.00
Cr	0.01	0.01	0.01	0.01	0.01	0.01	0.01	0.01	0.02
Al	0.05	0.05	0.05	0.03	0.05	0.07	0.06	0.07	0.08
Fe3+	0.00	0.00	0.00	0.00	0.00	0.00	0.00	0.00	0.00
Fe2+	0.09	0.09	0.09	0.08	0.09	0.10	0.10	0.10	0.10
Mn	0.00	0.00	0.00	0.00	0.00	0.00	0.00	0.00	0.00
Ni	0.00	0.00	0.00	0.00	0.00	0.00	0.00	0.00	0.00
Mg	2.91	2.89	2.89	2.88	2.91	2.88	2.89	2.89	2.89
Ca	0.00	0.00	0.00	0.00	0.00	0.00	0.00	0.00	0.00
Total Cations	5.02	5.01	5.01	4.99	5.02	5.01	5.01	5.02	5.02
XMg	0.97	0.97	0.97	0.97	0.97	0.97	0.97	0.97	0.97

Serpentine	T5_c4_serp29	T5_c4_serp30	T5_c4_serp31	T5_c4_serp32	T5_c4_serp33	T5_c4_serp34	T5_c5_serp1	T5_c5_serp2	T5_c5_serp3
SiO2	41.60	42.77	41.71	42.69	42.03	41.31	41.08	41.36	42.61
TiO2	0.02	0.01	0.01	0.01	0.01	0.01	0.00	0.01	0.00
Cr2O3	0.16	0.03	0.18	0.02	0.07	0.20	0.59	0.31	0.13
Al2O3	1.07	0.31	1.08	0.34	0.59	1.25	1.61	1.41	0.51
FeO	2.30	1.87	2.35	1.74	2.06	2.51	2.49	2.41	1.83
MnO	0.05	0.06	0.05	0.04	0.05	0.05	0.04	0.05	0.06
NiO	0.07	0.04	0.04	0.03	0.02	0.03	0.06	0.08	0.02
MgO	41.53	42.37	41.73	42.31	41.98	41.61	41.32	41.14	41.71
CaO	0.19	0.26	0.24	0.29	0.30	0.14	0.00	0.03	0.12
Total	86.98	87.73	87.39	87.47	87.12	87.10	87.20	86.80	86.98

Cation									
Si	1.95	1.98	1.95	1.98	1.96	1.94	1.92	1.94	1.99
Ti	0.00	0.00	0.00	0.00	0.00	0.00	0.00	0.00	0.00
Cr	0.01	0.00	0.01	0.00	0.00	0.01	0.02	0.01	0.00
Al	0.06	0.02	0.06	0.02	0.03	0.07	0.09	0.08	0.03
Fe3+	0.00	0.00	0.00	0.00	0.00	0.00	0.00	0.00	0.00
Fe2+	0.09	0.07	0.09	0.07	0.08	0.10	0.10	0.09	0.07
Mn	0.00	0.00	0.00	0.00	0.00	0.00	0.00	0.00	0.00
Ni	0.00	0.00	0.00	0.00	0.00	0.00	0.00	0.00	0.00
Mg	2.90	2.92	2.90	2.93	2.92	2.91	2.88	2.88	2.90
Ca	0.01	0.01	0.01	0.01	0.01	0.01	0.00	0.00	0.01
Total Cations	5.02	5.01	5.02	5.01	5.02	5.03	5.02	5.01	5.00
XMg	0.97	0.98	0.97	0.98	0.97	0.97	0.97	0.97	0.98

Serpentine	T5_c5_serp4	T5_c5_serp5	T5_c5_serp6	T5_c5_serp7	T5_c5_serp8	T5_c5_serp9	T5_c6_serp10	T5_c6_serp11	T5_c6_serp12
SiO2	42.43	41.50	41.61	42.40	42.02	41.54	42.02	41.77	41.35
TiO2	0.00	0.02	0.01	0.01	0.02	0.01	0.01	0.01	0.01
Cr2O3	0.05	0.17	0.15	0.23	0.11	0.36	0.07	0.27	0.15
Al2O3	0.35	1.18	1.12	0.54	0.68	1.36	0.56	1.16	1.33
FeO	1.84	2.33	2.42	2.00	1.91	2.16	2.19	2.45	2.51
MnO	0.04	0.05	0.05	0.04	0.03	0.04	0.05	0.03	0.05
NiO	0.08	0.05	0.04	0.10	0.07	0.07	0.03	0.04	0.07
MgO	41.93	41.23	41.26	41.59	41.52	41.07	41.40	41.32	41.29
CaO	0.03	0.18	0.03	0.08	0.09	0.08	0.00	0.06	0.05
Total	86.75	86.71	86.69	86.99	86.44	86.69	86.32	87.10	86.80
Cation									
Si	1.98	1.95	1.95	1.98	1.97	1.95	1.98	1.95	1.94
Ti	0.00	0.00	0.00	0.00	0.00	0.00	0.00	0.00	0.00
Cr	0.00	0.01	0.01	0.01	0.00	0.01	0.00	0.01	0.01
Al	0.02	0.07	0.06	0.03	0.04	0.08	0.03	0.06	0.07
Fe3+	0.00	0.00	0.00	0.00	0.00	0.00	0.00	0.00	0.00
Fe2+	0.07	0.09	0.10	0.08	0.08	0.08	0.09	0.10	0.10
Mn	0.00	0.00	0.00	0.00	0.00	0.00	0.00	0.00	0.00
Ni	0.00	0.00	0.00	0.00	0.00	0.00	0.00	0.00	0.00
Mg	2.92	2.89	2.89	2.89	2.91	2.87	2.90	2.88	2.89
Ca	0.00	0.01	0.00	0.00	0.00	0.00	0.00	0.00	0.00
Total Cations	5.01	5.01	5.01	5.00	5.01	5.01	5.01	5.01	5.02
XMg	0.98	0.97	0.97	0.97	0.97	0.97	0.97	0.97	0.97

Serpentine	T5_c6_serp13	T5_c6_serp14	T5_c7_serp15	T5_c7_serp16	T5_c7_serp17	T5_c7_serp18	T5_c7_serp19	T5_c8_serp20	T5_c8_serp21
SiO2	41.88	42.13	41.42	41.32	41.42	41.31	41.38	42.91	41.50
TiO2	0.00	0.00	0.01	0.00	0.00	0.02	0.03	0.03	0.02
Cr2O3	0.18	0.37	0.30	0.32	0.39	0.42	0.43	0.03	0.31
Al2O3	1.02	0.82	1.19	1.12	1.26	1.48	1.47	0.27	1.47
FeO	2.42	2.29	1.37	2.21	2.35	2.39	2.24	1.86	2.33
MnO	0.03	0.05	0.07	0.06	0.04	0.04	0.03	0.06	0.07
NiO	0.05	0.05	0.04	0.04	0.05	0.08	0.09	0.04	0.07
MgO	41.42	41.35	40.72	41.43	41.15	40.90	40.85	42.00	41.36
CaO	0.04	0.01	0.00	0.18	0.21	0.23	0.02	0.01	0.02
Total	87.04	87.07	85.12	86.68	86.88	86.86	86.53	87.22	87.14
Cation									
Si	1.96	1.97	1.97	1.94	1.94	1.94	1.95	1.99	1.94
Ti	0.00	0.00	0.00	0.00	0.00	0.00	0.00	0.00	0.00
Cr	0.01	0.01	0.01	0.01	0.01	0.02	0.02	0.00	0.01
Al	0.06	0.04	0.07	0.06	0.07	0.08	0.08	0.02	0.08
Fe3+	0.00	0.00	0.00	0.00	0.00	0.00	0.00	0.00	0.00
Fe2+	0.09	0.09	0.05	0.09	0.09	0.09	0.09	0.07	0.09
Mn	0.00	0.00	0.00	0.00	0.00	0.00	0.00	0.00	0.00
Ni	0.00	0.00	0.00	0.00	0.00	0.00	0.00	0.00	0.00
Mg	2.89	2.88	2.89	2.90	2.88	2.86	2.86	2.91	2.88
Ca	0.00	0.00	0.00	0.01	0.01	0.01	0.00	0.00	0.00
Total Cations	5.01	5.00	4.99	5.02	5.01	5.01	5.00	5.00	5.01
XMg	0.97	0.97	0.98	0.97	0.97	0.97	0.97	0.98	0.97

						T2			
Serpentine	T5_c8_serp22	T5_c8_serp23	T5_c8_serp24	T5_c8_serp25	T5_c8_serp26	T2_c1_serp120	T2_c1_serp121	T2_c1_serp122	T2_c1_serp123
SiO2	41.92	41.71	41.55	41.17	42.30	41.07	40.82	41.40	41.53
TiO2	0.00	0.02	0.00	0.00	0.02	0.01	0.03	0.04	0.00
Cr2O3	0.27	0.28	0.37	0.46	0.12	0.21	0.19	0.03	0.23
Al2O3	0.61	1.19	1.30	1.27	0.88	1.39	1.66	1.08	1.33
FeO	2.04	2.38	2.37	2.65	2.30	3.78	3.68	3.71	3.68
MnO	0.06	0.04	0.03	0.05	0.05	0.12	0.09	0.08	0.09
NiO	0.16	0.07	0.05	0.21	0.05	0.18	0.31	0.03	0.10
MgO	41.43	41.47	41.30	40.95	41.78	39.73	39.28	39.94	39.95
CaO	0.04	0.15	0.10	0.10	0.01	0.01	0.05	0.01	0.01
Total	86.54	87.29	87.08	86.86	87.51	86.49	86.09	86.32	86.92
Cation									
Si	1.97	1.95	1.94	1.94	1.97	1.95	1.95	1.96	1.96
Ti	0.00	0.00	0.00	0.00	0.00	0.00	0.00	0.00	0.00
Cr	0.01	0.01	0.01	0.02	0.00	0.01	0.01	0.00	0.01
Al	0.03	0.07	0.07	0.07	0.05	0.08	0.09	0.06	0.07
Fe3+	0.00	0.00	0.00	0.00	0.00	0.00	0.00	0.00	0.00
Fe2+	0.08	0.09	0.09	0.10	0.09	0.15	0.15	0.15	0.15
Mn	0.00	0.00	0.00	0.00	0.00	0.00	0.00	0.00	0.00
Ni	0.01	0.00	0.00	0.01	0.00	0.01	0.01	0.00	0.00
Mg	2.90	2.89	2.88	2.87	2.89	2.81	2.79	2.82	2.81
Ca	0.00	0.01	0.01	0.00	0.00	0.00	0.00	0.00	0.00
Total Cations	5.01	5.01	5.01	5.02	5.01	5.01	5.00	5.00	5.00
XMg	0.97	0.97	0.97	0.96	0.97	0.95	0.95	0.95	0.95

Serpentine	T2_c1_serp124	T2_c1_serp125	T2_c2_serp126	T2_c2_serp127	T2_c2_serp128	T2_c2_serp129	T2_c2_serp130	T2_c2_serp132
SiO2	41.23	41.40	40.53	41.47	41.45	40.78	40.89	41.32
TiO2	0.01	0.01	0.02	0.02	0.01	0.03	0.02	0.01
Cr2O3	0.20	0.27	0.14	0.10	0.26	0.26	0.20	0.13
Al2O3	1.34	1.53	1.99	1.25	1.57	2.00	1.62	1.37
FeO	3.87	3.73	3.96	3.66	3.77	4.00	3.83	3.68
MnO	0.11	0.08	0.07	0.10	0.10	0.08	0.08	0.13
NiO	0.14	0.14	0.24	0.11	0.08	0.03	0.20	0.05
MgO	39.82	39.67	39.27	39.65	39.85	39.34	39.25	39.81
CaO	0.02	0.02	0.10	0.09	0.18	0.24	0.25	0.41
Total	86.74	86.84	86.31	86.45	87.27	86.77	86.33	86.89

Cation								
Si	1.95	1.95	1.93	1.97	1.95	1.93	1.95	1.95
Ti	0.00	0.00	0.00	0.00	0.00	0.00	0.00	0.00
Cr	0.01	0.01	0.01	0.00	0.01	0.01	0.01	0.00
Al	0.08	0.09	0.11	0.07	0.09	0.11	0.09	0.08
Fe3+	0.00	0.00	0.00	0.00	0.00	0.00	0.00	0.00
Fe2+	0.15	0.15	0.16	0.15	0.15	0.16	0.15	0.15
Mn	0.00	0.00	0.00	0.00	0.00	0.00	0.00	0.01
Ni	0.01	0.01	0.01	0.00	0.00	0.00	0.01	0.00
Mg	2.81	2.79	2.79	2.80	2.79	2.78	2.78	2.80
Ca	0.00	0.00	0.01	0.00	0.01	0.01	0.01	0.02
Total Cations	5.01	5.00	5.01	5.00	5.00	5.01	5.00	5.01
XMg	0.95	0.95	0.95	0.95	0.95	0.95	0.95	0.95

Serpentine	T2_c3_serp134	T2_c3_serp135	T2_c3_serp136	T2_c3_serp138	T2_c3_serp139	T2_c3_serp140	T2_c4_serp143	T2_c4_serp147
SiO2	41.15	41.42	41.34	40.92	41.12	41.13	42.24	40.72
TiO2	0.04	0.04	0.02	0.02	0.03	0.02	0.01	0.04
Cr2O3	0.24	0.28	0.24	0.38	0.22	0.20	0.02	0.22
Al2O3	1.60	1.46	1.60	1.87	1.60	1.60	0.85	1.57
FeO	3.70	3.71	3.87	3.87	3.75	3.82	3.62	5.86
MnO	0.10	0.07	0.09	0.06	0.08	0.08	0.09	0.09
NiO	0.13	0.10	0.06	0.08	0.13	0.04	0.10	0.17
MgO	39.60	39.81	39.72	39.40	39.57	39.85	40.35	39.09
CaO	0.04	0.02	0.01	0.02	0.02	0.00	0.24	0.02
Total	86.61	86.91	86.95	86.61	86.51	86.75	87.52	87.78

Cation								
Si	1.95	1.95	1.95	1.94	1.95	1.94	1.98	1.93
Ti	0.00	0.00	0.00	0.00	0.00	0.00	0.00	0.00
Cr	0.01	0.01	0.01	0.01	0.01	0.01	0.00	0.01
Al	0.09	0.08	0.09	0.10	0.09	0.09	0.05	0.09
Fe3+	0.00	0.00	0.00	0.00	0.00	0.00	0.00	0.00
Fe2+	0.15	0.15	0.15	0.15	0.15	0.15	0.14	0.23
Mn	0.00	0.00	0.00	0.00	0.00	0.00	0.00	0.00
Ni	0.01	0.00	0.00	0.00	0.00	0.00	0.00	0.01
Mg	2.79	2.80	2.79	2.78	2.80	2.81	2.81	2.76
Ca	0.00	0.00	0.00	0.00	0.00	0.00	0.01	0.00
Total Cations	5.00	5.00	5.00	5.00	5.00	5.01	5.00	5.02
XMg	0.95	0.95	0.95	0.95	0.95	0.95	0.95	0.92

Serpentine	T2_c4_serp149	T2_c4_serp150	T2_c5_serp151	T2_c5_serp152	T2_c5_serp153	T2_c6_serp154	T2_c6_serp156	T2_c6_serp157
SiO2	42.18	40.83	41.06	41.25	41.29	40.85	40.61	39.06
TiO2	0.02	0.03	0.02	0.00	0.02	0.03	0.03	0.01
Cr2O3	0.03	0.31	0.21	0.10	0.10	0.34	0.36	0.16
Al2O3	0.85	1.63	1.64	1.53	1.53	1.72	1.93	1.26
FeO	4.33	4.45	3.84	3.74	3.84	3.76	4.07	3.52
MnO	0.09	0.08	0.07	0.09	0.09	0.07	0.08	0.10
NiO	0.15	0.17	0.23	0.04	0.04	0.24	0.09	0.07
MgO	40.57	39.19	39.36	39.86	39.92	39.08	39.09	38.78
CaO	0.16	0.06	0.03	0.16	0.12	0.04	0.01	1.89
Total	88.38	86.75	86.46	86.78	86.95	86.13	86.27	84.85

Cation								
Si	1.96	1.94	1.95	1.95	1.95	1.95	1.93	1.91
Ti	0.00	0.00	0.00	0.00	0.00	0.00	0.00	0.00
Cr	0.00	0.01	0.01	0.00	0.00	0.01	0.01	0.01
Al	0.05	0.09	0.09	0.09	0.09	0.10	0.11	0.07
Fe3+	0.00	0.00	0.00	0.00	0.00	0.00	0.00	0.00
Fe2+	0.17	0.18	0.15	0.15	0.15	0.15	0.16	0.14
Mn	0.00	0.00	0.00	0.00	0.00	0.00	0.00	0.00
Ni	0.01	0.01	0.01	0.00	0.00	0.01	0.00	0.00
Mg	2.81	2.77	2.79	2.81	2.81	2.78	2.78	2.82
Ca	0.01	0.00	0.00	0.01	0.01	0.00	0.00	0.10
Total Cations	5.01	5.01	5.00	5.01	5.01	5.00	5.00	5.05
XMg	0.94	0.94	0.95	0.95	0.95	0.95	0.94	0.95

Serpentine	T2_c7_serp158	T2_c7_serp159	T2_c7_serp161	T2_c8_serp162	T2_c8_serp164	T2_c9_serp167
SiO2	41.24	40.05	41.40	41.09	41.29	41.06
TiO2	0.01	0.04	0.03	0.01	0.01	0.03
Cr2O3	0.23	0.25	0.23	0.16	0.18	0.23
Al2O3	1.74	1.76	1.70	1.60	1.59	1.81
FeO	3.98	4.22	3.77	3.85	3.71	3.77
MnO	0.09	0.06	0.07	0.07	0.08	0.07
NiO	0.13	0.33	0.25	0.24	0.24	0.30
MgO	39.56	38.50	39.60	39.50	39.67	39.47
CaO	0.03	0.05	0.07	0.01	0.07	0.02
Total	87.01	85.26	87.13	86.52	86.83	86.76

Cation						
Si	1.95	1.94	1.95	1.95	1.95	1.94
Ti	0.00	0.00	0.00	0.00	0.00	0.00
Cr	0.01	0.01	0.01	0.01	0.01	0.01
Al	0.10	0.10	0.09	0.09	0.09	0.10
Fe3+	0.00	0.00	0.00	0.00	0.00	0.00
Fe2+	0.16	0.17	0.15	0.15	0.15	0.15
Mn	0.00	0.00	0.00	0.00	0.00	0.00
Ni	0.01	0.01	0.01	0.01	0.01	0.01
Mg	2.78	2.77	2.78	2.79	2.79	2.78
Ca	0.00	0.00	0.00	0.00	0.00	0.00
Total Cations	5.00	5.01	5.00	5.00	5.00	5.00
XMg	0.95	0.94	0.95	0.95	0.95	0.95

Serpentine	T2_c10_serp170	T2_c10_serp171	T2_c10_serp173
SiO2	40.53	41.13	41.51
TiO2	0.03	0.00	0.02
Cr2O3	0.24	0.18	0.09
Al2O3	2.19	1.72	1.28
FeO	3.98	3.79	3.69
MnO	0.06	0.09	0.07
NiO	0.52	0.08	0.07
MgO	38.87	39.59	39.91
CaO	0.04	0.33	0.30
Total	86.45	86.91	86.93

Cation			
Si	1.93	1.94	1.96
Ti	0.00	0.00	0.00
Cr	0.01	0.01	0.00
Al	0.12	0.10	0.07
Fe3+	0.00	0.00	0.00
Fe2+	0.16	0.15	0.15
Mn	0.00	0.00	0.00
Ni	0.02	0.00	0.00
Mg	2.76	2.79	2.81
Ca	0.00	0.02	0.01
Total Cations	5.00	5.01	5.00
XMg	0.95	0.95	0.95

	Sample	Weight (mg)	Ampl 44	Area All	Avg. d13C raw	std.dev.	Avg. d18O raw	std.dev.	$d^{13}C$ VPDB	$d^{18}O$ VPDB Calcite	$d^{18}O$ VSMOW Calcite	$d^{18}O$ VPDB Dolomite
	28-ZS-17	1606	1234	8.15	-0.84	0.06	19.32	0.05	-0.90			-20.04
	29-ZS-17	1511	876	5.82	-0.51	0.06	19.36	0.06	-0.57			-20.00
	30-ZS-17	1955	587	3.88	-1.70	0.10	20.72	0.15	-1.70			-18.41
	31-ZS-17	3421	165	0.63	-3.28	0.22	20.66	0.37	-3.29			-18.46
	32-ZS-17	2032	1144	7.61	-0.59	0.08	20.70	0.07	-0.59			-18.42
	33-ZS-17	1665	737	4.81	-1.02	0.09	19.46	0.14	-1.08			-19.90
	28-ZS-17(R) (spot)	183	1660	11.03	-0.26	0.04	19.67	0.04	-0.32			-19.70
	28-ZS-17(R) (vein)	268	2518	16.85	-1.03	0.09	19.20	0.09	-1.09			-20.15
	29-ZS-17 (1)	150	1511	10.39	-0.13	0.07	19.55	0.06	-0.19			-19.82
	29-ZS-17 (2)	133	1478	9.77	0.04	0.08	19.61	0.08	-0.02			-19.75
	32-ZS-17	334	2563	17.02	-0.13	0.10	20.22	0.07	-0.19			-19.17
E	33-ZS-17	213	925	6.11	-0.86	0.09	19.77	0.06	-0.92			-19.60

	Sample	$d^{18}O$ VSMOW Dolomite	$d^{18}O$ VPDB Magnesite	$d^{18}O$ VSMOW Magnesite	Yield % as Carbonate	Comment	Type of carbonate	
	28-ZS-17	10.25			3.68	Reacted for 1 hrs	DOLOMITE	WHOLE ROCK
	29-ZS-17	10.30			2.80	Reacted for 1 hrs	DOLOMITE	WHOLE ROCK
	30-ZS-17	11.94			2.58	Reacted for 24 hrs	?	WHOLE ROCK
	31-ZS-17	11.88			0.24	Reacted for 24 hrs	?	WHOLE ROCK
	32-ZS-17	11.92	-18.56		4.86	Reacted for 24 hrs	MAGNESITE	WHOLE ROCK
	33-ZS-17	10.39			2.10	Reacted for 1 hrs	?	WHOLE ROCK
	28-ZS-17(R)	10.60			43.75	Reacted for 1 hrs	DOLOMITE	GRAIN
	28-ZS-17(R)	10.14			45.65	Reacted for 1 hrs	DOLOMITE	GRAIN
	29-ZS-17 (1)	10.48			50.26	Reacted for 1 hrs	DOLOMITE	GRAIN
	29-ZS-17 (2)	10.55			53.31	Reacted for 1 hrs	DOLOMITE	GRAIN
	32-ZS-17	11.15	-19.31		36.99	Reacted for 1 hrs	MAGNESITE	GRAIN
E	33-ZS-17	10.70			20.81	Reacted for 1 hrs	?	GRAIN

Analyses Majeurs FRX (19) ** T. STROMO ** projet n° 932, TSM1117.xls , 23- novembre- 2017															
Echant.	SiO2	TiO2	Al2O3	Fe2O3	MnO	MgO	CaO	Na2O	K2O	P2O5	LOI	Cr2O3	NiO	Somme	
	wt-%	wt-%	wt-%	wt-%	wt-%	wt-%	wt-%	wt-%	wt-%	wt-%	wt-%	wt-%	wt-%	wt-%	
UB-N	44.84	0.12	3.32	9.39	0.15	39.97	1.38	0.13	0.02	0.02	0.00	0.39	0.28	100.01	std
TS2T	39.97	0.02	1.04	7.44	0.11	41.54	0.00	0.00	0.00	0.01	9.09	0.40	0.31	99.93	
TS2B	39.35	0.03	5.14	6.40	0.12	28.12	11.09	0.34	0.05	0.01	8.79	0.25	0.20	99.89	
TS4	38.57	0.02	0.61	10.42	0.13	41.48	0.19	0.00	0.00	0.01	7.75	0.50	0.31	100.00	
TS6	36.49	0.02	0.51	6.94	0.10	39.27	0.17	0.00	0.00	0.01	15.67	0.25	0.28	99.70	
TS9	36.72	0.03	0.59	8.95	0.10	35.87	2.90	0.00	0.00	0.01	14.21	0.36	0.22	99.95	
TS13	34.23	0.02	1.78	5.65	0.12	29.16	10.98	0.10	0.02	0.01	17.37	0.31	0.22	99.96	
TS15	50.11	0.04	3.90	4.98	0.09	25.16	9.38	0.77	0.08	0.01	5.02	0.18	0.16	99.89	
TS16	53.87	0.03	0.55	4.43	0.10	21.05	16.21	0.59	0.06	0.01	2.77	0.09	0.11	99.87	
TS18	36.13	0.02	1.16	7.85	0.11	34.94	4.01	0.00	0.00	0.01	15.01	0.35	0.25	99.83	
TS19T	40.95	0.02	1.45	7.42	0.10	37.59	0.11	0.00	0.00	0.01	11.64	0.33	0.25	99.85	
TS19M	29.32	0.02	1.67	8.50	0.13	31.51	8.09	0.00	0.00	0.01	19.62	0.32	0.24	99.43	
TS19B	25.82	0.02	2.10	6.73	0.14	30.15	11.24	0.00	0.00	0.01	23.18	0.31	0.25	99.96	
TS20 (center)	36.95	0.02	1.02	8.34	0.10	38.97	0.08	0.00	0.00	0.01	13.62	0.32	0.28	99.72	
TS28	40.53	0.02	1.40	5.73	0.10	37.28	1.17	0.00	0.00	0.01	13.05	0.25	0.27	99.81	
TS29	38.69	0.03	2.10	8.95	0.09	35.92	1.00	0.00	0.00	0.01	12.44	0.43	0.26	99.91	
TS30	37.34	0.11	0.90	11.81	0.14	40.09	0.16	0.00	0.00	0.01	8.64	0.47	0.23	99.90	
TS31	40.88	0.02	1.42	6.15	0.09	38.75	0.01	0.00	0.00	0.01	11.85	0.33	0.29	99.81	
TS32	39.12	0.02	1.32	8.14	0.10	38.06	0.00	0.00	0.00	0.01	12.41	0.31	0.30	99.77	
TS33	40.70	0.03	1.80	6.53	0.11	37.17	0.74	0.00	0.00	0.01	12.18	0.35	0.29	99.91	
NIM-P	50.71	0.19	4.21	12.74	0.23	25.19	2.64	0.36	0.09	0.02	0.00	3.47	0.07	99.92	std
PCC-1	43.96	0.02	0.80	8.65	0.13	44.84	0.58	0.05	0.02	0.01	0.00	0.42	0.31	99.79	std

Analyses pro-Trace FRX (19) *** T. STROMO ***, projet n° 932, TST1117C.xls, 23- novembre- 2017																					
Echant.	Sc	V	Cr	Mn	Co	Ni	Cu	Zn	Ga	Ge	As	Se	Br	Rb	Sr	Y	Zr	Nb	Mo	Ag	Cd
	(ppm)	(ppm)	(ppm)	(ppm)	(ppm)	(ppm)	(ppm)	(ppm)	(ppm)	(ppm)	(ppm)	(ppm)	(ppm)	(ppm)	(ppm)	(ppm)	(ppm)	(ppm)	(ppm)	(ppm)	(ppm)
LLD	1	2	1	2	2	1	1	1	1	1	3	1	1	1	1	1	1	1	1	3	3
TS2T	4	24	2268	663	114	2068	11	32	1	<LLD	20	<LLD	<LLD	<LLD	<LLD	<LLD	<LLD	<LLD	<LLD	<LLD	<LLD
TS2B	3	26	2046	727	116	2041	10	28	2	<LLD	16	<LLD	<LLD	<LLD	<LLD	<LLD	<LLD	<LLD	<LLD	<LLD	<LLD
TS4	4	27	2898	883	121	2177	12	44	1	<LLD	16	<LLD	<LLD	<LLD	1	<LLD	<LLD	<LLD	<LLD	<LLD	<LLD
TS6	4	17	1453	701	105	1884	8	25	<LLD	<LLD	16	<LLD	<LLD	<LLD	1	<LLD	<LLD	<LLD	<LLD	<LLD	<LLD
TS9	5	21	2013	726	92	1572	9	38	1	<LLD	8	<LLD	<LLD	<LLD	87	<LLD	<LLD	<LLD	<LLD	<LLD	<LLD
TS13	6	18	1793	869	93	1530	14	27	2	<LLD	<LLD	<LLD	<LLD	1	259	<LLD	<LLD	<LLD	<LLD	<LLD	<LLD
TS15	7	41	1081	559	67	1138	5	30	3	1	<LLD	<LLD	<LLD	<LLD	21	<LLD	<LLD	<LLD	<LLD	<LLD	<LLD
TS16	10	26	527	606	66	724	5	22	<LLD	1	<LLD	<LLD	<LLD	<LLD	51	2	1	<LLD	<LLD	<LLD	<LLD
TS18	4	22	2044	787	100	1754	16	40	2	<LLD	6	<LLD	<LLD	<LLD	140	<LLD	<LLD	<LLD	<LLD	<LLD	<LLD
TS19T	3	27	1991	628	94	1697	16	45	2	<LLD	3	<LLD	<LLD	<LLD	2	<LLD	<LLD	<LLD	<LLD	<LLD	<LLD
TS19M	6	30	1993	995	96	1756	22	35	2	<LLD	5	<LLD	<LLD	<LLD	272	<LLD	<LLD	<LLD	<LLD	<LLD	<LLD
TS19B	8	28	1942	1028	100	1739	19	29	2	<LLD	5	<LLD	<LLD	2	300	1	<LLD	<LLD	<LLD	<LLD	<LLD
TS20	12	34	1530	783	71	1296	10	28	3	<LLD	<LLD	<LLD	<LLD	<LLD	131	<LLD	<LLD	<LLD	<LLD	<LLD	<LLD
TS28	6	25	1506	638	98	1747	25	37	2	<LLD	<LLD	<LLD	<LLD	<LLD	17	<LLD	2	<LLD	<LLD	<LLD	<LLD
TS29	7	45	2577	555	106	1927	4	34	2	<LLD	<LLD	<LLD	<LLD	<LLD	13	<LLD	<LLD	<LLD	<LLD	<LLD	<LLD
TS30	6	36	2998	967	106	1571	7	41	1	<LLD	21	<LLD	<LLD	<LLD	<LLD	<LLD	<LLD	<LLD	<LLD	<LLD	<LLD
TS31	3	17	1938	552	100	2009	13	32	1	<LLD	10	<LLD	<LLD	<LLD	<LLD	<LLD	<LLD	<LLD	<LLD	<LLD	<LLD
TS32	3	20	1941	660	108	2113	13	34	1	<LLD	10	<LLD	<LLD	<LLD	<LLD	<LLD	<LLD	<LLD	<LLD	<LLD	<LLD
TS33	4	22	2088	760	101	1870	8	39	2	<LLD	<LLD	<LLD	<LLD	<LLD	16	<LLD	<LLD	<LLD	<LLD	<LLD	<LLD
Contrôle sur standards																					
BHVO	30	318	280	1346	45	118	147	107	24	<LLD	<LLD	<LLD	<LLD	11	400	27	175	17	<LLD	<LLD	<LLD
NIMG	<LLD	<LLD	12	137	<LLD	5	12	52	31	<LLD	13	<LLD	<LLD	330	9	136	286	51	1	<LLD	<LLD

Echant.	Sn	Sb	Te	I	Cs	Ba	La	Ce	Nd	Sm	Yb	Hf	Ta	W	Hg	Tl	Pb	Bi	Th	U
	(ppm)	(ppm)	(ppm)	(ppm)	(ppm)	(ppm)	(ppm)	(ppm)	(ppm)	(ppm)	(ppm)	(ppm)	(ppm)	(ppm)	(ppm)	(ppm)	(ppm)	(ppm)	(ppm)	(ppm)
LLD	**2**	**3**	**3**	**3**	**2**	**5**	**7**	**5**	**3**	**3**	**2**	**2**	**1**	**1**	**4**	**2**	**1**	**1**	**1**	**1**
TS2T	<LLD	<LLD	<LLD	<LLD	2	<LLD	<LLD	<LLD	<LLD	<LLD	<LLD	<LLD	<LLD	106	<LLD	<LLD	<LLD	<LLD	<LLD	<LLD
TS2B	<LLD	<LLD	<LLD	<LLD	<LLD	<LLD	<LLD	<LLD	<LLD	<LLD	<LLD	<LLD	<LLD	111	<LLD	<LLD	<LLD	<LLD	<LLD	<LLD
TS4	<LLD	<LLD	<LLD	<LLD	<LLD	<LLD	<LLD	<LLD	<LLD	<LLD	<LLD	<LLD	<LLD	130	<LLD	<LLD	<LLD	<LLD	<LLD	<LLD
TS6	<LLD	<LLD	<LLD	<LLD	<LLD	<LLD	<LLD	<LLD	<LLD	<LLD	<LLD	<LLD	<LLD	63	<LLD	<LLD	<LLD	<LLD	<LLD	<LLD
TS9	<LLD	<LLD	<LLD	<LLD	<LLD	<LLD	<LLD	<LLD	<LLD	<LLD	<LLD	<LLD	<LLD	60	<LLD	<LLD	<LLD	<LLD	<LLD	<LLD
TS13	<LLD	<LLD	<LLD	<LLD	2	<LLD	<LLD	<LLD	<LLD	<LLD	<LLD	<LLD	<LLD	55	<LLD	<LLD	<LLD	<LLD	1	<LLD
TS15	<LLD	<LLD	<LLD	<LLD	<LLD	<LLD	<LLD	<LLD	<LLD	<LLD	<LLD	3	<LLD	87	<LLD	<LLD	<LLD	<LLD	<LLD	<LLD
TS16	<LLD	<LLD	<LLD	<LLD	3	<LLD	<LLD	<LLD	<LLD	<LLD	<LLD	<LLD	<LLD	105	<LLD	<LLD	<LLD	<LLD	<LLD	<LLD
TS18	<LLD	<LLD	<LLD	<LLD	<LLD	<LLD	<LLD	<LLD	<LLD	<LLD	<LLD	4	<LLD	60	<LLD	<LLD	<LLD	<LLD	<LLD	<LLD
TS19T	<LLD	<LLD	<LLD	<LLD	<LLD	<LLD	<LLD	<LLD	<LLD	<LLD	<LLD	<LLD	<LLD	61	<LLD	<LLD	<LLD	<LLD	<LLD	<LLD
TS19M	<LLD	<LLD	<LLD	<LLD	3	<LLD	<LLD	<LLD	<LLD	<LLD	<LLD	<LLD	<LLD	63	<LLD	<LLD	1	<LLD	<LLD	1
TS19B	<LLD	<LLD	<LLD	<LLD	2	<LLD	<LLD	<LLD	<LLD	<LLD	<LLD	<LLD	<LLD	61	<LLD	<LLD	2	<LLD	2	1
TS20	<LLD	<LLD	<LLD	<LLD	3	<LLD	<LLD	<LLD	<LLD	<LLD	<LLD	<LLD	<LLD	59	<LLD	<LLD	<LLD	<LLD	<LLD	<LLD
TS28	<LLD	<LLD	<LLD	<LLD	<LLD	<LLD	<LLD	<LLD	<LLD	<LLD	<LLD	<LLD	<LLD	58	<LLD	<LLD	<LLD	<LLD	<LLD	<LLD
TS29	<LLD	<LLD	<LLD	<LLD	<LLD	<LLD	<LLD	<LLD	<LLD	<LLD	<LLD	<LLD	<LLD	69	<LLD	<LLD	<LLD	<LLD	<LLD	<LLD
TS30	<LLD	<LLD	<LLD	<LLD	<LLD	<LLD	<LLD	<LLD	<LLD	<LLD	<LLD	<LLD	<LLD	88	<LLD	<LLD	<LLD	<LLD	<LLD	<LLD
TS31	<LLD	<LLD	<LLD	<LLD	<LLD	<LLD	<LLD	<LLD	<LLD	<LLD	<LLD	<LLD	<LLD	67	<LLD	<LLD	<LLD	<LLD	<LLD	<LLD
TS32	<LLD	<LLD	<LLD	<LLD	<LLD	<LLD	<LLD	<LLD	<LLD	<LLD	<LLD	<LLD	<LLD	71	<LLD	<LLD	<LLD	<LLD	<LLD	<LLD
TS33	<LLD	<LLD	<LLD	<LLD	<LLD	<LLD	<LLD	<LLD	<LLD	<LLD	<LLD	<LLD	<LLD	69	<LLD	<LLD	<LLD	<LLD	<LLD	<LLD
Contrôle sur standards																				
BHVO	<LLD	<LLD	<LLD	3	<LLD	142	25	41	26	6	<LLD	4	<LLD	<LLD	<LLD	<LLD	2	<LLD	1	1
NIMG	6	<LLD	<LLD	<LLD	2	110	120	199	70	15	14	13	4	2	<LLD	<LLD	40	<LLD	57	21